Numerical simulation of the Helicon Double Layer Thruster Concept

ESA Contract No. Ariadna 05/3201

Prepared by: Marco Manente , Ivano Musso, Johan Carlsson

Contributions by:

Checked by: Daniele Pavarin

Approved by: Daniele Pavarin

ESA CONTRACT no.	SUBJECT	CONTRACTOR
Ariadna 05/3201	Numerical Simulations of the Helicon Double Layer Thruster Concept – Final Report	CISAS "G. Colombo"

ABSTRACT

The Australian National University and the Laboratoire de Physique et Technologie des Plasmas (LPTP) of Ecole Polytechnique in Palaiseau (France) obtained experimental results of current free helicon double layer originating with electropositive and electronegative gases. The experimental evidence of a current free helicon double layer envisages tantalizing performance of a thruster exploiting this effect. Although some progress has been achieved, at the present time a number of aspects related to this phenomenon are still partially understood. This research report presents the resulted obtained by a deep numerical investigation on Double layer, formation, stability and characteristic and to explore the applicability of this concept to space mission. The analysis has been conducted through a combination of 1-D and 2-D code numerical code.

A 1-D code named PPDL was developed specifically for the porpoise of this study . It is a hybrid code with Boltzmann electrons and drift-kinetic ions, inclusion of dominant 2-D effects and high computational efficiency through implicit nonlinear Boltzmann solver. With the hybrid Boltzmann electron/drift-kinetic ion approach, the time step is only limited by ion period which is two orders of magnitude larger than electron plasma period and ion gyro period which can become very short. Simulations have been performed with several models for thrusters to identify the critical parameters. We analyzed the effects of ions and electrons temperatures, magnetic field strength and gradient. The plasma density and plasma source rates have been changed as well.

The 2D model adopted in this study is the Object Oriented Particle in Cell Code (OOPIC). The hybrid configuration has been found to not fulfill our requirements therefore we had to use the full PIC method, where electrons are computed as real particles like ions.

The geometry has been defined as near as possible to the experimental apparatus, like the properties of electrons and ions that are charged with Maxwellian distributions inside the source tube. The static magnetic field has been reconstructed adopting two coils with shape and current as reported by Charles, in order to have a axial field inside the source with two peaks of almost 150G.

We have conducted three campaigns of simulations with growing source rates and ions densities. The first two campaigns shown the main border conditions' effects on the plasma potential and ions velocity distribution. We have changed the electrons and ions temperatures, the electrical properties of the source walls, neutral pressure, magnetic field and plasma production rates and distributions. The third campaign has been devoted to the evaluation of higher densities plasmas with biased left source walls and, enlarging the diffusion chamber length, the thrust and specific impulse.

The results show a high energy ions flux at almost two times the ion sound speed. The potential jump is larger than the experimental measurements and, sometimes, lower. The effect of the neutral pressure increase, which reduces the high energy flux, appears similar to the one reported by Charles while the magnetic field has not been able to switch it off.

The combined approach resulted very useful since the 1-D code has been used to screen many different experimental conditions and to identify the right boundary conditions and the 2-D code has been then used to refine 1-D results.

ESA CONTRACT no.	SUBJECT	CONTRACTOR
Ariadna 05/3201	Numerical Simulations of the Helicon Double Layer Thruster Concept – Final report	CISAS "G. Colombo"

INDEX

ESA CONTRACT no.	SUBJECT	CONTRACTOR
Ariadna 05/3201	Numerical Simulations of the Helicon Double Layer Thruster Concept – Final report	CISAS "G. Colombo"

SECTION 3: Replication of experiments: understanding of the double layer formation and stability, thrust evaluation

ESA CONTRACT no.	SUBJECT	CONTRACTOR
Ariadna 05/3201	Numerical Simulations of the Helicon Double Layer Thruster Concept – Final report	CISAS "G. Colombo"

1 HELICON DOUBLE LAYER THEORY AND EXPERIMENTS

1.1 INTRODUCTION

The helicon double layer has been first reported by Charles and Boswell [6-9,31]. Successively some research groups have reproduced their results [22,23,24] while, analyzing older plasma experiments, one finds that similar conditions were met by other authors [5,19], under different conditions and with partial or original interpretations of the phenomenon.

This section exposes the actual theoretical understanding of the Helicon Double Layer formation processes and the experimental results.

1.2 DOUBLE LAYER

Double-layers (DLs) are electrostatic structures able to support a potential jump in a narrow spatial region of plasmas. DLs have been studied intensively interpreting and reproducing magnetospheric, solar and extragalactic plasma phenomena [1,2]. The motions of charged particles determine the internal structure of a DL and, by the net charge distribution, its electric field. In the most general DL structure both free and reflected electrons and ions are required (Fig 1.1).

ESA CONTRACT no.	SUBJECT	CONTRACTOR
Ariadna 05/3201	Numerical Simulations of the Helicon Double Layer Thruster Concept – Final report	CISAS "G. Colombo"

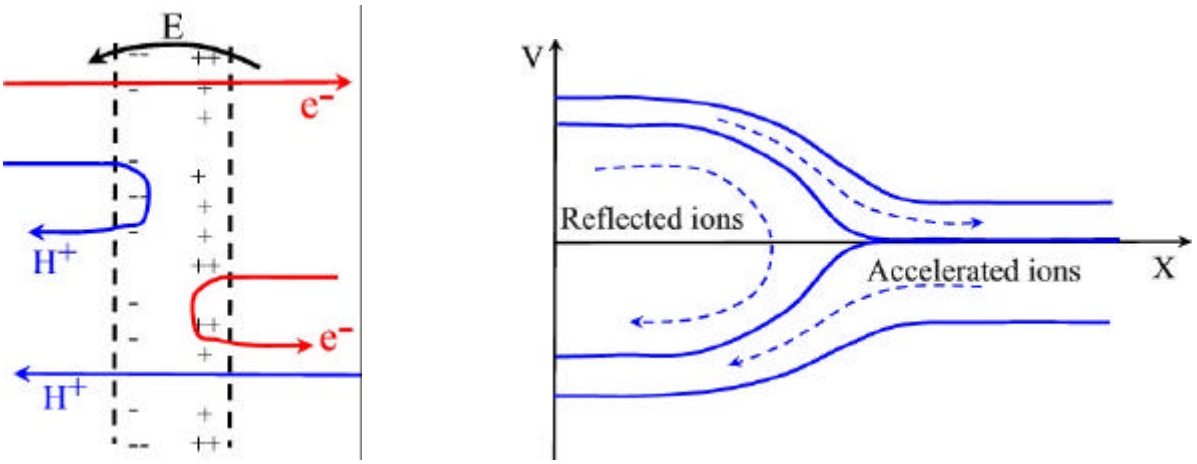

FIG 1.1: Double layer structure. Left: charge density distribution gives the electric field; incoming particles are reflected or accelerated depending on their charge, velocity and side of entry. Right: areas of phase space occupied by populations of ions.

The electric field acts as a barrier for the reflected particles while the accelerated ones emerge downstream as energetic beams. The current is carried by the free particles. Usually DLs studied by laboratory tests and theoretical models require an electron current or an external imposed electric field. Sometimes their formation is ascribed to evolution of plasma instabilities.

The most used way to determine the structure of a DL is the *Sagdeev* or *Classical Potential* method. Solution of the Vlasov equations

$$\frac{Df_{i,e}}{Dt} = \frac{\partial f_{i,e}}{\partial t} + v\frac{\partial f_{i,e}}{\partial x} + \frac{q_{i,e}\cdot E}{m_{i,e}} = 0$$

are determined by defining the ions and electrons distribution functions to be functions of the energies $w_{i,e}=½m_{i,e}v^2+q_{i,e}f$, which are integrals of the motion. The particles densities are obtained by integrating the distribution functions over velocity, so they depend only on the electric potential. Poisson's equation

$$e_0\frac{d^2 j}{dx^2} = -\left[q_i n_i(j) + q_e n_e(j)\right] \tag{1.1}$$

can be integrated once assuming $V(j) = \int^{j} V(y)\cdot dy$ (the Sagdeev potential) and giving

$$\frac{1}{2}e_0\left(\frac{dj}{dx}\right)^2 + V(j) = \Pi = \cos t \tag{1.2}$$

Formally the integral may be regarded as the energy of a fictitious particle located at position f where the time is given by x.
The matching conditions between DL and the ambient plasma require that the net charges and the electric filed at the edge of the DL tend to zero. These conditions ensure that the plasma in contact with the DL is shielded from the internal structure of the DL and hence undisturbed. In terms of the Sagdeev potential this means:

$$V'(0)=V'(j_{DL})=0 \qquad V(0)=V(j_{DL})=\Pi \tag{1.3}$$

Then from (1.2) V(f)<p everywhere inside the DL. These existence criteria require that the Sagdeev potential has two equal maximum at f=0 and f=f_{DL} and, in terms of the fictitious particle interpretation, the solution may be regarded to a particle starting at rest at one of the maxima, rolling down the potential V(f) and then upward coming to rest at the other maxima.

1.3 CURRENT FREE DOUBLE LAYER

Double Layers have generally appeared to require a relative electron-ion drift but some experiments, computer simulations and theoretical studies have shown the possibility of low amplitude potential drops with little or no plasma currents. Since they may be related to electrostatic plasma modes they are termed *ion-acoustic* double layers and *slow ion-acoustic* double layers by Raadu in his monumental work [2].
One of the first study of this sort was reported by Sato [13] more than twenty years ago, simulating double layers along the auroral field lines, where the electron drift velocity was supposed much lower then the thermal one. He studied ion-acoustic instabilities by performing one-dimensional particle simulations and considering a long system with Maxwellian electrons with low drift velocity. Then he found that, no matter how small, the starting dc potential associated with the instability, became high enough to accelerate electrons and be enhanced by a sort of bootstrap processes. Double layers were generated when the system was long enough and they became stronger as the system length became longer. This process required that the anomalous resistivity, associated with the ion-acoustic instability, persisted by the time the double layer was formed. The final current was only a tiny fraction of its original value and the resistivity was negligible. The DL potential jump was comparable to the electron thermal potential and it required a system with a fundamental length of about 10^3 times the $?_d$ (Debey Length) to form. A negative potential dip at the low potential side was seen to be associated to this type of DL which, for that, does not have a monotonic shape.

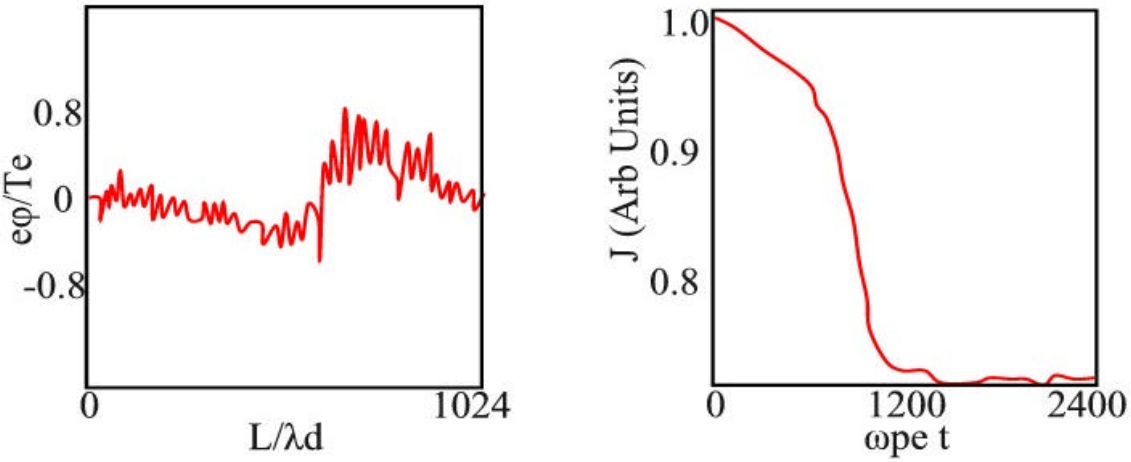

Fig 1.2: potential profile at t? $_{pe}$=960 and time evolution of the electric current of the Sato one-dimensional simulations

Successively Perkins [3] demonstrated the possibility for current-free DL, solving the Vlasov-Poisson equations. The key to obtaining these solutions was to recognize that electrostatically trapped ions can exist on the double layer's low-density, low-potential side. The density of these trapped ions, together with the magnitude of the potential drop, provided the two parameters that were sufficient to satisfy the criteria for double layer formation: quasi neutrality of the low potential side and zero total charge in the double layer (zero electric filed at the borders). The electron distribution function was Maxwellian everywhere and it was shown that without trapped ions it would be impossible to satisfy the double layer conditions. These type of DLs have a monotonic potential function, without the negative potential dip reported by Sato, and they have been defined elsewhere as *slow ion-acoustic* or *currentless.*

A similar analytic evidence of small amplitude monotonic double layers was then expressed by Kim [14]. A two temperature Maxwell-Boltzmann electron distribution function was assumed, while the ions function was drawn with trapped particles distribution shaped as a hole: have a minimum for zero velocity. Then, again imposing charge neutrality and zero electric field at the borders (equations 1.3), the author obtained the electric potential. The solution did not require a discontinue trapped-particle distribution and could exist with an ion drift velocity lower than the electron thermal velocity, so compatible with the simulations of Sato.

Chan, few years later, made experiments in his triple-plasma device were ion-acoustic [5] and slow ion-acoustic [4] DLs, similar to the Perkins solutions, were found. If we exclude some controversial observations in the auroral plasma [10] this is probably the first time that such DLs were measured. The device consisted of two source plasmas bounding a target plasma, where potential and density could be varied separately. Five grids were used to separate the target plasma from the sources and pulsing one of them an electron drift was produced, exciting an ion-acoustic wave. The double layer was found to evolve from a virtual cathode potential well at the electron injection boundary, born to limit the injection of unneutralized electrons into a collisionless plasma. The potential well evolved in a stable

DL of length 50/60 l_d after about 500μs. The current-limiting nature of these double layer, the measured properties of ef/T_e~1, the propagating velocity near the ion thermal velocity and the small drift velocity associated them with the *currentfree*, *currentless* or *slow ion-acoustic* DL type previously reported.

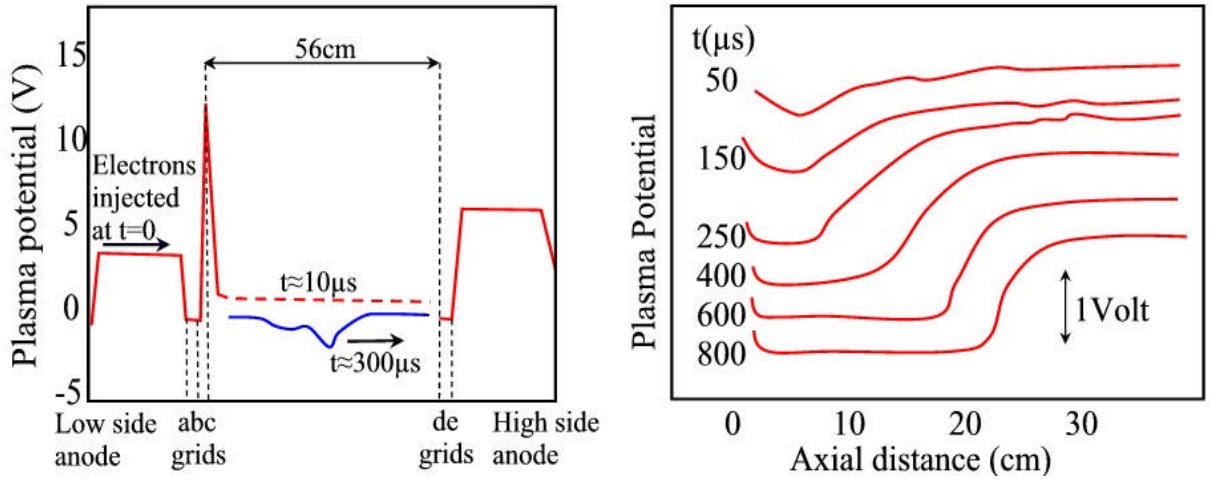

Fig 1.3: Left: axial potential profile along the device. Grid b was switched from -30V to ground at t=0. Rigth: temporal evolution of the target-plasma potential of the Chan triple-plasma experiment.

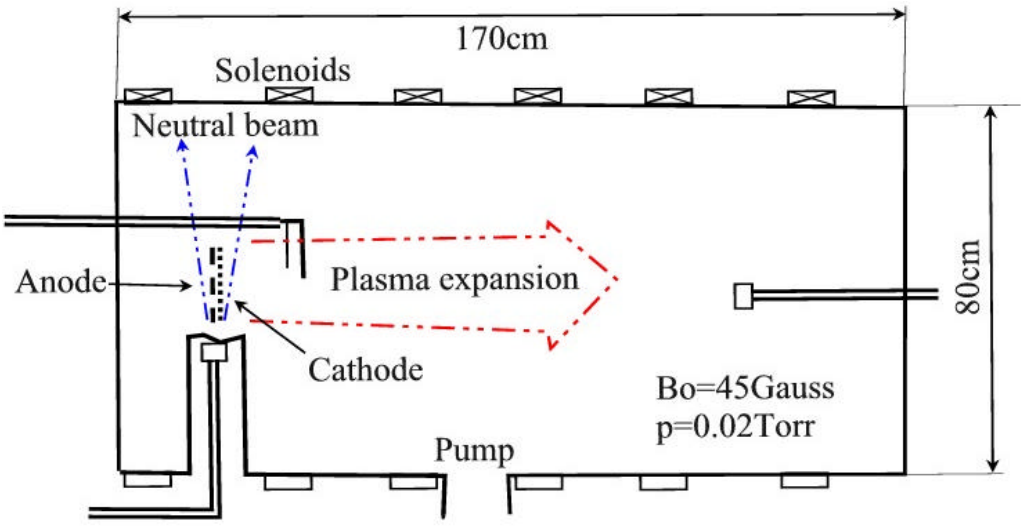

Fig 1.4: Hairapetian experiment: filamentary cathode and plasma expansion under a weak axial magnetic field

ESA CONTRACT no.	SUBJECT	CONTRACTOR
Ariadna 05/3201	Numerical Simulations of the Helicon Double Layer Thruster Concept – Final report	CISAS "G. Colombo"

More recently a *currentfree* DL was found by Hairapetian [19]. The plasma, made by a filamentary cathode, expanded under a weak axial magnetic field producing a current-free DL. In this case after its production the DL propagated along the magnetic field, it slowed down in 1-2 hundreds μs and then it evolved in a steady-state current-free DL.
The physical interpretation was that few energetic electrons, directly produced by the plasma source (Fig 1.4), realized a space charge potential that trapped the colder ones. In fact the source produced a non-Maxwellian electron distribution, composed of a Maxwellian plus an energetic tail. The expansion front propagated along the vacuum chamber at a velocity near the ion sound speed, until it reached the stable configuration. The importance of the high-speed electrons on the DL formation was proved deflecting their trajectories with a permanent magnet and changing the end-plate potential allowing the collection of more electron current: the DL became weak or didn't form. The steady-state DL position and amplitude changed with the ratio of the two electrons families' densities: highest tail density increased the potential jump and moved it upstream.
Two distinct electron temperature were measured upstream and downstream the double layer and a supersonic ion beam was measured on the low-potential side, which disappeared increasing the chamber pressure.

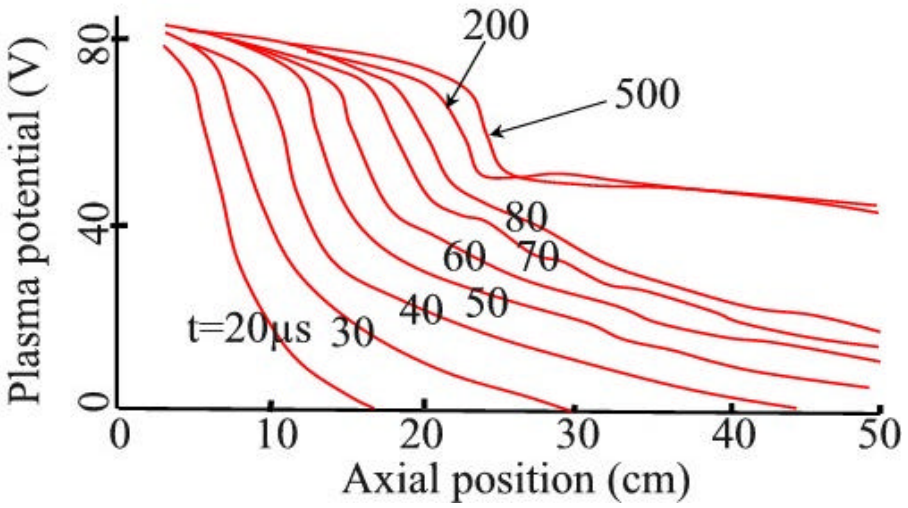

Fig 1.5: Hairapetian experiment: measured temporal evolution of the axial plasma potential profile.

ESA CONTRACT no.	SUBJECT	CONTRACTOR
Ariadna 05/3201	Numerical Simulations of the Helicon Double Layer Thruster Concept – Final report	CISAS "G. Colombo"

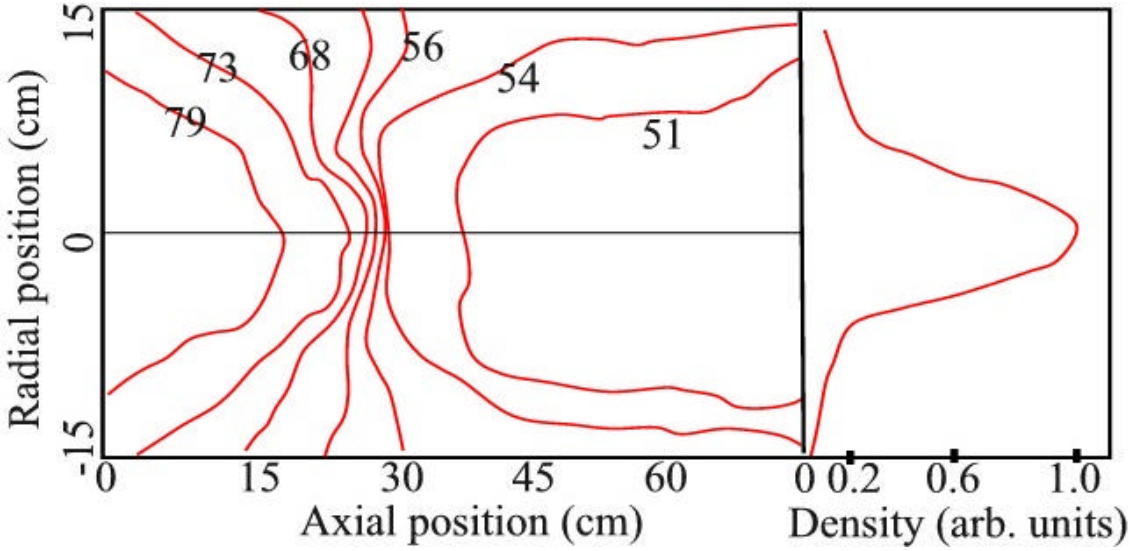

Fig 1.6: Hairapetian experiment: contour of constant plasma potential showing the steady state double layer.

1.4 HELICON DOUBLE LAYER

As partially anticipated by Hairapetian, the plasma expansion in a weak magnetic field can form a stable current-free DL. Charles and Boswell have first shown the existence of a similar phenomenon for helicon discharges along a diverging magnetic field [6-9]. Their experiment then has been reproduced by Sun [21,22] and Cohen [20] with some differences. Successively the helicon double layer has been reported by Plihon [28] in a similar reactor but using an electronegative mixture and without magnetic field.

In a recent paper Fruchtman [25] has analyzed the "double layer" electric and magnetic fields configuration. It is shown that the net momentum delivered by the large electric field inside a one-dimensional double layer is zero. Considering a double layer in a current-free plasma expanding along a divergent magnetic field, an analysis of the evolution of the radially averaged variables shown that the increase of plasma thrust results from the magnetic-field pressure balancing the plasma pressure in the direction of acceleration, rather than from electrostatic pressure.

ESA CONTRACT no.	SUBJECT	CONTRACTOR
Ariadna 05/3201	Numerical Simulations of the Helicon Double Layer Thruster Concept – Final report	CISAS "G. Colombo"

1.4.1 Charles-Boswell experiment

The Charles-Boswell experiment consisted of a horizontal helicon system composed of a 15 cm diameter helicon source (31 cm long cylindrical glass tube terminated with a 0.5 cm thick glass plate and surrounded by an 18 cm long double-saddle antenna) is attached contiguously to a 30 cm long 16 cm radius earthed aluminum diffusion chamber. The antenna operated at 13.56MHz providing a plasma column, which expands in the vacuum diffusion chamber along an axial diverging magnetic field (Fig 1.7). The gas could be introduced on the side of the chamber or at the closed end of the source.
Deeply changes in the plasma potential have been reported just inside the source, accompanied by a dip in its density (Fig 1.8). The potential drop is around 25V. The typical experiment conditions were: chamber pressure 0.3mTorr, axial magnetic field in the source center 150 Gauss, radio-Frequency power between 250 and 800W, gas Argon or Hydrogen.

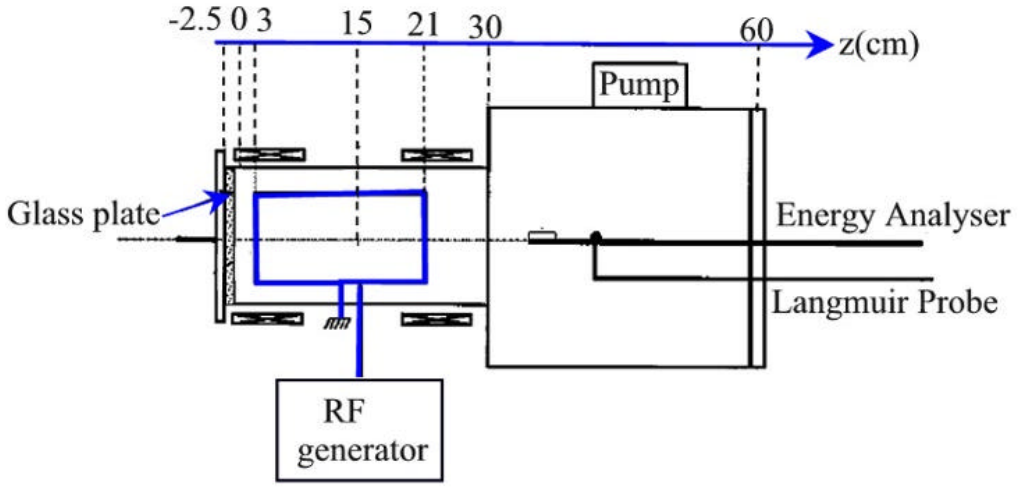

Fig 1.7.1: The Charles-Boswell (up) and Sun (down) helicon discharge experiments

ESA CONTRACT no.	SUBJECT	CONTRACTOR
Ariadna 05/3201	Numerical Simulations of the Helicon Double Layer Thruster Concept – Final report	CISAS "G. Colombo"

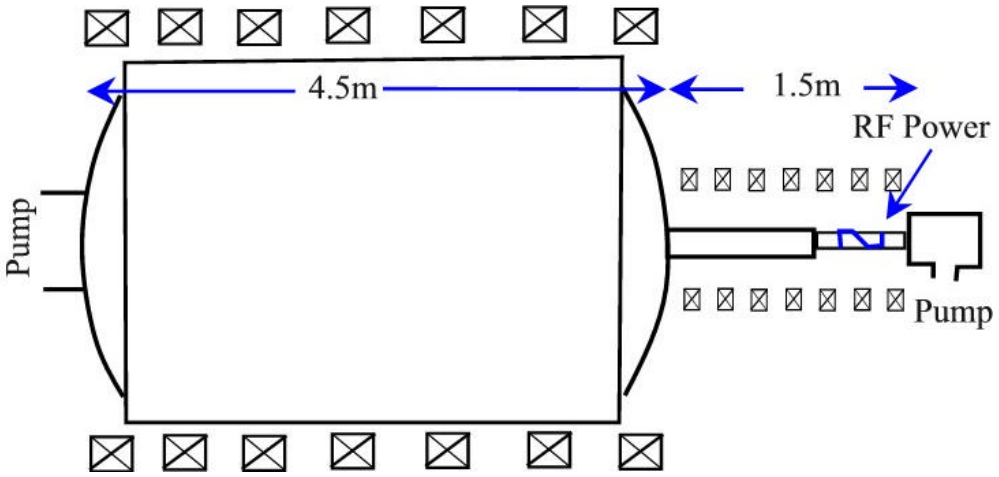

Fig 1.7.2: The Charles-Boswell (up) and Sun (down) helicon discharge experiments

In some ways the plasma expansion, associated with an axial diverging magnetic field and low chamber pressures, evolved to a stable current-free DL.
Comparing the floating plasma potential of two pulsed discharges, with and without DL, its formation was found during plasma break-down, during the first 100μs (when high energy electrons are present). For a stable DL pressure had to be below 1mTorr, while the magnetic field along the source had to be higher than 125 Gauss.
Axial ion energy distribution function (IEDF) measurements have been done just downstream the source-chamber connection (z=37cm); they showed a function with two peaks (29 and 47V, Fig 1.9), the second representing a supersonic ion beam at

$$v_{beam} = \sqrt{\frac{2e\left(V_{beam} - V_p\right)}{m_i}} = \sqrt{\frac{2e\cdot(47-29)}{m_i}} \approx \sqrt{\frac{4.5\cdot kT_e}{m_i}} \cong 2.1\cdot c_s \qquad (1.4)$$

where $c_s=v(kT_e/m_i)$ is the ion-sound speed and considering T_e, downstream the double layer, around 8eV (9eV for hydrogen discharge).
The second peak cannot be seen during the "non DL" experiment: higher chamber pressure 1.3mTorr, lower magnetic field 100Gauss (Fig 1.9). The axial ion energy distribution function measurements (IEDF) were interpreted as the collection of two families of ions: one with density n_s and velocity c_s, the second, n_{beam} and v_{beam}, was accelerated by the DL. Comparing the two data the beam density has been evaluated as: $n_{beam}/n_s \tilde{} 0.15$ for Ar and 0.17 for H, but higher beam densities were successively reported reducing the source length. In that case a movable glass plate was inserted in the source at z=2cm so at the maximum of the magnetic field at the source's closed end (Fig 1.10) [31]. The potential drop remained approximately constant while the ratio between the beam density and the downstream density was increased from 0.15 to 0.5.
For pressures below 2mTorr high potentials have been measured in the middle of the helicon source

ESA CONTRACT no.	SUBJECT	CONTRACTOR
Ariadna 05/3201	Numerical Simulations of the Helicon Double Layer Thruster Concept – Final report	CISAS "G. Colombo"

(Fig 1.10), while an energetic ion beam is detected in the diffusion chamber, an indirect evidence of the double layer.
The experiment has been reproduced reducing the magnetic filed near the closed end of the source [31]. As can be seen in Fig 1.11 low values of the first solenoid currents, corresponding to lowest magnetic fields, did not show the double peak distributions typical of the double layer.

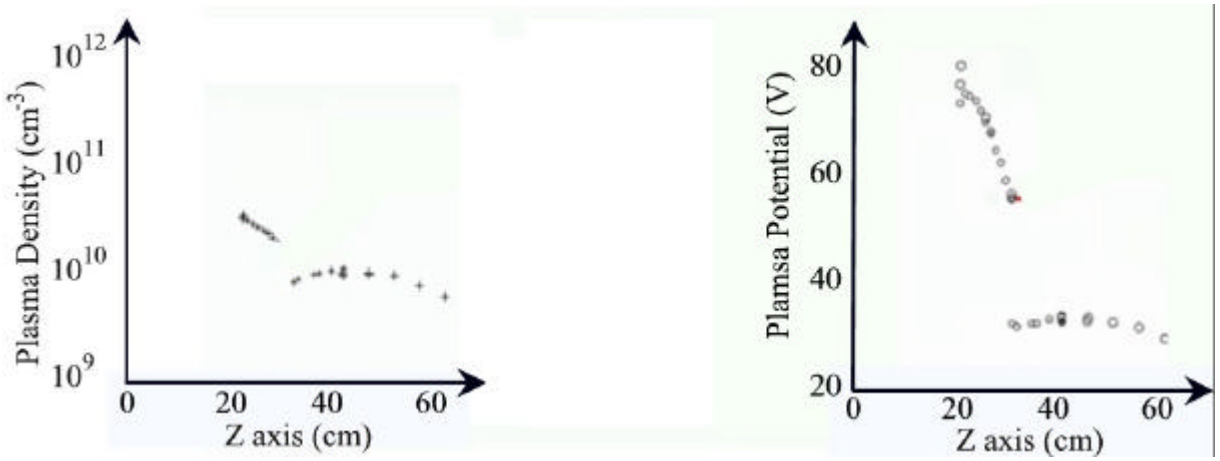

Fig 1.8: Plasma potential and density of the Charles-Boswell experiment

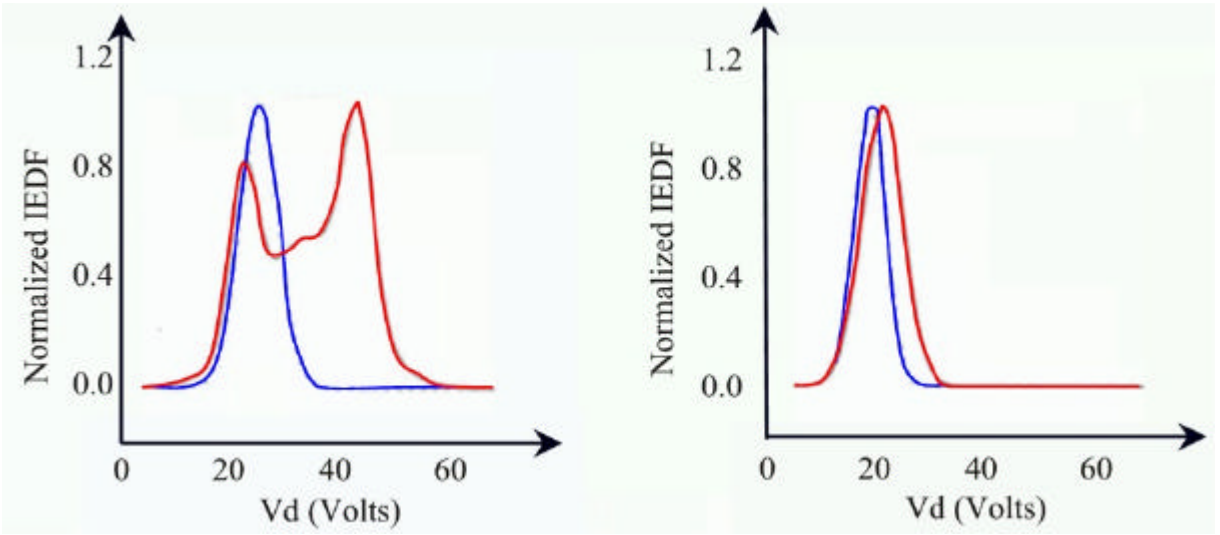

Fig 1.9: IEDF with (red) and without (blue) DL. Radial (right) and axial (left) at z = 37cm

The ion beam was detected near the source radius (r<6.8cm) and its divergence very low. In other words, no ion acceleration was seen near the chamber wall. The ion beam appears as a plasma column. It also means that the diverging magnet field does not have big effects on the ion beam and DL

ESA CONTRACT no.	SUBJECT	CONTRACTOR
Ariadna 05/3201	Numerical Simulations of the Helicon Double Layer Thruster Concept – Final report	CISAS "G. Colombo"

acceleration process. Figure 1.12 shows the ions' energy functions and density ratio calculated across the chamber radius at z=37cm, far downstream the double layer. Similar results were described by Sun: ion flow velocity did not change varying the chamber magnetic field strength and source frequency.

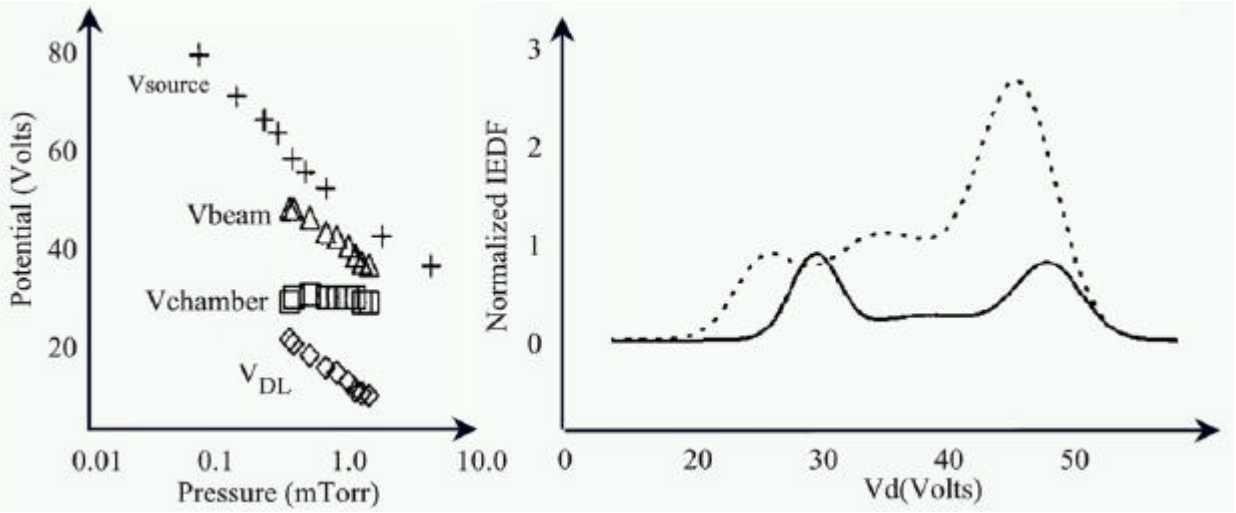

Fig 1.10: Left: plasma potential in the source, ion beam energy, chamber and double-layer potential drop as function of gas pressure. Right: ion energy distribution functions with (dotted) and without (solid) the addition of a second glass plate at z=2cm

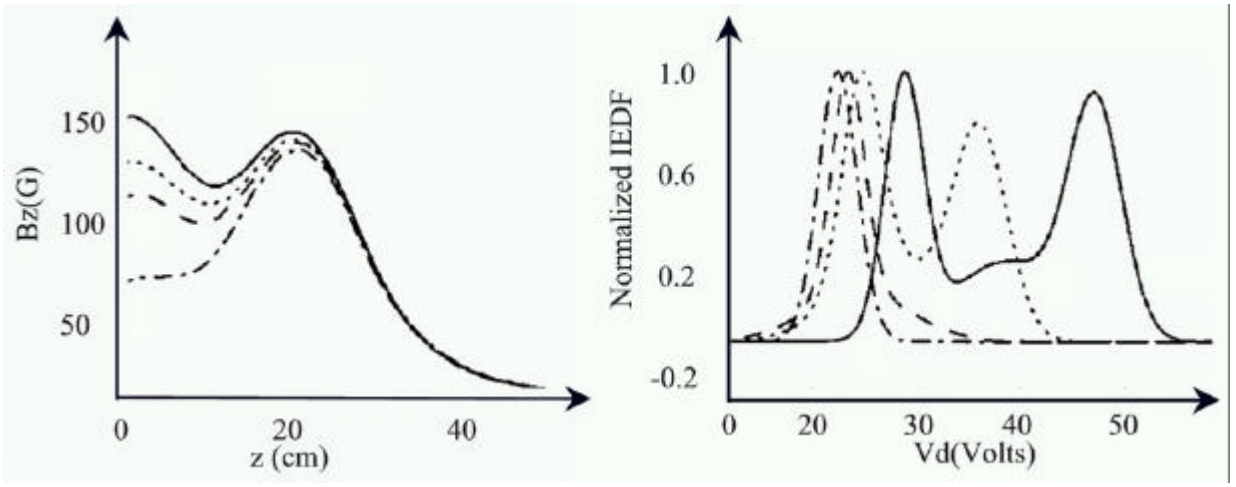

Fig 1.11: Left: axial components of the static magnetic field measured along axis for different solenoid currents near the closed end of the source. Right: ion energy distribution functions for those magnetic field configurations.

ESA CONTRACT no.	SUBJECT	CONTRACTOR
Ariadna 05/3201	Numerical Simulations of the Helicon Double Layer Thruster Concept – Final report	CISAS "G. Colombo"

It is important to stress that Langmuir probe data near the closed end of the source (z=3cm) were compatible with the presence of an electrons beam. The data have also been considered consistent with some charging of the source walls.
It has to be noted also that the DL was located close to the source-chamber diameter change, so near the highest value of the magnetic field, and its thickness was less than 1 cm (about 50 l_d).

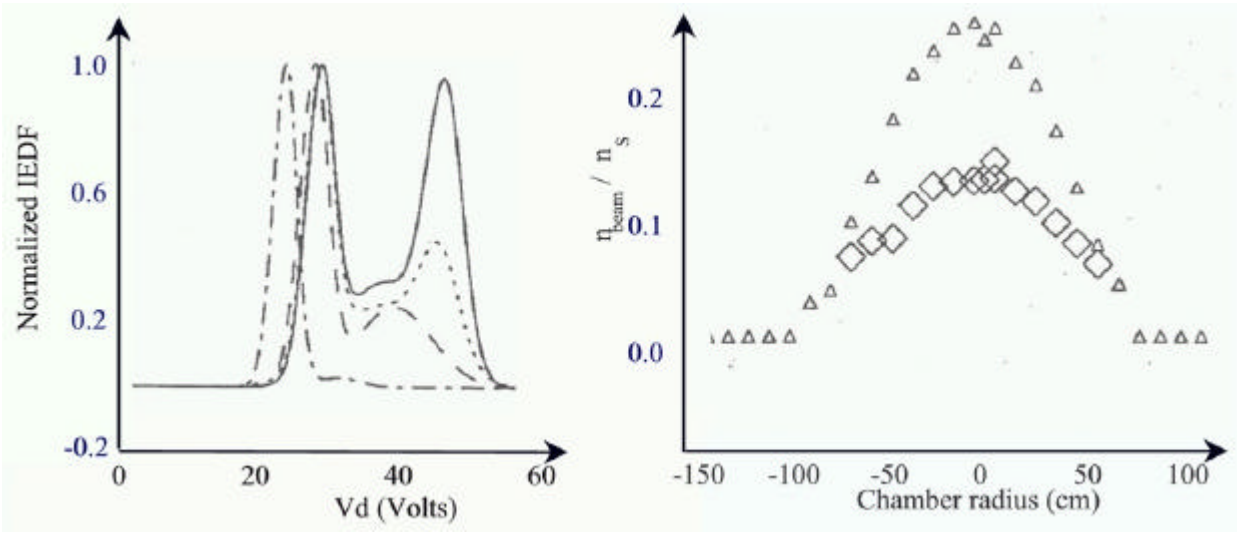

Fig 1.12: Left: IEDF obtained at z=37cm and for different radius: 0 (solid), 5.5 (dotted), 7.5 (dashed) and 13.5 (dotted-dashed). No energetic beams were collected for radius greater than the source radius (6.8cm). Right: Beam-plasma density ratio calculated with IEDF measurements across the chamber radius for z=37cm.

Boswell, at the end of his papers, suggested some important hypotheses:

1) The condition for DL existence came from the electrons dynamic
2) The DL formation should happen during the first 100μs of the discharge, when high- energy electrons are important
3) The source walls should be allowed to charge.

1.4.2 Plihon experiment

Similar results have been obtained by the Ecole Polytechnique de Paris and reported by Plihon [23,24] (Fig 1.13 and Fig 1.14). Early work by this group has shown that DLs can form without a magnetic field when traces of electronegative plasmas (SF_6) are mixed in with electropositive ones (Ar). As

previously reported [30] for radio-frequency sources, helicon electronegative discharges are subject to transport instability, occurring downstream when a sufficiently long expanding chamber is present. The instability has been interpreted as a DL formation and propagation at a velocity around 150 m/s (near ion thermal velocity). The double-layer formation frequency and the propagation speed are such that the first double layer had not reached the bottom of the diffusion chamber when a new double layer formed upstream (Fig 1.15).
The DL formation requires a certain fraction of negative ions. For negative ions concentrations between 8 and 13% the DL was stationary, at the source-chamber interface. The stable DL separated high-density low-electronegative plasma upstream from a low-density high-electronegative downstream and the minimum required power increased increasing neutral pressure. Electrons were near the Boltzmann equilibrium both upstream and downstream.
It is important to remember that the DL formed also when no chamber-source diameter discontinuities were present.
Fig 1.13 shows some experimental results. The electronegative mixture produces a strong reduction of electron density that, in some way, could reproduce the diverging magnetic field plasma conditions of the Charles experiment.

The same authors have also reproduced the Charles approach [28] reporting some important considerations (see figure 1.16):

- minimum magnetic field required for the DL formation is around 45G
- DL amplitude is independent of the magnetic field, as plasma and beam potentials, but may vary with the field gradient
- pressure has to be below 3 and above 0.1mTorr
- DL amplitude and beam flux increase decreasing pressure
- DL amplitude remains almost constant increasing antenna power while plasma and beam potential decrease
- beam density slightly increases with power, but not at the same rate of plasma density

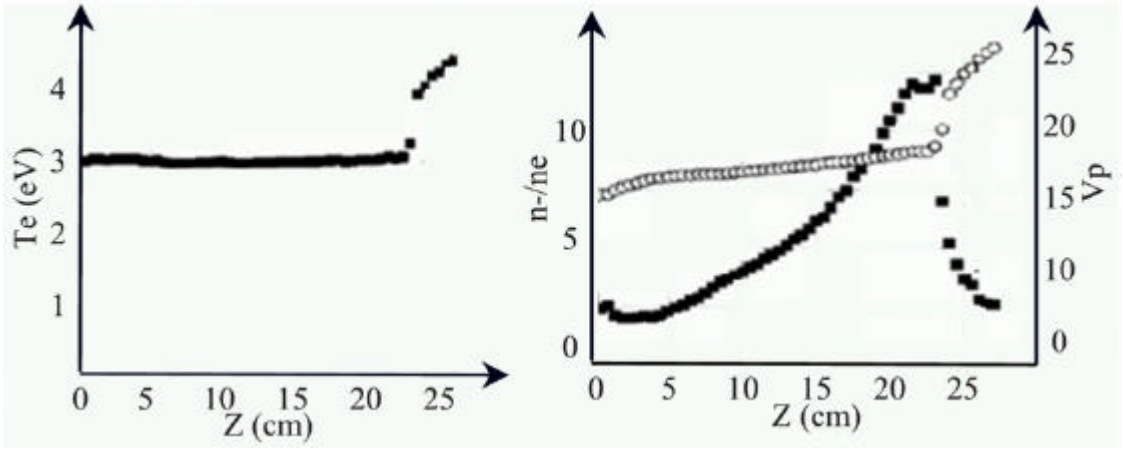

ESA CONTRACT no.	SUBJECT	CONTRACTOR
Ariadna 05/3201	Numerical Simulations of the Helicon Double Layer Thruster Concept – Final report	CISAS "G. Colombo"

Fig 1.13.1: Plihon experiment: electronegativity and potential; electron temperatures

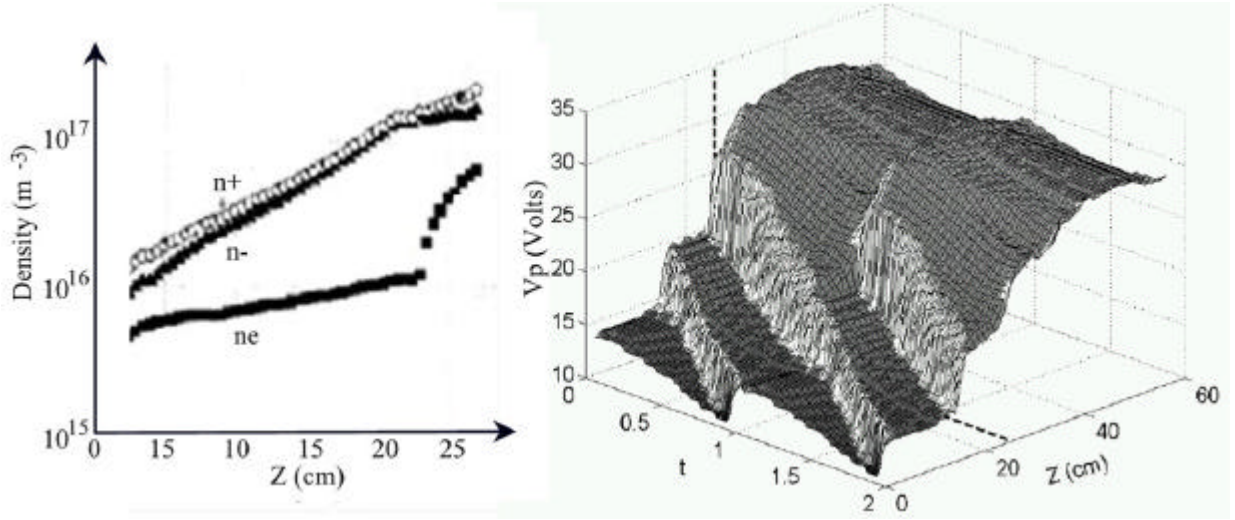

Fig 1.13.2: Plihon experiment: particles densities and mapping of the plasma potential, showing the propagation of the unstable double layer

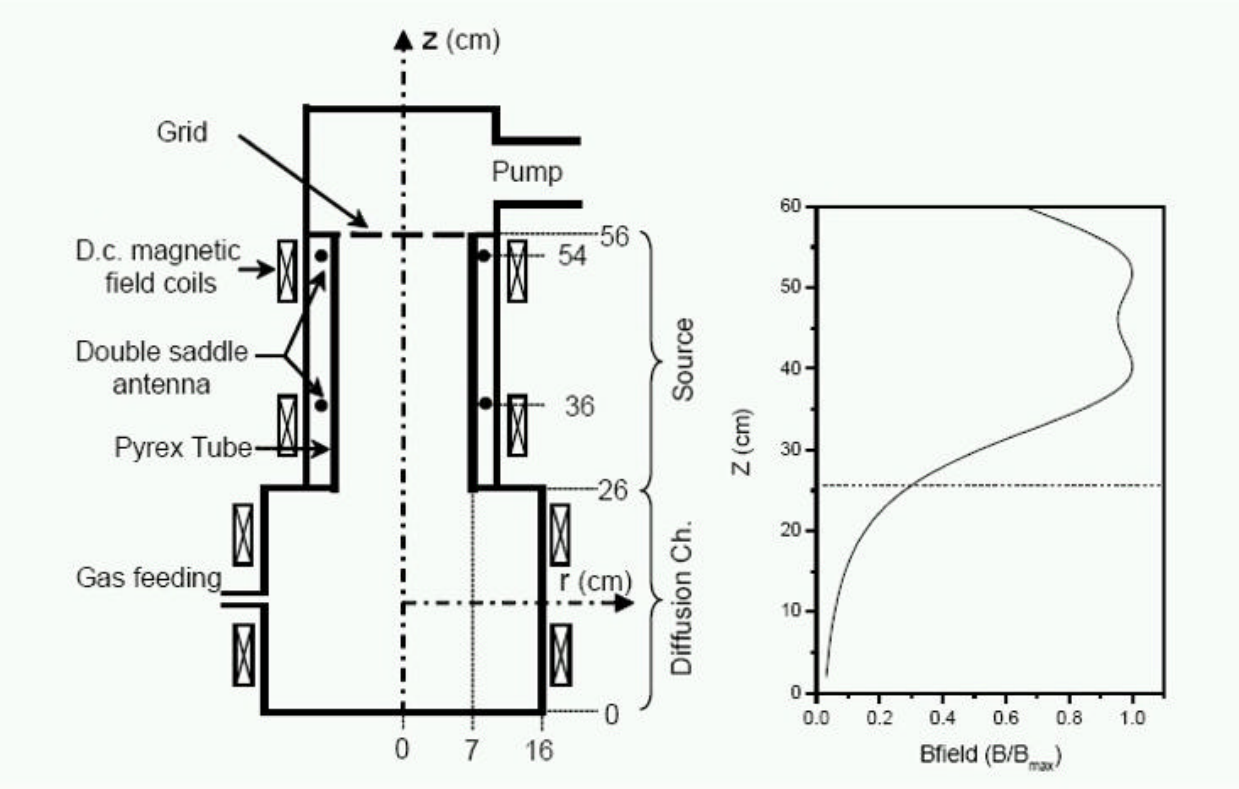

ESA CONTRACT no.	SUBJECT	CONTRACTOR
Ariadna 05/3201	Numerical Simulations of the Helicon Double Layer Thruster Concept – Final report	CISAS "G. Colombo"

Fig 1.14: Left: the experiment of LPTP - Ecole Polytechnique in Palaiseau. Left: axial static magnetic field configuration.

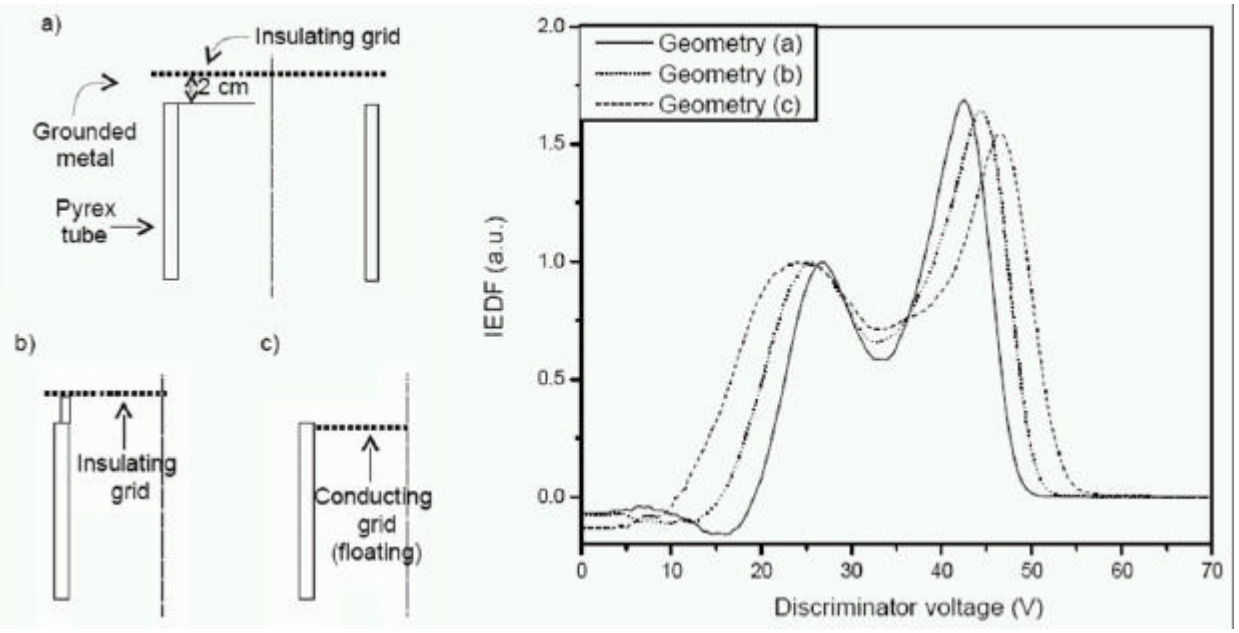

Fig 1.15: Left: the three end wall geometries of the source tested by Plihon had an insulating grid with (b) and without (a) a connection made by a pyrex tube and a conducting floating grid (c). Right: IEDFs for operating conditions 0.17 mT, 250 W and a magnetic field of 90G

It appeared that the position of the glass tube in the Charles' experiment plays an important role in the beam amplitude [31]. To evidence the effects of the source wall geometry, three configurations have been tested, showing some differences on the beam potential (Fig 1.15). The peaks amplitudes decreased by a few percent from geometry (a) to geometry (c), the local plasma potential decreased (26.5, 25.5 and 24.5 V), while the beam potential increased (42.5, 44.2, 46.5 V) for geometry (a), (b) and (c) respectively. However the broadening of the peaks slightly grew when scanning from geometry (a) to geometry (c), with significantly differences from those published in [31].
The double layer was found for all boundary conditions, including the dc connected (condition a) case, but its amplitude changed noticeably with the boundary conditions: the higher DL amplitude was obtained for the floating conducting grid (16 V case a, against 22 V for condition c). It has to be noted that the system was operating with the pump at the closed end of the source tube, so with a different geometry respect the Charles' experiments.

ESA CONTRACT no.	SUBJECT	CONTRACTOR
Ariadna 05/3201	Numerical Simulations of the Helicon Double Layer Thruster Concept – Final report	CISAS "G. Colombo"

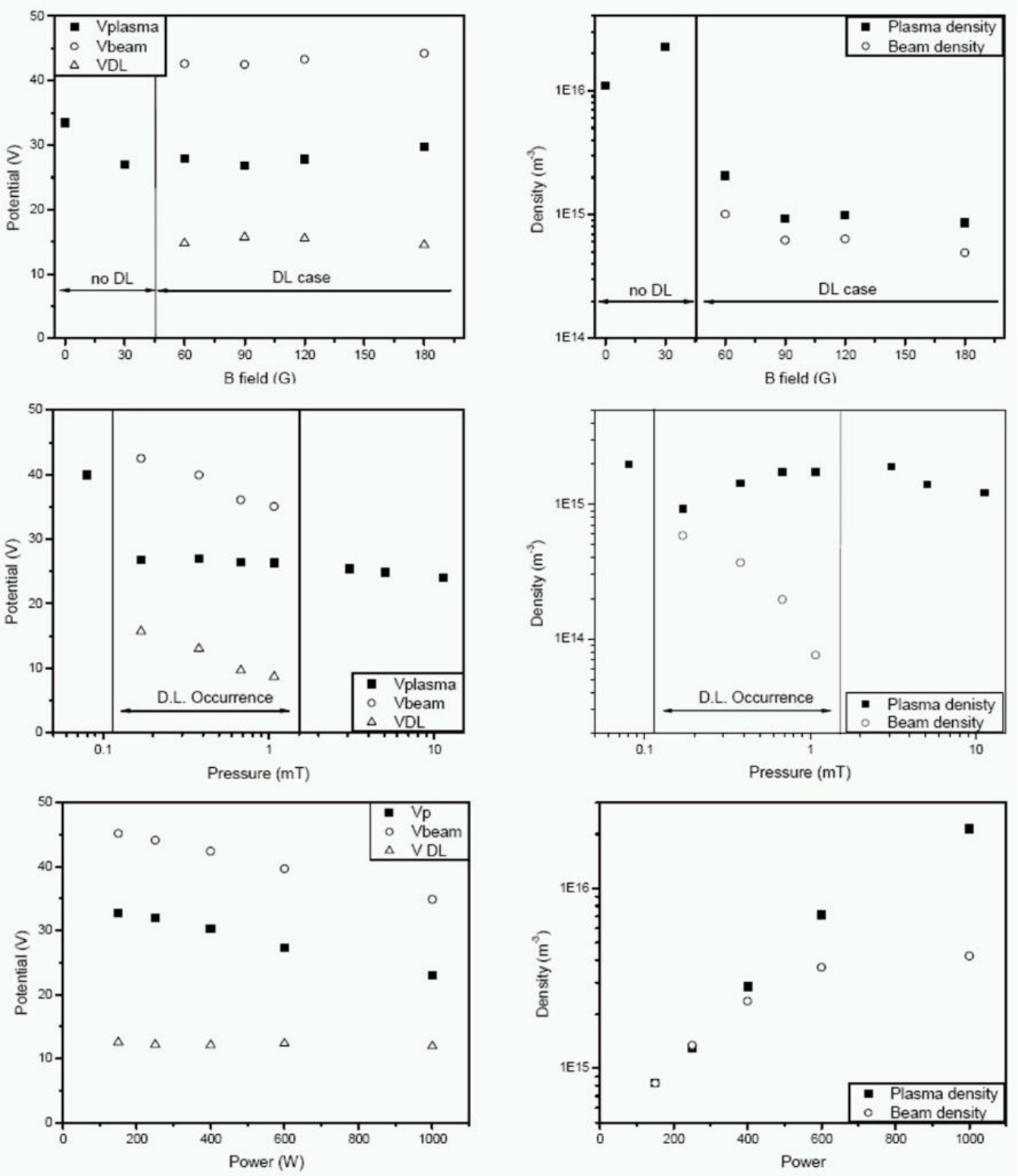

Fig 1.16: Main results of the Plihon [28] reproduction of the Charles' experiment.

ESA CONTRACT no.	SUBJECT	CONTRACTOR
Ariadna 05/3201	Numerical Simulations of the Helicon Double Layer Thruster Concept – Final report	CISAS "G. Colombo"

1.5 CHEN STUDIES

A different theoretical explanation of the phenomenon first reported by Charles has been proposed by Chen [18]. He wrote that the so called double layers are in fact the result of a sheath instability connected with the Bohm criterion. Diverging magnetic field lines cause presheath acceleration of ions, causing a potential jump resembling that of a double layer. To demonstrate his hypothesis he has considered the classical sheath theory, normally applied to boundaries, with only one assumption, that of Maxwellian electrons:

$$n_e = n_0 \cdot e^{-h} \qquad h = \frac{-eV}{kT_e} \tag{1.5}$$

When ?=1/2 the Bohm criterion is satisfied: the ions, assumed cold, will have fallen through a potential of ½kT_e/e and thus achieved a speed of $(KT_e/M)^{1/2}$= cs. The ions cannot be accelerated much further since, in the absence of a biased electrode, there is no energy source to drive them.
The ions will have a density that falls more slowly than that of the electrons as ? increases further, and the quasi-neutral solution becomes unstable. A further increase in z causes n to drop and ? to increase. With ni > ne, V''(z) drops rapidly, and an ion sheath must form, even in "mid-air". This occurs at a position where $n/n_0=e^{-1/2}$. Thus, considering a plasma frozen to the field lines, where the field B(z) and the density n(z) in the expansion region are related to the plasma radius r by $B/B_0=n/n_0=(r_0/r)^2$, it happens when the plasma radius has expanded by 28%.
Normally in sheath theory, the ion energy of ½*KT*e is gained in a presheath field, whose extent is governed by collisions and ionization and is therefore specific to each plasma discharge. The author supposed that in the Charles experiments the plasma expansion has taken the place of the presheath in accelerating ions to the Bohm velocity, even in collisionless plasma conditions. As ni and ne separate, quasi-neutrality is broken, the sheath builds up until it reaches the floating potential which imposes the forward fluxes of ions and electrons to be equal; at this point a current-free single layer is formed.

ESA CONTRACT no.	SUBJECT	CONTRACTOR
Ariadna 05/3201	Numerical Simulations of the Helicon Double Layer Thruster Concept – Final report	CISAS "G. Colombo"

2 SIMULATIONS OF THE HELICON DOUBLE LAYER

2.1 INTRODUCTION

Computer simulations are used for verification, interpretation and extension of the experimental data. In the "Double Layer" thrusters the simulations have also the intention of enhance the physical knowledge of the phenomenon. The thrust efficiency can be evaluated calculating the particles trajectories of the exhaust beam. The ions have to detach from the magnetic field lines to allow a high force production. In this section a bibliographic review of the current simulations is proposed.

2.2 MEIGE SIMULATIONS

1D-PIC simulations have been made by Meige and Boswell [16] as shown in Fig 2.1. Two separated parts took care of plasma heating and expansion. The left wall is allowed to charge while the right one is grounded, in order to reproduce the experimental setup and impose the current absence.
The heating process, in the first half of the model, did not solve the field equations: an oscillating electric field of 10MHz was applied, orthogonal to the PIC axis and evaluated by finite difference method. This simplified approach reduced the computational time. If J_0 is the current density amplitude (around 100A/m^2), $v_{e,y,i}$ the orthogonal velocity of the ith electron inside the source, L the source length and N_s the weight of a macroparticle per square meter:

$$J_{tot} = J_0 \cdot \sin(w_0 \cdot t) = e_0 \frac{\partial E_y}{\partial t} + e\Gamma_{e,y} \qquad \Gamma_{e,y} = n_e \overline{v_{e,y}} = \frac{N_s}{L} \sum_{i \in source} v_{e,y,i} \tag{2.1}$$

$$\frac{\partial E_y}{\partial t} = \frac{1}{e_0}\left[J_0 \sin(w_0 t) - \frac{eN_s}{L} \sum_{i \in source} v_{e,y,i} \right] \tag{2.2}$$

After demonstrating that this heating process did not produce any particular effect on the plasma potential at low pressure (even if different source positions and dimensions were considered) they

started to study the plasma expansion. This was modeled with a routine that removed particles with a given loss frequency function. Different loss frequency functions have been used, those are null in the source and have a maximum at the beginning of the expansion or few centimeters after it. The DL formation has been reported for particular expansion functions (the loss frequency must be above a threshold which depends on the ionization frequency) and the potential jumps were similar to the experimental values.
Most of the electrons were Maxwellian (both upstream and downstream) and in Boltzmann equilibrium ($n=n_0 \exp[ef/kT_e]$) also within the DL. Two population coexisted: colder downstream (3.9eV) and warmer upstream (5.2eV) (for the Tab1 case). No electron beams were reported upstream the DL. The ion beam is accelerated downstream to twice the sound speed.

The study of the DL formation has shown that:

- The simplified heating model does not affect the potential jumps for low pressures
- Both the profile and amplitude of the loss function are critical for the DL formation
- The DL is current-free if the source wall is floating in potential
- DL position and potential jump are not affected by the right grounded wall position
- The potential drop reduces increasing the gas pressure

A paper about two dimensional simulations of electronegative plasmas has been recently presented by the same authors [17].The computer code assumed Boltzmann electrons while both, positive and negative ions were treated as particles. The simulated space has been divided into two regions, the source and the diffusion chamber. The effects of the ionization, attachment and recombination profiles

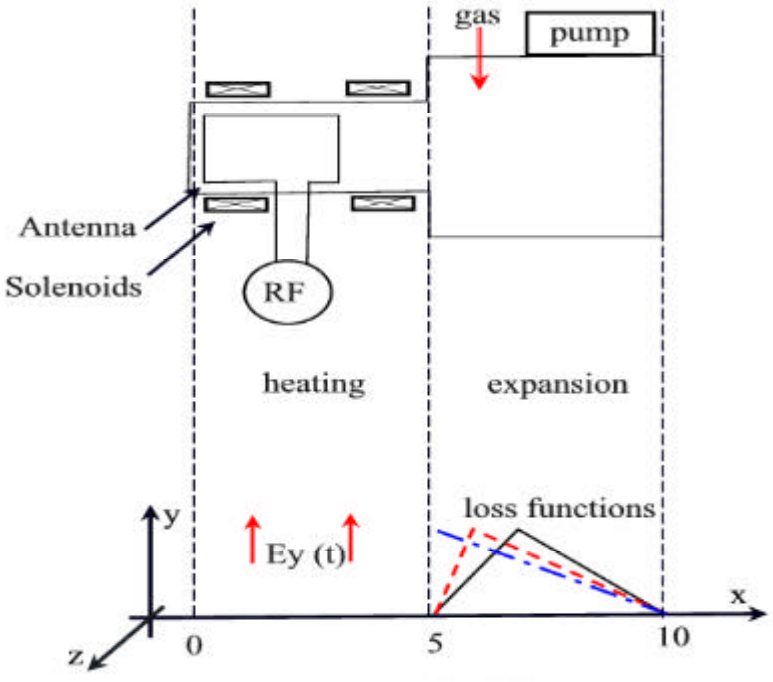

Standard parameters of the simulations

QUANTITY	VALUE
Neutral Pressure	1 mTorr
Electron density	$6\ 10^{14}$ m^{-3}
rf frequency	10 MHz
Current density	$100 A/m^2$
Length	10 cm
Cell number	250
Total duration	25 μs
Time step	$5\ 10^{-11}$ s
Macroparticle weight	$4\ 10^{9}$ m^{-2}
Ion mass (Ar)	$6.68\ 10^{-26}$
Room temperature	297 K
Capacitance	22 nF

Fig 2.1: Left: 1D-PIC model description. Right: its standard parameters

are studied with respect to the formation of the double-layer. Electric double-layers (DLs) are formed in the expanding region of the electronegative plasma. Different regimes have been found: from a non double-layer state to a stable double-layer state, via an unstable double-layer state depending on the different coefficients that have been used to reproduce ionization, attachment and recombination in the source and expansion regions. The results agree with the Plihon measurements.

2.3 IONS DETACHMENT

The expanding magnetic field, produced by the solenoids, creates a "magnetic nozzle" which influences the shape of the ion beam as it expands into space, giving the beam divergence and thereby affecting the net thrust. In the extreme case no thrust will be provided, where the magnetic-field intensity is high enough and the charged particles exiting the nozzle will be attached to the closed magnetic-field lines returning to the flight vehicle. A charged particle is unmagnetized if its trajectory has zero curvature. At that point the ion is totally detached and it provides thrust pushing not only against the vacuum magnetic field but also against the double-layer electric field, as it flows out of the nozzle volume. The net thrust generated over time depends upon these reaction forces.
Simulations of the ions detachment from the helicon double layer has been made by Gesto and Blackwell [15]. The authors reproduced ions trajectories imposing an analytic diverging magnetic field and a stable orthogonal potential difference near the magnetic field maximum. The simulations have been guided by the experiments, where the low divergence of the ion beam downstream of the electric double layer suggests that the ion beam is well neutralized and that a transport mechanism exists that allows the electrons to follow the ions. It was not believed that the electron motion can change the trajectories of the ions substantially so the authors have investigated only them, remembering also that the momentum carried by the ion beam provides the main source of thrust and is directly measurable in the laboratory experiment. In reality, the faster transport of electrons along the magnetic field lines, because of their smaller mass, will set up an ambipolar electric field that will allow the high-energy tail of the electron distribution to drift toward the ions. In fact the neutralization of the ion beams by electrons cannot be simply explained by linear fluid or particle dynamics and it is still an active area of research.
For the purpose of the study the arbitrary detachment point for an orbit on the beam cross section has been defined as the point on the orbit of maximum curvature. Past this point, the centrifugal force provided by the magnetic field begins its asymptotic approach to zero. The results shown that the ion beam detaches from the magnetic field and that the simulated flow has a small angle of divergence,

ESA CONTRACT no.	SUBJECT	CONTRACTOR
Ariadna 05/3201	Numerical Simulations of the Helicon Double Layer Thruster Concept – Final report	CISAS "G. Colombo"

which increases radially in the direction of magnetic-field curvature. The geometry of the simulated beam in the detachment region was in substantial agreement with laboratory measurements.

ESA CONTRACT no.	SUBJECT	CONTRACTOR
Ariadna 05/3201	Numerical Simulations of the Helicon Double Layer Thruster Concept – Final report	CISAS "G. Colombo"

3 OOPIC GENERAL DESCRIPTION

3.1 INTRODUCTION

The Particle-In-Cell algorithm (PIC) [10] is a popular way to solve the coupled Maxwell-Vlasov equations. The Maxwell equations are solved on a discrete grid and at discrete times. The Vlasov equation for each charged particle species is solved by aggregating a large number of physical particles into numerical macroparticles, which are advanced by solving their time-discretized equation of motion. The particles acceleration follow the Lorentz force $F=q(E + v \times B)$. The macroparticles move in contiguous space and the Lorentz force is found by interpolating the fields between discrete gridpoints. The velocity moment of the solution to the Vlasov equation provides the current closure to the Maxwell equations. Practically this is done by current weighting, basically an inverse interpolation where the current at the particle location is distributed between surrounding gridpoints of the discretized fields. The PIC algorithm structure is illustrated in Fig. 3.1.

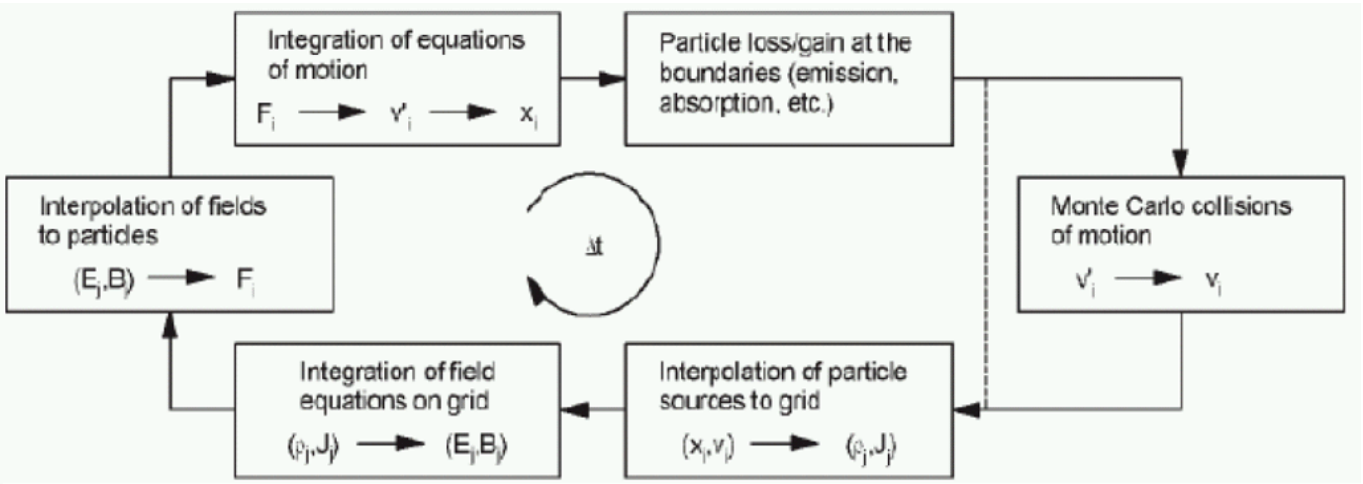

Fig 3.1. MCC PIC structures

The great advantage of PIC is that it provides a first-principles, detailed model of low-collisional plasmas, including nonlinear effects. The disadvantage of PIC is that it is computationally demanding due to strict limitations on cell size (spacing between gridpoints) and timestep. If the Debye sphere is not resolved, spurious, numerical grid heating will increase the particle temperature until the Debye sphere fills the cell. The timescale of this process is a few dozen plasma periods. Several limits are imposed on the timestep. If the standard PIC field solver, the explicit Yee solver, is used a Courant condition is imposed on the

timestep. The Courant condition demands that the fastest mode that satisfies the Maxwell equations (light waves) does not cross a cell in a single timestep. As will be discussed below, the Courant condition can impose a severe limitation on the timestep. The Courant condition can be avoided by using an implicit field solver or if the electrostatic approximation is valid.

Implicit field solvers are considerably harder to implement than the explicit Yee solver. Also, to our knowledge no implicit field solver exists that can handle as general boundary conditions (time-dependent Dirichlet, etc.) as Yee and still have the same good convergence properties (second-order accurate in both space and time).

If the electrostatic approximation is valid, Maxwell's equations can be replaced by the Poisson equation, which is independent of time and therefore is not subject to a Courant condition. Even without a Courant limit, the particle advance has it own timestep limitations. If the standard leapfrog or Boris particle advances are used, both the gyromotion and the plasma oscillation (Langmuir wave) must be temporally resolved. If the gyration is not relevant for the physics under study, it can be removed by using drift kinetic particles. Similarly, if the plasma oscillation is irrelevant, it can be suppressed by an implicit particle advance.

In some cases more drastic simplifications can be made. E.g., on electron timescales, the ions can sometimes be treated as immobile (and ambipolar effects neglected). For slow phenomena it is sometimes sufficient to use fluid electrons. However, one should be careful not to exclude relevant physics by using too simplistic approximations. For example, some physical processes such as air breakdown phenomena involve energy distributions that are partially Maxwellian but include a long, high energy tail. The particles in the high-energy tail are those responsible for the majority of interactions that lead to a qualitative change in physical behavior. Thus, a fluid description that neglects the high-energy tail fails to capture the physics of interest. A hybrid plasma description simultaneously employs the fluid and PIC treatments, which has the potential to capture the relevant physics in a tractable computational time .

Developing a consistent way to divide the simulated plasma into fluid and particle portions is one of the most complicated aspects of this approach. Several details need to be considered. Most importantly, the distinction between the fluid and particle descriptions is not a physical one, but rather a computational necessity. As such, it is crucial that dividing the plasma into two separate populations does not introduce any spurious observable behaviors in the physics. The mechanism for exchanging particles into fluid (and vice versa) must be seamless enough that it does not affect the global properties of the plasma. Besides, the fluctuations in density, pressure, and temperature in the fluid must affect the dynamics of the PIC particles in exactly the same way as if those fluctuations had occurred in a purely PIC model. In the special case where the density contained in the fluid is significantly greater than the density in the particles, it may be a good approximation to neglect these fluctuations in the PIC particles.

Another important priority in the development of a useful hybrid model is to determine the optimal way to divide the plasma. An appropriate criterion must be found for the exchange of PIC particles with fluid density.

It is important to treat as much of the plasma as possible with the fluid model, since this minimizes computation time. On the other hand, if the decision criterion is computationally expensive, it would not be sensible to perform the particle-fluid exchange in every time step. A balance must be found between the time saved by moving particles into the fluid and the time spent deciding whether the particles can be moved without sabotaging the accuracy of the simulation.

The standard PIC algorithm neglects collisions. To allow simulations of low-temperature plasmas, where collisions with neutrals play an important role, PIC has been extended with Monte-Carlo collisions The direct simulation Monte Carlo (DSMC) method models the collisions of the heavy particles (ions and atoms) while the Particle In Cell (PIC) method models the transport of the ions in electric fields.

3.2 OOPIC MAIN FEATURES

The adopted code is OOPIC (or XOOPIC, which has a GUI), both of them are opensource from Berkeley (University of California).
OOPIC (Object-Oriented Particle-In-Cell) is a 2D-3V relativistic electromagnetic PIC code. The object-oriented paradigm provides an opportunity for advanced PIC modelling, increased flexibility, extensibility and efficiency [11]. One of the principal advantages of the object-oriented method is the potential for rapid extension and enhancement of the code, adding algorithms to extend it to model a new phenomenon or adjusting an existing model.
The X11 version, XOOPIC, uses the XGrafix package and some additional diagnostics can be added without recompiling the code. The applicability of this code ranges from plasma discharges, such as glow and RF discharges, to microwave-beam devices.
Researchers around the world have used the OOPIC physics kernel since 1995 to simulate a wide range of challenging problems. These include plasma display panels, ion implantation, high-power microwave devices, advanced particle acceleration concepts, and many other systems.
OOPIC includes 2-dimensional orthogonal grid: cartesian (x,y) or cylindrically symmetric (r,z) and moving window, 2D x-y (slab) and r-z (cylindrical) models, electrostatic and electromagnetic fields, and relativistic particles. The boundaries can be determined at runtime and include many models of emitters, collectors, wave boundary conditions and equipotentials.
Because the dependence on the azimuthal angle is not expected to be relevant for DL experiments, we can use a 2D r-z cylindrical PIC simulation. The OOPIC code [11] fits this and most other of our requirements.
The code can handle an arbitrary number of species, particles, and boundaries. It also includes Monte Carlo collision (MCC) algorithms for modelling collisions of charged particles with a variety of neutral background gasses, including such effects as ion/neutral charge exchange, elastic electron scattering, inelastic scattering due to electron impact excitation, and electron impact ionization. OOPIC can also simulate field-induced tunneling ionization of selected neutral gasses and charged macro-particles. The particles follow the relativistic equations of motion in electric and magnetic fields, generating a source current for the field equations. OOPIC employs the relativistic time-centered Boris advance.
The object-oriented methodology is employed ranging from the physical device to the mathematical model, and finally to the discrete model for simulation. The mathematical model may divide the device into various regimes with different physical properties, which are best described with heterogeneous sets of equations.
XOOPIC permits to use parallel and distributed processing to optimize the simulation of large problem. It may use parallel libraries such MPI (Message Passing Interface).

ESA CONTRACT no.	SUBJECT	CONTRACTOR
Ariadna 05/3201	Numerical Simulations of the Helicon Double Layer Thruster Concept – Final report	CISAS "G. Colombo"

3.3 OOPIC DIAGNOSTIC TOOLS AND OUTPUT

OOPIC can work with its Graphical User Interface (GUI) which permits to display some default diagnostics while the user can define new output of his specific interest. OOPIC presents several types of diagnostics:

- 2D particle plots
- 2D vector plot
- 3D surface plot of scalar field component
- Time history of scalar diagnostic

Usually, to reduce the memory requested by the software, the simulation is launched without the GUI in batch mode. In this way it is also possible to write sequential output files that contain the particles and some field data of the simulation's time step when they have been created. Another important feature is the possibility to start a simulation from one of those: the calculation begins from time and particles' configuration saved on the specified file. When the user defines new diagnostics he can decide whether they have to be saved in the output files or not. Consequently the post-processing methods can be the following:

- Display pictures by using the OOPIC GUI and save them in graphical or text modes
- Read directly the output files of OOPIC with external Matlab or IDL routines
- Define new diagnostics and display them with the GUI or store and read from the output files

We have preferred the first two methods: from the GUI we have obtained the field data like the plasma potential and particle densities that are part of the default diagnostics, from the output files we have read the particles' positions and velocities that there are stored. We have used some user defined diagnostics but only occasionally also because their storage inside the output files can make the necessary disk and memory space big and therefore difficult to manage.

ESA CONTRACT no.	SUBJECT	CONTRACTOR
Ariadna 05/3201	Numerical Simulations of the Helicon Double Layer Thruster Concept – Final report	CISAS "G. Colombo"

4 DEFINITION OF THE MODEL

4.1 GEOMETRY

A detailed model of the helicon source is not our intention. It should require a radiofrequency electromagnetic solver working in parallel with the PIC model and the electromagnetic fields generated by the antenna should be defined and considered during the calculation of particle trajectories. This approach needs high computational power and specific physical assumptions.
The heating process can be avoided by imposing ad hoc electron and ions families, emerging from the helicon. This is a versatile approach because we could change the parameters, simulating plasma expansion in different conditions. The resolution of the particles motion can be done under electrostatic assumption.
Modeling the Charles-Boswell experiment we must draw a first dielectric open-ended cylinder connected to a conducting one, representing the source and diffusion chamber walls. The source and chamber radiuses are 6 and 16 cm while the length is 30 cm for both. We could implement a half thruster stressing its cylindrical symmetry (Fig 4.1). The source walls can be defined using the *Dielectric* and *DielectricRegion* objects of OOPIC. They permit to define a wall and a rectangle with particular permittivity and reflection properties. The region object is used for the upper source wall. The variable *Quseflag* can switch off the dielectric charge accumulation, neglecting the wall/plasma potential difference like the charged particles drain off through the wall. This allows a sort of wall floating which is like the case of an *ExitPort*, so the plasma is not confined. The chamber walls could be realized by using the *Equipotential* or *Conductor* objects. The first realizes a wall maintaining it at a potential, which can be defined by the user (put to zero but also time-dependent functions could be used). A multiple *Segments* line reproduces the experimental configuration. To set the cylindrical geometry we must define the *Geometry* flag equal to zero inside the *Grid* block of the input file. Then we have to give the axis position by writing its coordinates in the *CylindricalAxis* block at the end of the input file. The *ExitPort* object should be used to model the pump absorption at the chamber walls.

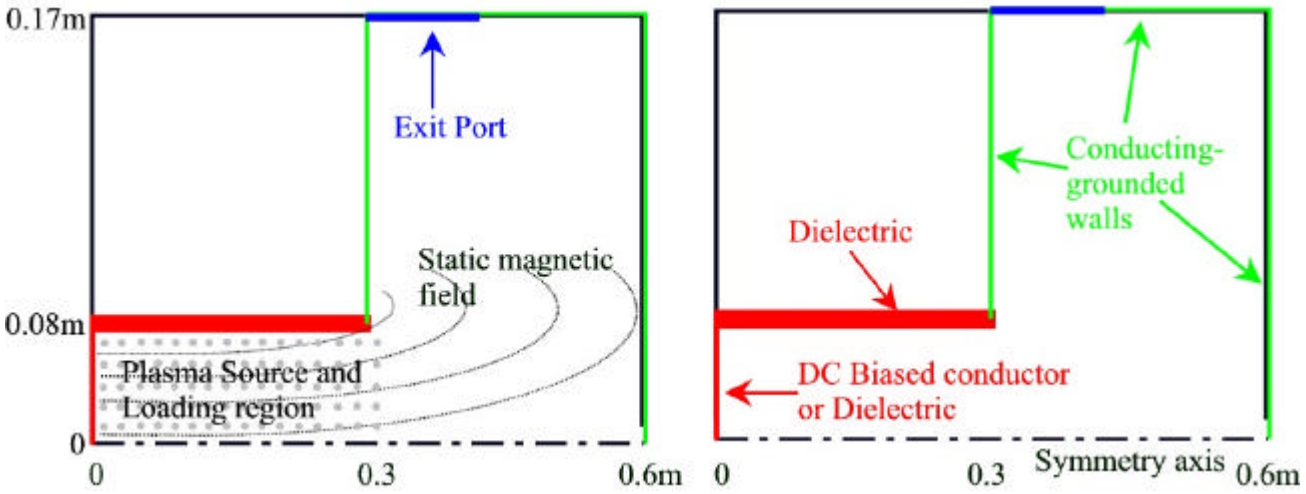

Fig 4.1: OOPIC Geometry adopted to simulate the Charles experiment

The particles passing along this segment will be treated as if they were escaping the boundaries of the simulation. Only one segment can be defined, so it should be carefully positioned. Particular attention must be paid to set the port resistance and impedance because sometimes it can produce reflections and absorptions of particles and/or electromagnetic waves. Few particles are immediately loaded into the source region, to represent the high energy electrons produced during the breakdown and to start without a empty region, while the most are created during the simulation. The plasma production is represented by the OOPIC *PlasmaSource* object. The particles are created at a given rate in a rectangular area and with Maxwellian velocity distribution and a changeable density distribution. The plasma production density is defined in order to model the typical helicon source behaviour: maximum density near r=0 and after the tube half (see Fig 4.2).

4.2 STATIC MAGNETIC FIELD

The static magnetic field has been calculated by solving the equations for circular filamentary coils. The two solenoids of the Charles-Boswell and Plihon experiments are located around the source tube. Their dimensions have been extrapolated from the figures of the ANU and LPTP publications, from there we can also figure out that the current is below 12A and the magnetic field has two maximums along the axis inside the helicon. Each solenoid is schematized as a series of filamentary coils along r and z, at constant current and inside the areas defined from the published pictures: radius between 10 and 13cm, axial

ESA CONTRACT no.	SUBJECT	CONTRACTOR
Ariadna 05/3201	Numerical Simulations of the Helicon Double Layer Thruster Concept – Final report	CISAS "G. Colombo"

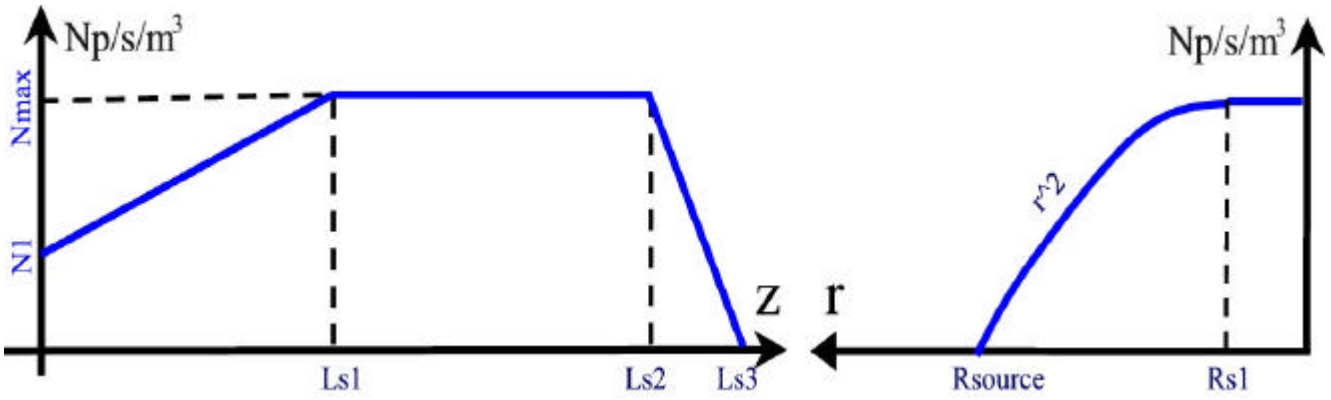

Fig 4.2: Plasma rate density distribution: $L_{s3}=L_{source}$=30cm, R_{s1}=1.5cm and $N_1=N_{max}/3$

positions of 1 and 20cm (from the left source wall) and 8cm long. The total magnetic field is obtained as sum of the fields generated by each coil, calculated for the greed points and stored in a text file which can be imported by OOPIC at the initialization of the simulation.

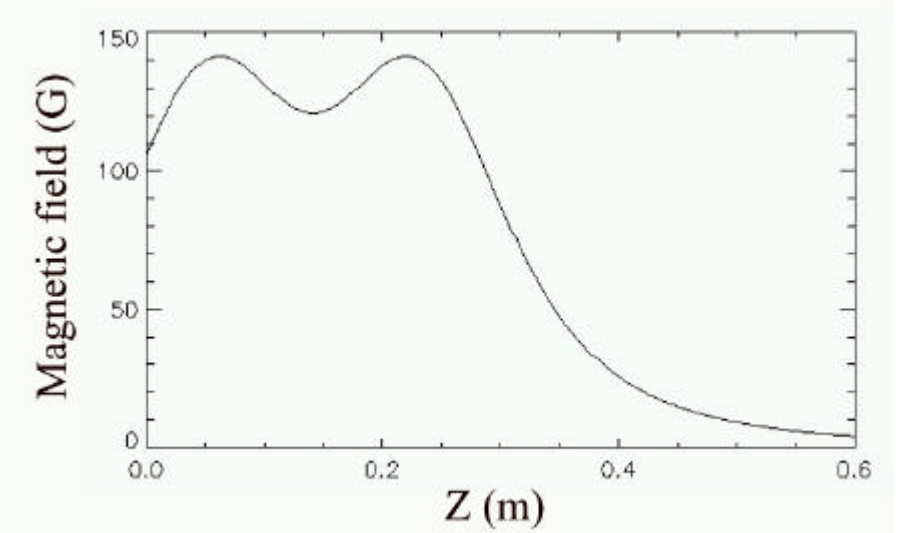

Fig 3.4: Axial static magnetic field

4.3 TEST OF THE OOPIC HYBRID CONFIGURATION

While ions are always computed as real particles, the electrons can be considered like a fluid at isothermal equilibrium. This assumption is usually reported as "Hybrid" PIC paradigm and allows a space

and time scales enhancing because electrons, that move faster then ions due to their lower inertia, can be treated as a uniform background.
The measurements and simulations reported by Charles and Meige suggest the utilization of a hybrid configuration. In this case the electrons can be assumed to be in Boltzmann equilibrium:

$$n_e(r,t) = n_o(r,t) \cdot esp\left[\frac{e \cdot f(r,t)}{k_B \cdot T_e(r,t)}\right] \tag{1}$$

Where *e* is the elementary charge and Ø is the electrostatic potential. The total charge density becomes:

$$r(r,t) = e\left(\sum_i Z_i \cdot n_i(r,t) - n_0(r,t) \cdot \exp\left[\frac{e \cdot f(r,t)}{k_B \cdot T_e(r,t)}\right]\right) \tag{2}$$

If the plasma is quasi neutral we must then have:

$$n_0(r,t) = \sum_i Z_i \cdot n_i(r,t) \tag{3}$$

In electrostatic approximation the Poisson's equation determines the field in the plasma, but with (2) and (3) it becomes nonlinear:

$$\nabla^2 f + \frac{e \cdot n_0}{e_0}\left(1 - \exp\left[\frac{e \cdot f(r,t)}{k_B \cdot T_e(r,t)}\right]\right) = 0 \tag{4}$$

The above relation can be linearized but only in absence of sheaths or DLs.
OOPIC admits Boltzmann electrons and it has both linear and nonlinear Poisson solves but it had to be modified in order to use always the nonlinear solve, except the initialization of the simulation. In the original source codes OOPIC decided to use the linear or nonlinear solve from the total charge of the system. Our modifications have just changed the subroutines call sequence, eliminating the linear solve utilizations.
Two equation solves can be used: Dynamic Alternating Direction Implicit (DADI) and, with a better performance, MultiGrid. Unfortunately, during our tests, the Poisson solve does not converge properly: the system-equations residue remains too high also after several iterations and these errors remain also with the original OOPIC code. Fig 3.5 shows the plasma potential differences between full and hybrid-PIC inside the source tube (to solve the simulation with the hybrid method we had to allow a residue of the Poisson solve five times bigger then the default value). Using the fluid electrons the plasma potential is 20-25% higher then the case with particle electrons and remains almost constant after the first 5-6 μs when the full PIC simulation still change.
These results suggested to change the paradigm of the simulations and adopt a new method which does not involve the Boltzmann electrons. Both ions and electrons will be computed as real particles.

ESA CONTRACT no.	SUBJECT	CONTRACTOR
Ariadna 05/3201	Numerical Simulations of the Helicon Double Layer Thruster Concept – Final report	CISAS "G. Colombo"

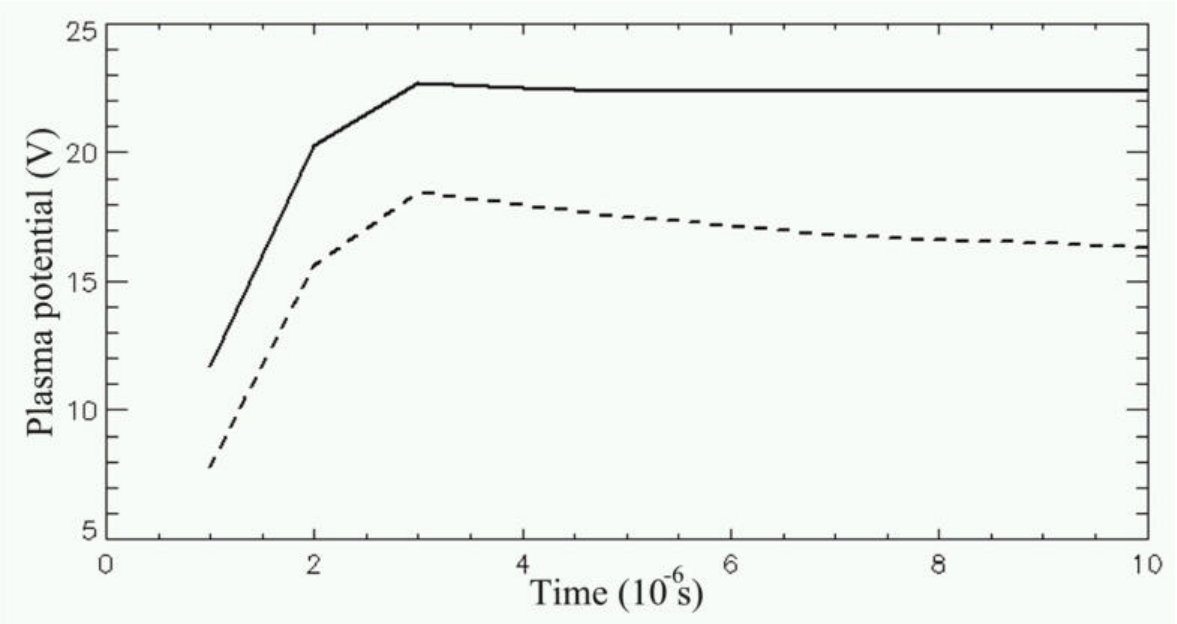

Fig 3.5: Example of plasma potential difference for hybrid and full (dashed) DL OOPIC simulations

ESA CONTRACT no.	SUBJECT	CONTRACTOR
Ariadna 05/3201	Numerical Simulations of the Helicon Double Layer Thruster Concept – Final report	CISAS "G. Colombo"

5 PPDL GENERAL DESCRIPTION

5.1 THEORY

For the application of primary interest to us the boundary conditions for the nonlinear Poisson equation are Dirichlet/Neumann (prescribed f and prescribed ∇j , respectively), rather than the pure Dirichlet.

More specifically the Neumann condition is for a wall with floating potential, where the lost electrons and ions build up a net surface charge that determines the normal component of the electric field $-\nabla j$. To make the nonlinear Poisson solve robust in this case we had to calculate n_0 and the surface charge density s fully self-consistently with j . We do this by extending the nonlinear system of equations given by the discretized Poisson equation with equations for the conservation of charge in the plasma and on the floating-potential wall, respectively.

In the simulation the floating wall is always on the right side.

So sometimes the direction of magnetic field can change: the position of system depends if we choose a floating wall near the source or far from it.

For many plasma applications the electrostatic approximation is valid and the physics of interest occurs on ion time and length scales. In such cases full particle-in-cell (PIC) simulation can be impractical due to the need to resolve the fast electron time scales and short length scales to avoid numerical instability. Hybrid schemes with kinetic ions but Boltzmann electrons, i.e. inertialess electrons in instantaneous thermodynamic

equilibrium, allow larger time steps before numerical instability occurs

In the Boltzmann approximation the electron density is given by

$$n_e = n_0 \exp\left(\frac{j(x)}{T_e}\right) \tag{5.1}$$

where j is the electrostatic potential, T_e is the electron temperature measured in eV and n_0 is the Boltzmann density parameter.

With Boltzmann electrons the Poisson equation becomes nonlinear because the electrostatic potential j depends on the charge density r , which exponentially depends on r .

In the presence of sources or sinks, the density parameter n_0 will change over time and if it is not done self-consistently with j electron charge will not be conserved. When a plasma is in contact with a material wall n_0 will in general be reduced by the electron flux from the plasma to the wall. Cartwright et al.[32] were the first to introduce a nonlinear Poisson solver, using the Newton-Raphson scheme, where

ESA CONTRACT no.	SUBJECT	CONTRACTOR
Ariadna 05/3201	Numerical Simulations of the Helicon Double Layer Thruster Concept – Final report	CISAS "G. Colombo"

n_0 is updated without heuristic assumptions about the electron flux.
They also noted the importance of charge conservation for the numerical stability of the solver. However, in the Cartwright algorithm n_0 is not fully self-consistent with j but lags one iteration behind in the Newton loop. For many applications the charge conservation of the Cartwright solver is nevertheless sufficient to give acceptable numerical stability.

5.2 MODEL DESCRIPTION

The goal of the simulation is to reproduce the potential drop sometimes seen in an expanding magnetic field downstream from a helicon plasma source.
The relevant geometry is cylindrical with azimuthal symmetry and the magnetic configuration, generated by solenoids, can be changed from the input file. We used two different type of magnetic field configuration as shown in figures.
A plasma source is located in the high-field region to the right.
The boundary condition to the right is a floating-potential wall. In this case the field lines expand to the left and we will assume that detachment occurs and the appropriate boundary condition is ground. Fig 5.1 shows the axial magnetic field $B_z(r=0,z)$ and its gradient $\hat{z}\cdot\nabla B = \partial B_z/\partial z$, dashed and dotted lines, respectively. The solid line is the radius, r_z, of the magnetic field line that is infinitesimally close to the inside of the solenoid to the right.

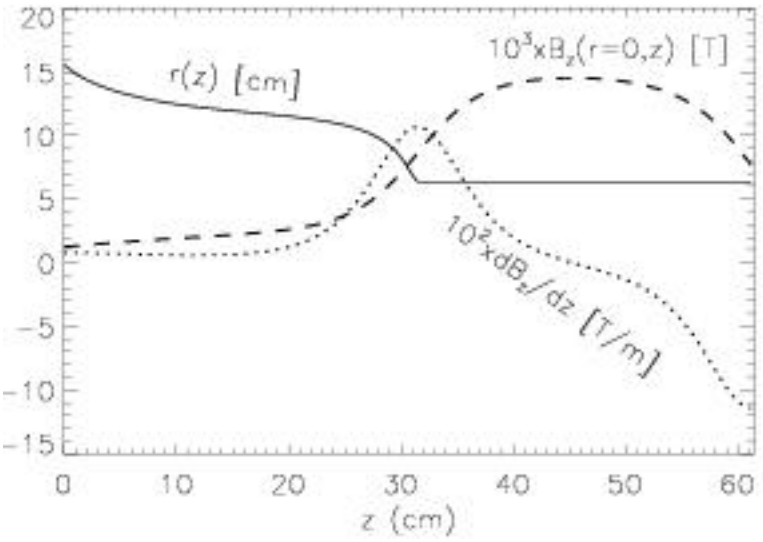

Fig 5.1: Solid line is distance of field line from axis, dashed is magnetic field and dotted line is magnetic gradient

ESA CONTRACT no.	SUBJECT	CONTRACTOR
Ariadna 05/3201	Numerical Simulations of the Helicon Double Layer Thruster Concept – Final report	CISAS "G. Colombo"

Following Chen [33] we will assume that the dominant radial effect is the dilution of density due to the expanding magnetic field. The electron and ion densities are then of the form

$$n_{e,i}(r,z) = n_{e,i}(z)\frac{r^2(L)}{r^2(z)} \tag{5.2}$$

The fixed-fixed boundary condition permits to choose the potential of right and left wall.
This quasi-2D assumption reduces the dimensionality from two to one, while retaining the dominant 2D effect: the reduction of density as the magnetic field expands. We will additionally include the ∇B force on the ions by using the drift-kinetic approximation for the ion dynamics. The magnetic field is calculated as a superposition of elemental loops that formed the solenoids, solving the helmoltz equations in 2D.

An implicitly charge-conserving algorithm has been derived from PadPIC, a previous software for solving the nonlinear Poisson equation that results from the use of Boltzmann electrons.
The new algorithm solves for the Boltzmann density parameter and, in case of a Neumann boundary condition, the surface charge density simultaneously as it solves for the discretized electrostatic potential.
Stability is demonstrated for time steps exceeding the electron plasma period and spatial resolution much coarser than the Debye length. Both temporal and spatial convergence is shown to be quadratic.

A Monte-Carlo algorithm is used to simulate elastic collisions between ions and neutrals. With drift-kinetic ions the velocity coordinates are V_z , $V_\perp = v(2\mu B/m)$, where μ is the adiabatically invariant magnetic moment, B is the magnetic field strength and m is the ion mass. The probability for a collision during a time step Δt is $n_n Q(v)vDt$, where n_n is the neutral density, Q is the cross section and v is the ion speed $V^2 = V_z^2 + V_\perp^2$. For each ion macroparticle during each time step a random number z , uniform in the interval [0, 1), is generated. If the random number is smaller than the collision probability, the velocity coordinates of the macroparticle are changed according to the type of collision. For collisions between Ar+ and Ar we use the cross sections suggested by Phelps [35]

We assumed that the plasma detaches from the magnetic field when the kinetic pressure $P_e + P_i$ exceeds the magnetic pressure $P_m = B^2/(2\mu_0)$.
Pressure from Boltzmann electrons is:

$$P_e = n_e(z)k_B T_e \tag{5.3}$$

where $n_e(z)$ includes the rarefaction due to the magnetic-field expansion.
For the ion pressure we assumed the P_{zz} term of the stress tensor dominates. This follows if we assume B? 0 in the detachment region ($v_\perp$? 0 if μ constant of motion). The ion pressure then becomes:

$$P_i \approx n_i m_i \left\langle v_z^{\,2} \right\rangle \tag{5.4}$$

This is of course an approximation, but this is all lowest-order stuff.

The experimental models are implemented by the modification of the input file which allows to change all the relevant parameters:

For every simulations we provide the input file:
All parameters must be set in S.I. (except temperatures (eV))

```
 length = 0.6144,        (Length of System)
 Rpipe  = 0.0634,        (Initial Plasma Pipe Radius)
 Lrpipe = 0.6144,        (Plasma Pipe right end)
 Llpipe = 0.3168,        (Plasma Pipe left end)
 sLr    = 0.6044,        (Plasma Source right end)
 sLl    = 0.3168,        (Source left end)
 srate  = 1e32,          (Source Rate)
 time   = 11.14e-6,      (Simulation time length)
 ne     = 1e14,          (Initial particle density)
 te     = 100.0,         (Electron Temperature in eV)
 ti     = 100.0,         (Ion Temperature in eV)
 mi     = 6e-26,         (Ion Mass)
 Zi     = 1,             (Degree of Ionization)
 posit1 = 0.1,           (z-position 1 for potential diagnostics)
 posit2 = 0.3,           (z-position 2 for potential diagnostics)
 posit3 = 0.5,           (z-position 3 for potential diagnostics)
 ndens  = 2e10,                (Neutral Density)
 dcbO   = 0              (Left boundary DCBIAS - for FIXED-FIXED case only)
 dcbN   = 0,             (Right boundary DCBIAS - for FIXED-FIXED case only)
 fixfix = 1,             (FIXED-FIXED case Flag [1=fixfix, 0=fixflo])
 bins   = 512,           (Number of Cells)
 detach  = 1,            (DETACHMENT Flag [0=no detachment,1=detachment])
 nu     = 120000,        (Number of Macro-Particles)
 steps  = 1600           (Number of time steps in simulation time)
/
&pcoil0
 sl0 = 0.3168,           (Coil 0 left end z-position)
 sr0 = 0.6144,           (Coil 0 right end z-position)
 ri0 = 0.0634,           (Coil 0 internal radius)
```

ESA CONTRACT no.	SUBJECT	CONTRACTOR
Ariadna 05/3201	Numerical Simulations of the Helicon Double Layer Thruster Concept – Final report	CISAS "G. Colombo"

```
 re0 = 0.0734,          (Coil 0 external radius)
 iw0 = -25.0,           (Coil 0 current per wire)
 nw0 = 500              (Coil 0 number of wires / unit length)
/
&pcoil1
 sl1 = 0.0,             (Coil 1 left end z-position)
 sr1 = 0.3168,          (Coil 1 right end z-position)
 ri1 = 0.1636,          (Coil 1 internal radius)
 re1 = 0.1736,          (Coil 1 external radius)
 iw1 = -4.0,            (Coil 1 current per wire)
 nw1 = 500              (Coil 1 number of wires / unit length)
/
&pcoil2
 sl2 = 11,              (Coil 2 left end z-position)
 sr2 = 11,              (Coil 2 right end z-position)
 ri2 = 23,              (Coil 2 internal radius)
 re2 = 24,              (Coil 2 external radius)
 iw2 = 0,               (Coil 2 current per wire)
 nw2 = 47               (Coil 2 number of wires / unit length)
/
&pcoil3
 sl3 = 0.3168,          (Coil 3 left end z-position)
 sr3 = 0.6144,          (Coil 3 right end z-position)
 ri3 = 0.1636,          (Coil 3 internal radius)
 re3 = 0.1736,          (Coil 3 external radius)
 iw3 = 0.0,             (Coil 3 current per wire)
 nw3 = 500              (Coil 3 number of wires / unit length)
/
&description
Boswell test simulation          (Brief simulation description; multiple lines
                                  descriptions allowed)
```

The output files provided for all simulation are in the following form:

basename(FILE).out	output file if -o option selected (it contains status and message obtained during the run)
basename(FILE)_Netot.out	(Total number of particles: time, step number , Number of electrons

ESA CONTRACT no.	SUBJECT	CONTRACTOR
Ariadna 05/3201	Numerical Simulations of the Helicon Double Layer Thruster Concept – Final report	CISAS "G. Colombo"

	inside the source, total number of electrons inside the system, total number of ions inside the system
basename(FILE)_pot.out	(potential phi[j] for current step)
basename(FILE)_pothistory.out	(potential phi[j] history for all steps cell vs time vs phi[j])
basename(FILE)_phasespace.out	(x, v, Mach number for each particle at the end of simulation)
basename(FILE)_errorslog.out	(error-warning message storage file for Debye Length and plasma time criterions – empty if no problem occurs)
basename(FILE)_thrust.out	(step,t,thrust) [only for detachment]
basename(FILE)_neNerho.out	(electron density, ion density, electron number, ion number, charge density in functio of space)
basename(FILE)_Bconf.out	(First-> radius of magnetic tube, axial magnetic field, axial magnetic gradient, source position)
basename(FILE)_Bconf2.out	(Last-> radius of magnetic tube, axial magnetic field, axial magnetic gradient, source position)
basename(FILE)_phipoint.out	(potential in three points: phi[pos[1-3]])
basename(FILE)_density2.out	(cell position, initial number of particles per cell, initial ion density per cell, final number of particles per cell, final ion density per cell, initail numebr of macroparticle per cell, final numeber of macroparticle per cell)
basename(FILE)_pmpi.out	(cell index, electron kinetic pressure, ion kinetic pressure per cell, magnetic pressure, total kinetic pressure)
basename(FILE)_temp.out	(Cell position, Ion temperature)
basename(FILE)_magnlinesB.dat	(cell,Bz[i],dBz[i])
basename(FILE)_tube#i.dat	(x,y,Bx,By) for i-th magnetic tube line
basename(FILE).tex	report latex file
basename(FILE).gp	gnuplot file for ps graphs creation

ESA CONTRACT no.	SUBJECT	CONTRACTOR
Ariadna 05/3201	Numerical Simulations of the Helicon Double Layer Thruster Concept – Final report	CISAS "G. Colombo"

6 OOPIC SPARSE GRID SIMULATIONS

As we pointed out before, due to the low Hybrid-OOPIC performances the simulations had to be made using a full electrostatic configuration. The analysis have been done by considering high time steps and low plasma densities: this permits to reduce the particles' number and the spatial grid, which is scaled with $?_d$, and the dimension of the fields' matrixes that consequently OOPIC can manipulate without the need of a supercomputer in a reasonable time. The time step has been set at 10^{-9}s in accordance with the electron cyclotron and plasma frequencies and a comparison test between the case with $dt=10^{-11}$s showed a low discrepancies, of the order of 1%, on the plasma potential after 5 μs.

6.1 COMPARISION WITH NOT CONFINED PLASMA EXPANSION

The source walls' characteristics can be chosen by adopting three OOPIC objects: conducting surface with constant potential, dielectric and dielectric without the accumulated surface charge property. This last configuration has been chosen as reference case because it represents a non confining wall. The dielectric in the reference simulation has a relative permittivity of 1, so as the free space.

ESA CONTRACT no.	SUBJECT	CONTRACTOR
Ariadna 05/3201	Numerical Simulations of the Helicon Double Layer Thruster Concept – Final report	CISAS "G. Colombo"

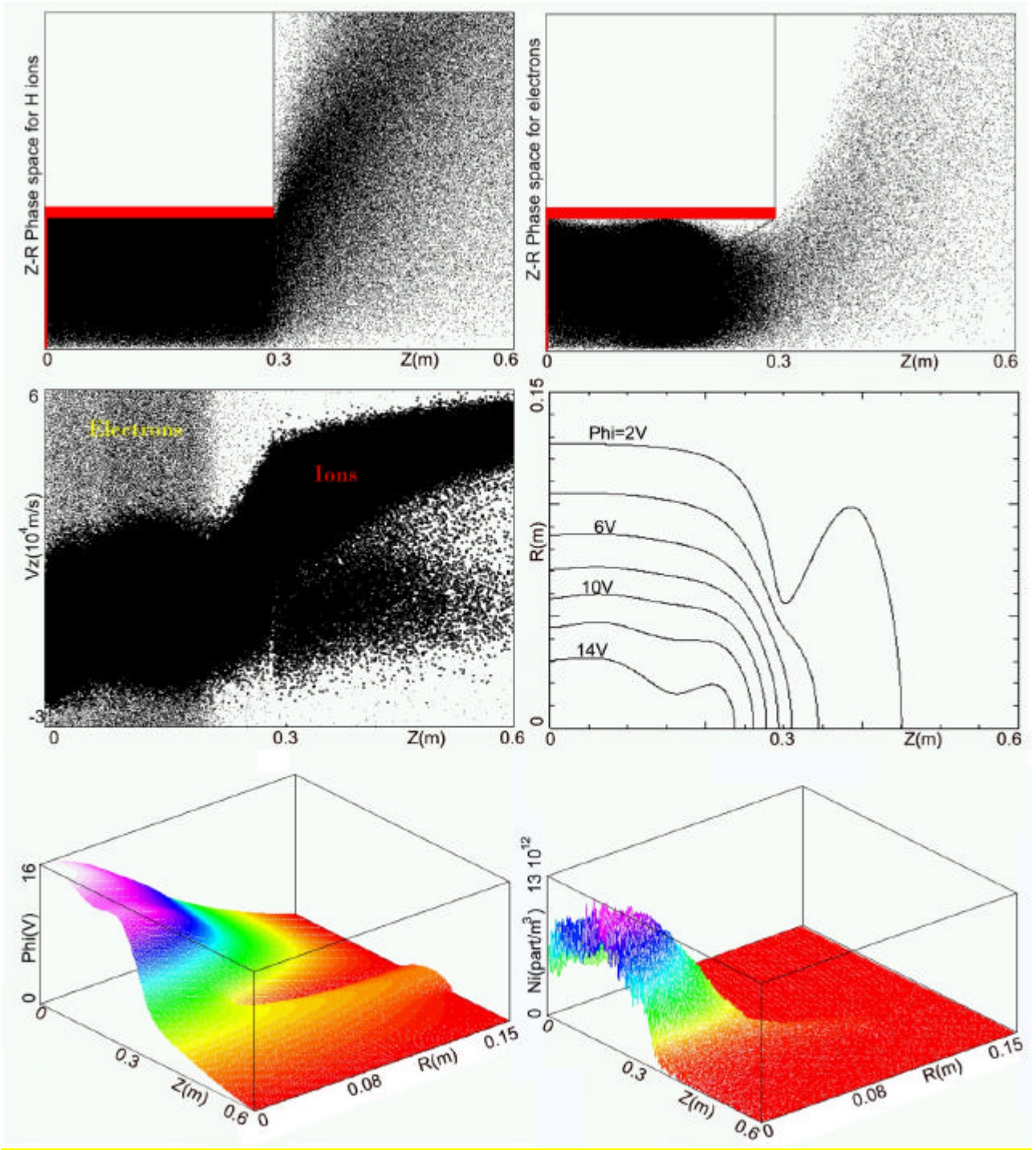

Fig 6.1: Plasma r-z phase space, ions axial velocity, potential and ions number density for the reference case at t=11μs. The source walls are not confining and the parameters of Tab 6.1 applies.

ESA CONTRACT no.	SUBJECT	CONTRACTOR
Ariadna 05/3201	Numerical Simulations of the Helicon Double Layer Thruster Concept – Final report	CISAS "G. Colombo"

In our dual-core computers the simulations took 20-30 hours each to reach 15-20 μs, their results are shown below and the reference parameters follow:

Particles	H		Neutral Density (mT)	1.6
Magnetic field (G)	125		Time Step (s)	10^{-9}
Macro-part relative weight	10^3		Duration (μs)	11
R Space Step (mm)	1.2		Z Space Step (mm)	1.2
PRODUCED PARTICLES			IMMEDIATELY LOADED PARTICLES	
Te (eV)	7		Te (eV)	10
Ti (eV)	0.5		Ti (eV)	0.5
Source Rate (s^{-1} m^{-3})	$5*10^{17}$		Density (m^{-3})	10^9

Tab 6.1: Parameters of the reference case simulation

From Fig 6.2 one can suggest that, for the reference case, the plasma potential and its jump are well defined after 10μs, therefore our simulations, that last 15-20μs, should be indicative of the phenomenon. The plasma potential at z>30cm increases between 5 and 10μs but it remains almost unchanged during the successive 5μs, showing that also the ions flux inside the chamber should be stable after 10μs. In fact the ions travel around the ion sound speed which is now $v(k\ Te/m_i)\sim 2.5\ 10^4$ m/s, so they should pass the 30cm diffusion chamber and reach its right wall after 10-11μs. With the adopted source rate the densities inside the source after 10μs are few times 10^{12} m^{-3} so more than two orders of magnitude lower than the experimental values.

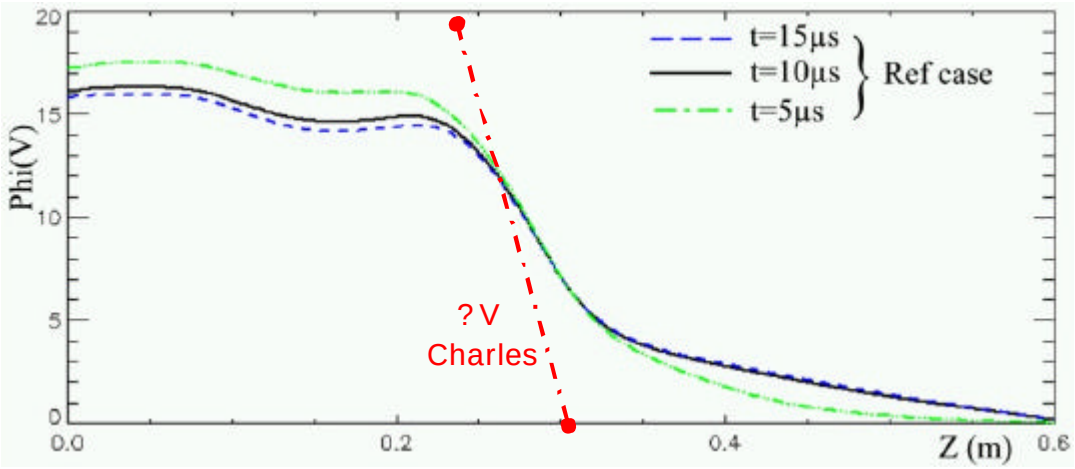

Fig 6.2: Plasma potential at r=0 for non confining (non-accumulating surface charge) dielectric source walls. The parameters of Tab 6.1 applies. After 10μs the potential jump becomes almost

ESA CONTRACT no.	SUBJECT	CONTRACTOR
Ariadna 05/3201	Numerical Simulations of the Helicon Double Layer Thruster Concept – Final report	CISAS "G. Colombo"

stable. The red arrow represents the width of the potential jump measured by Charles. T_e=7eV final N_{ions}~10^{12} m^{-3}.

6.1.1 Axial magnetic field effects

Switching off the magnetic field, particles are not confined and electrons are uniformly spread inside the helicon tube. Also the ions' trajectories change and their divergence increases. See Fig 6.3 for more details. The divergence remains around 50 and 60 degrees.

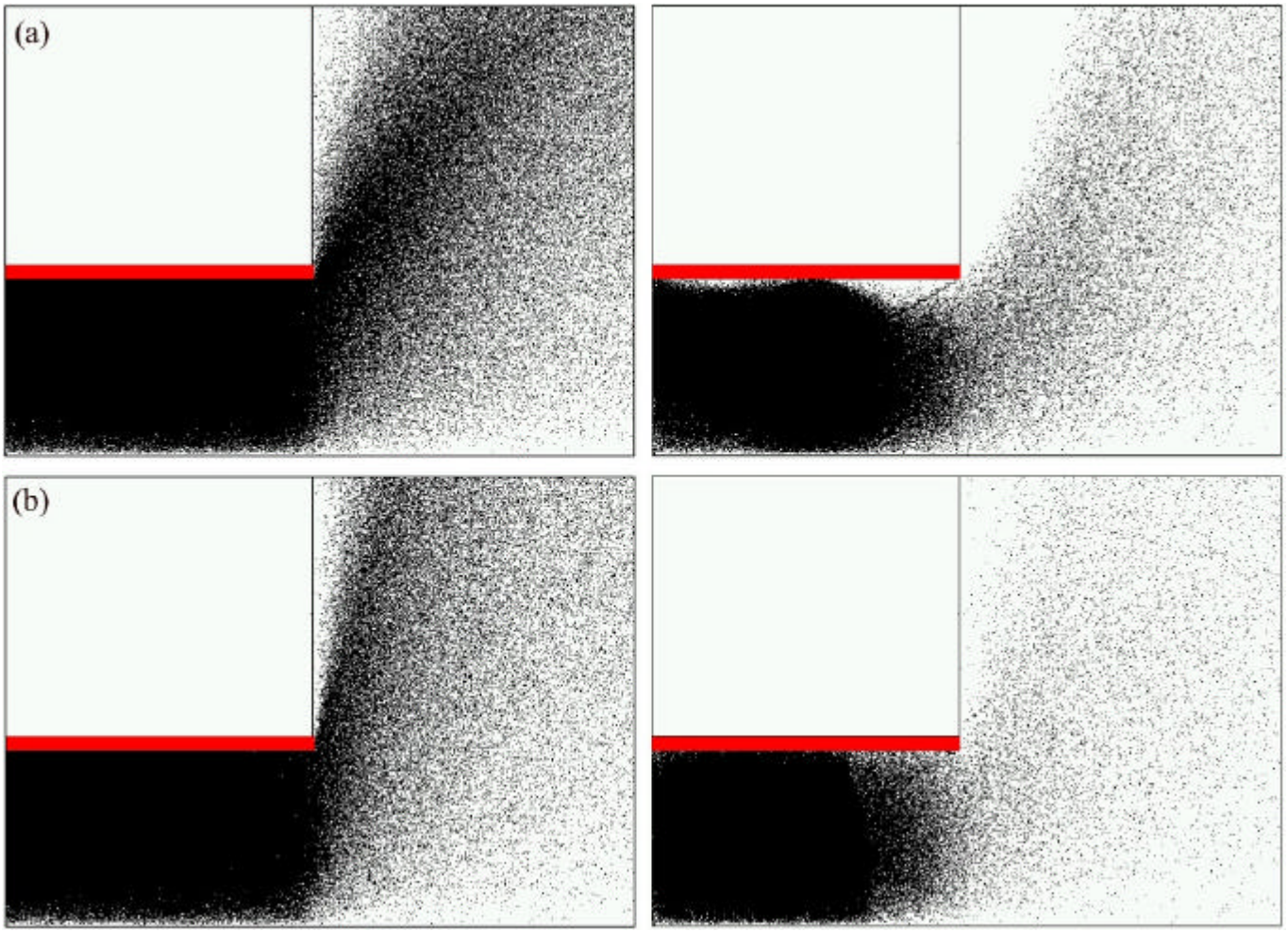

Fig 6.3a: Ions (left) and electrons positions after 11μs for the non confining source walls with (a) and without magnetic field (b).

ESA CONTRACT no.	SUBJECT	CONTRACTOR
Ariadna 05/3201	Numerical Simulations of the Helicon Double Layer Thruster Concept – Final report	CISAS "G. Colombo"

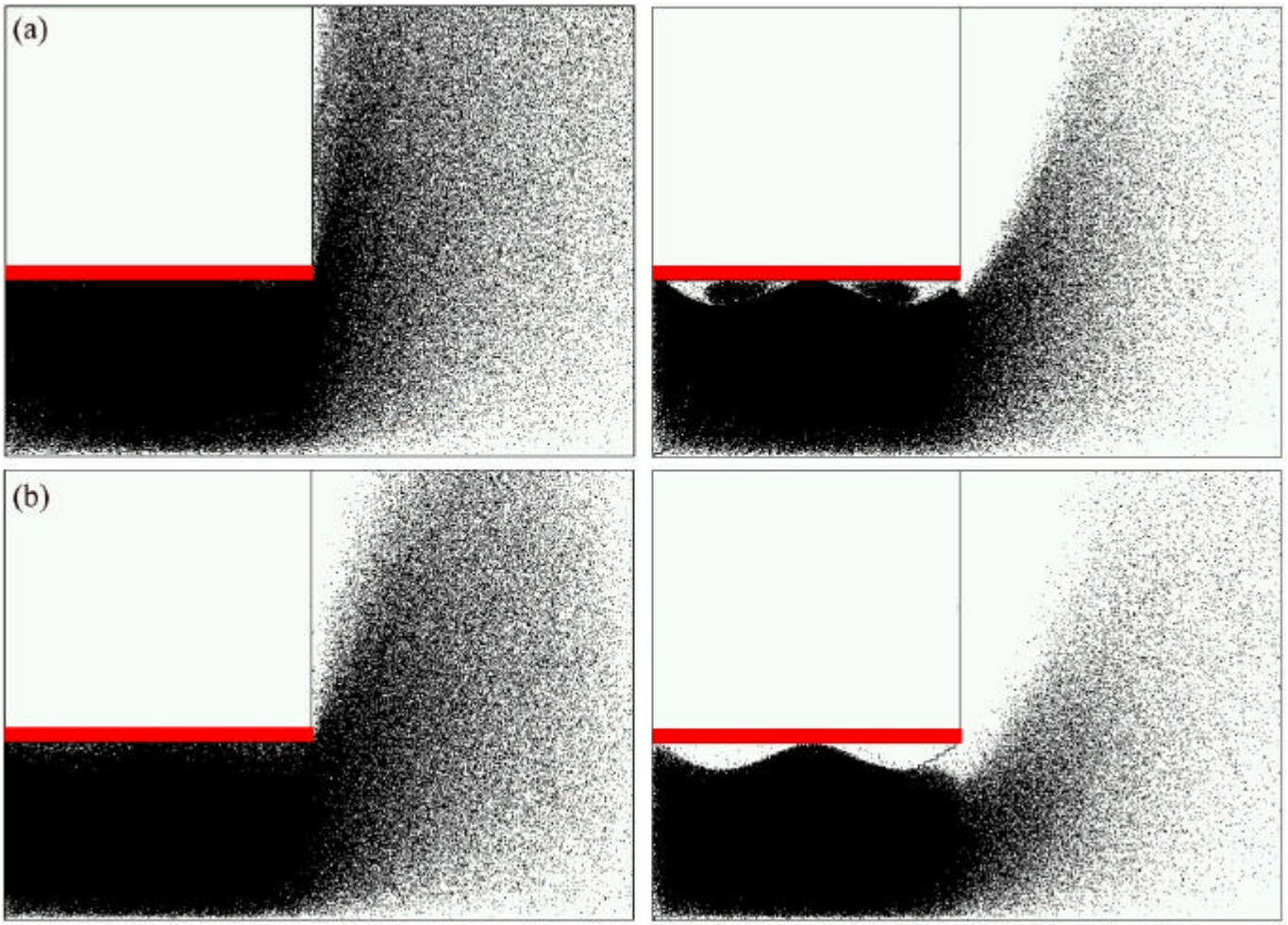

Fig 6.3b: Ions (left) and electrons positions after 11μs for true dielectric source walls (accumulating surface charge) with e_r=1 (a) and e_r=4 (b) both with magnetic field.

6.1.2 Source tube walls effects

Using "real" dielectric as source walls the confining effect of the magnetic field seams to be enhanced and it grows using high permittivity. In particular electrons are much more confined at lower radius inside the helicon and the ions density at $r<R_{source}$ grows inside the diffusion chamber. See Fig 6.3b.

Fig 6.4 confirms the Boswell suggestion: the potential of the left source wall is a critical point for the formation of the potential jump. If the left wall is made of conductors set to a low fixed potential or dielectric (so if it is able to produce a sheath mainly lowering its potential to negative values by accumulating the faster electrons in order to attract ions and neglect the total current) the source plasma potential is sensibly reduced. Another information coming from the picture is that increasing the left wall potential above the value obtained in the not biased case, the potential jump varies, but only of few Volts.

ESA CONTRACT no.	SUBJECT	CONTRACTOR
Ariadna 05/3201	Numerical Simulations of the Helicon Double Layer Thruster Concept – Final report	CISAS "G. Colombo"

Finally allowing the accumulation charge (true dielectric surface) both at the left and up source walls, the potential jump is drastically reduced, showing that the ion flux is sensibly changed.

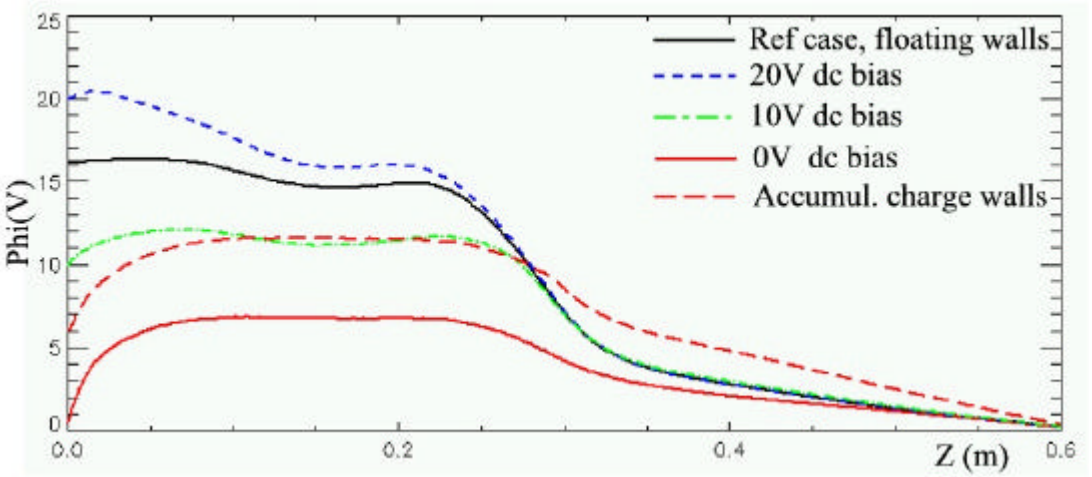

Fig 6.4: Plasma potential at r=0 and t=11μs for different dc biased source left walls. T_e=7eV final N_{ions}~10^{12} m^{-3}.

Fig 6.5 and 6.6 represent the time evolutions of axial plasma potential and density for three left source walls, they show that the stabilization of the flux is not an easy attempt. The up source wall is there a non confining dielectric wall (*QuseFlag* is 1). For all the three cases the plasma potential change very rapidly during the first 5-6 μs, when the ions flux starts to penetrate the expanding chamber, and almost it does not change after 9-10 μs. Not the same happens for the plasma density: if the left wall potential remains far below the plasma's one, the ions' density does not stop to grow, reaching values three times greater and the potential jump decreases of about 25%.

ESA CONTRACT no.	SUBJECT	CONTRACTOR
Ariadna 05/3201	Numerical Simulations of the Helicon Double Layer Thruster Concept – Final report	CISAS "G. Colombo"

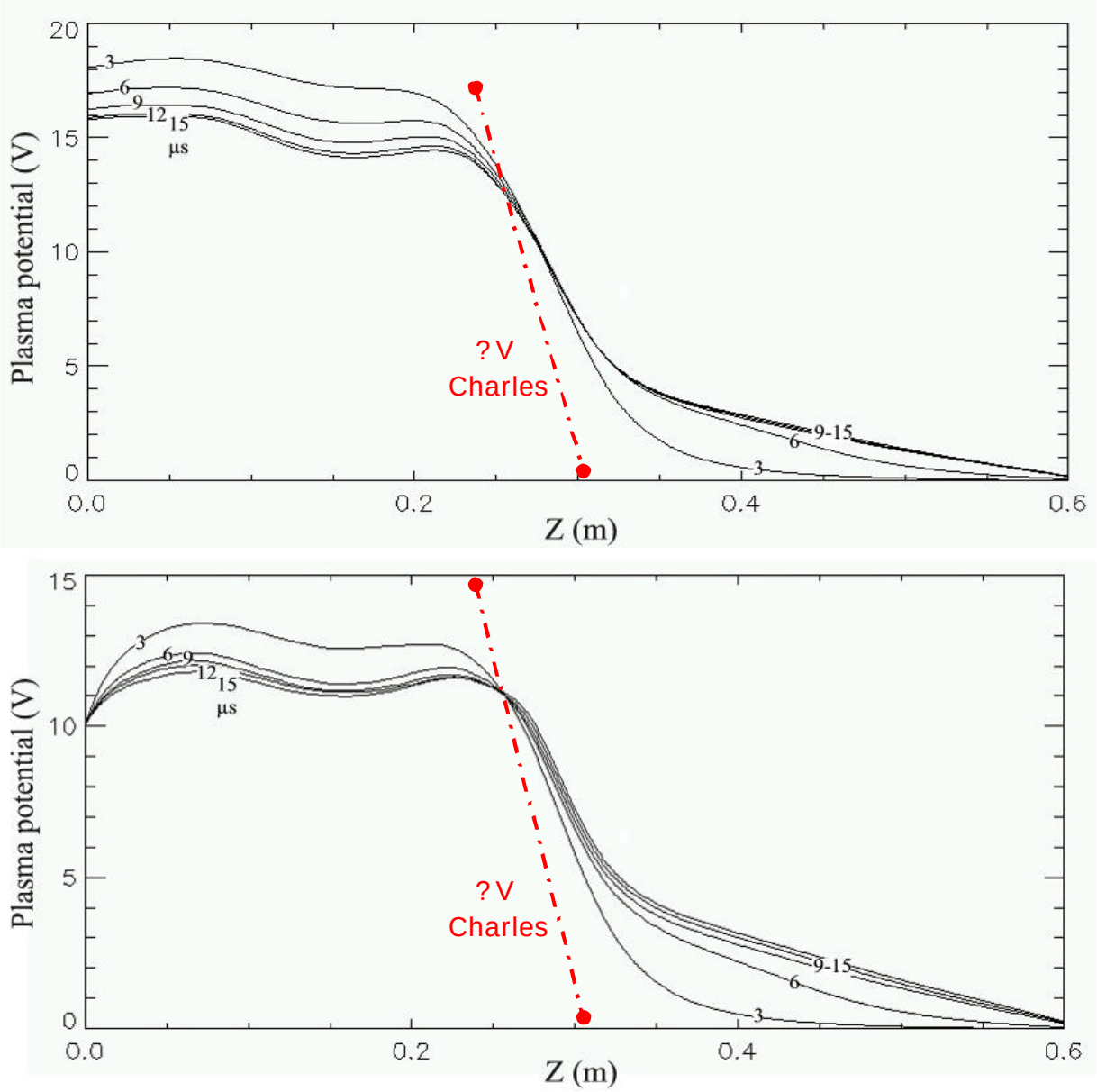

Fig 6.5a: Axial plasma potentials for reference case (non confining left wall) and conducting 10V dc biased source left wall (down). The up wall is a non confining dielectric. The red arrow represents the width of the potential jump measured by Charles. T_e=7eV final N_{ions}~10^{12} m^{-3}.

ESA CONTRACT no.	SUBJECT	CONTRACTOR
Ariadna 05/3201	Numerical Simulations of the Helicon Double Layer Thruster Concept – Final report	CISAS "G. Colombo"

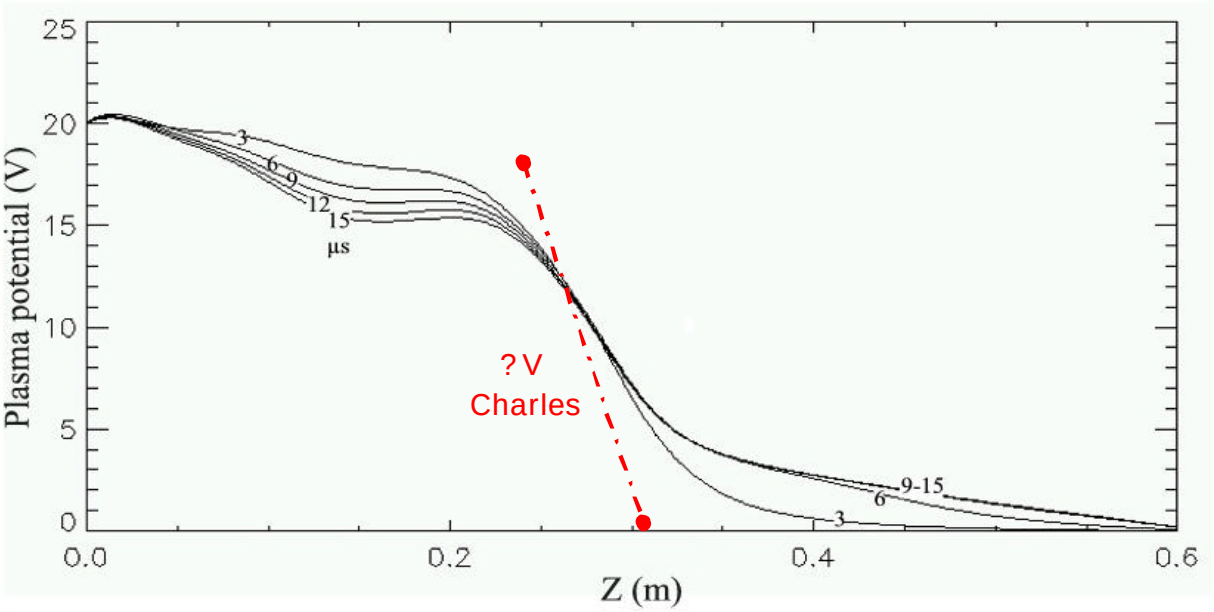

Fig 6.5b: Axial plasma potentials for conducting 20V dc biased source left wall. The up wall is a non confining dielectric. The red arrow represents the width of the potential jump measured by Charles. T_e=7eV final N_{ions}~10^{12} m^{-3}.

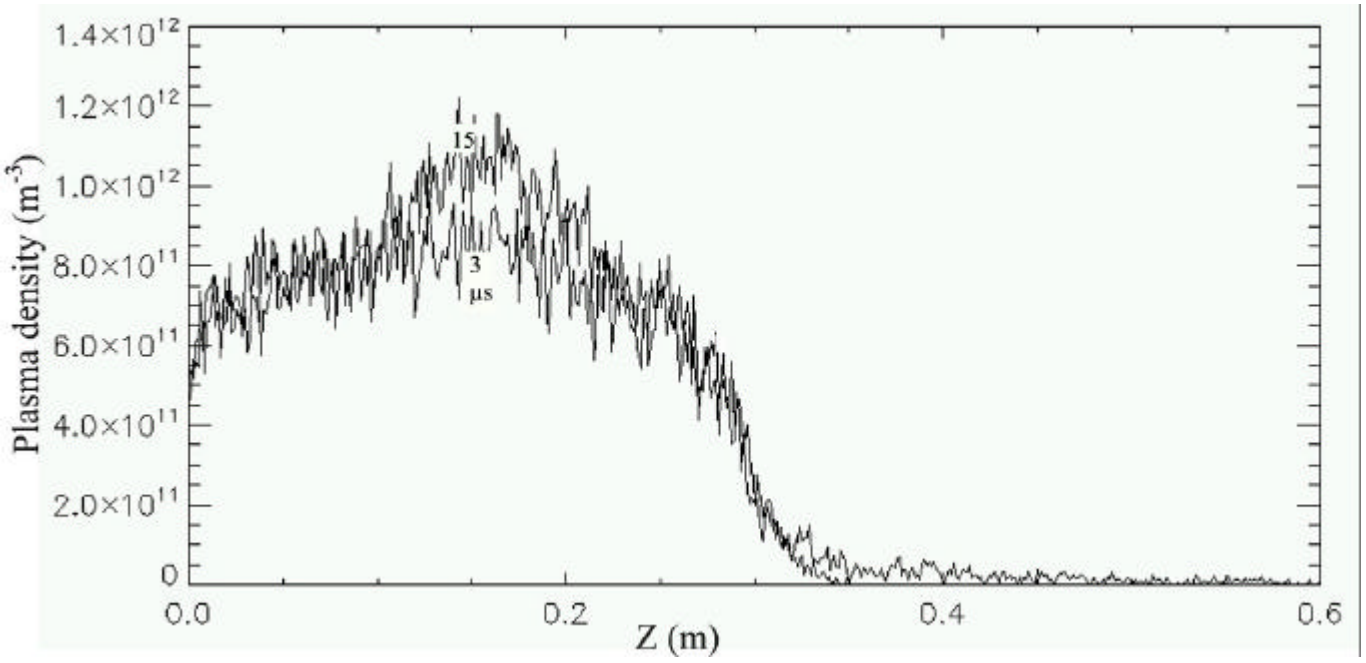

Fig 6.6a: Axial plasma density for reference case (non confining source left wall). The up wall is a non confining dielectric.

ESA CONTRACT no.	SUBJECT	CONTRACTOR
Ariadna 05/3201	Numerical Simulations of the Helicon Double Layer Thruster Concept – Final report	CISAS "G. Colombo"

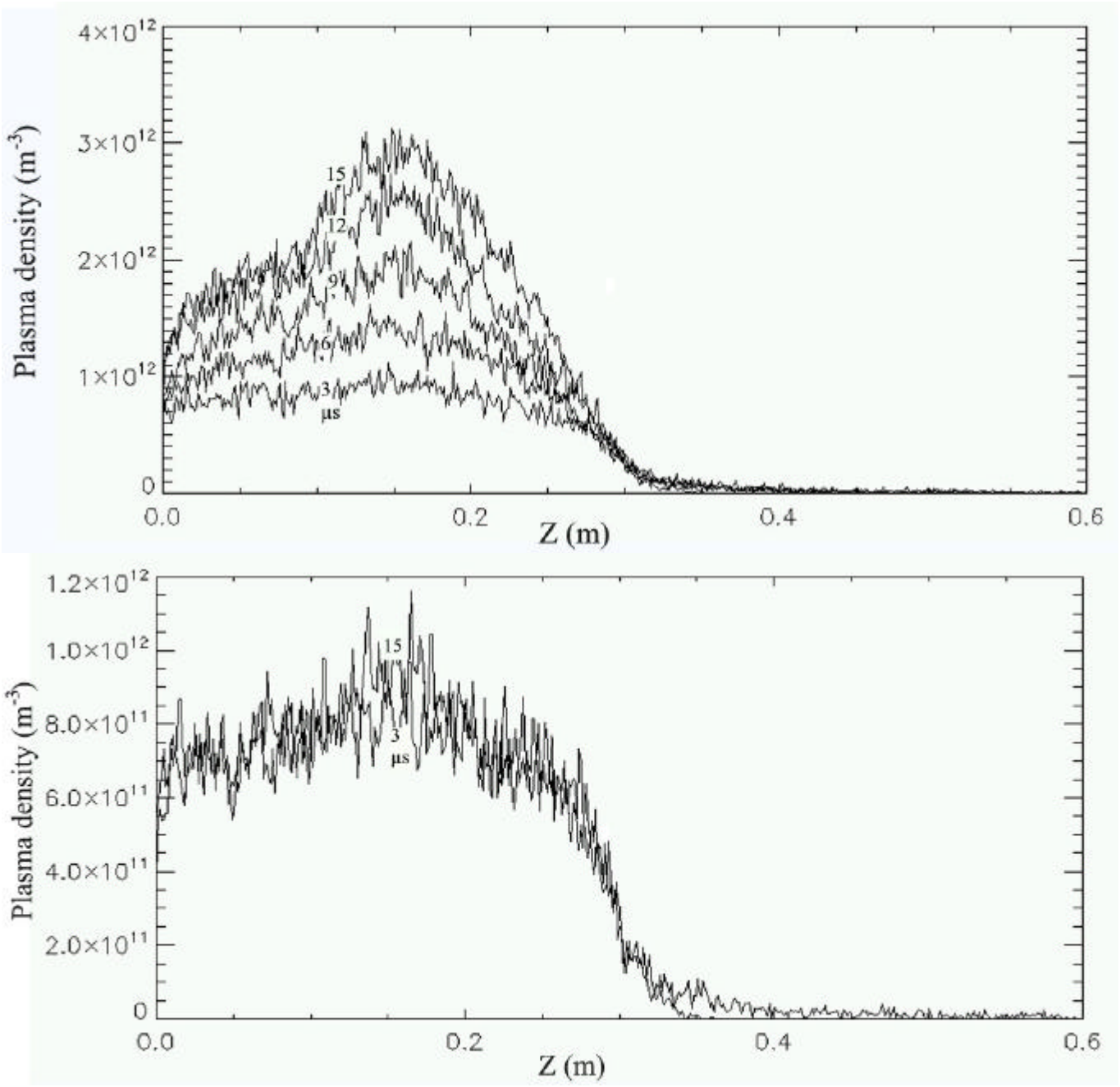

Fig 6.6b: Axial plasma density for conducting 10 (up) and 20V (down) dc biased source left walls. The up wall is a non confining dielectric.

ESA CONTRACT no.	SUBJECT	CONTRACTOR
Ariadna 05/3201	Numerical Simulations of the Helicon Double Layer Thruster Concept – Final report	CISAS "G. Colombo"

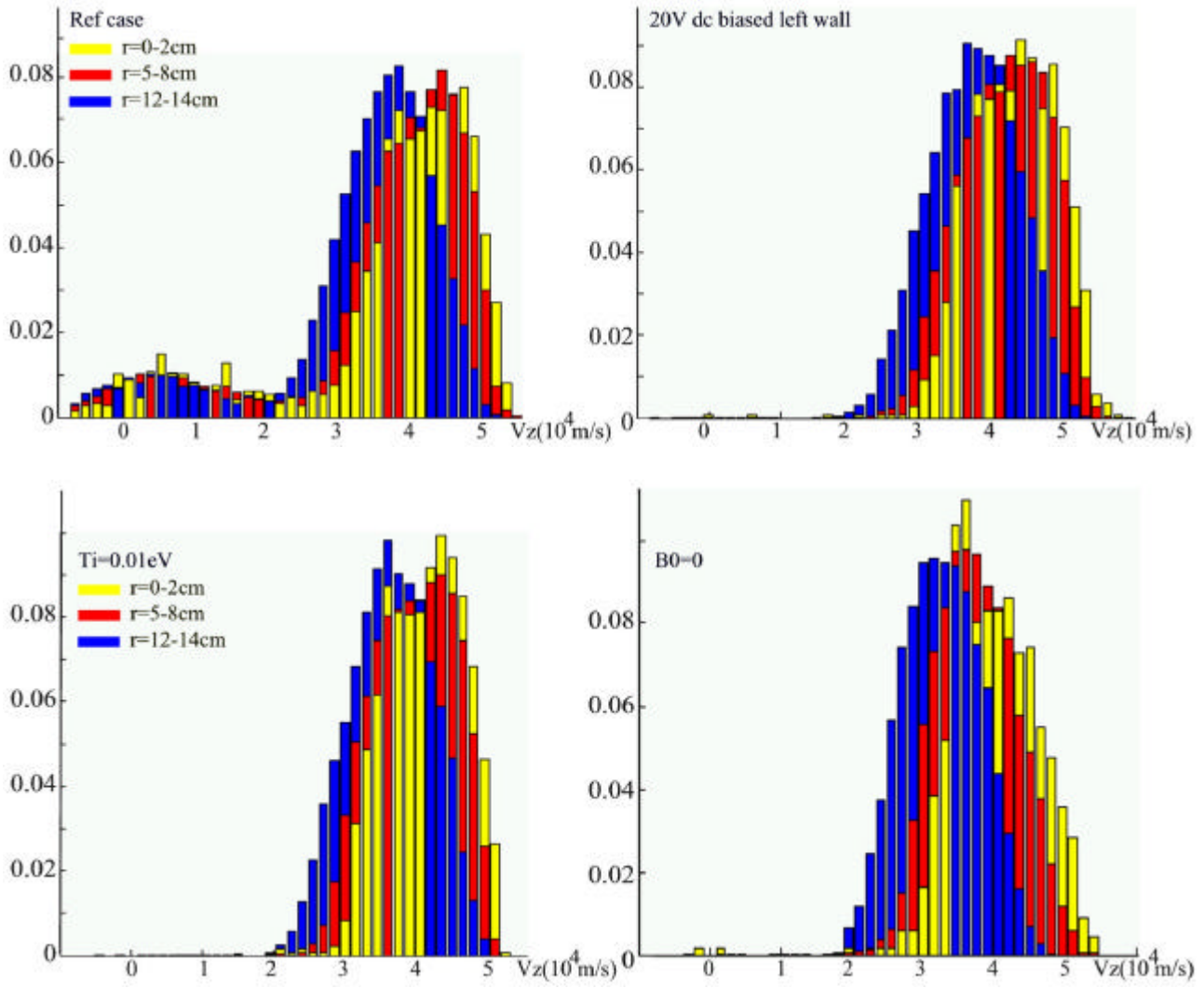

Fig 6.7a: Ions relative density as function of the axial velocity and radius and for z=40-45cm (10cm outside the helicon tube). The height of each bar represents the relative density of ions having that velocity; e. g. for the reference case 4.5% of the ions at r=12-14cm have axial velocity of 3 10^4m/s while less then 1% of the ions at r=0-2cm have that value.

ESA CONTRACT no.	SUBJECT	CONTRACTOR
Ariadna 05/3201	Numerical Simulations of the Helicon Double Layer Thruster Concept – Final report	CISAS "G. Colombo"

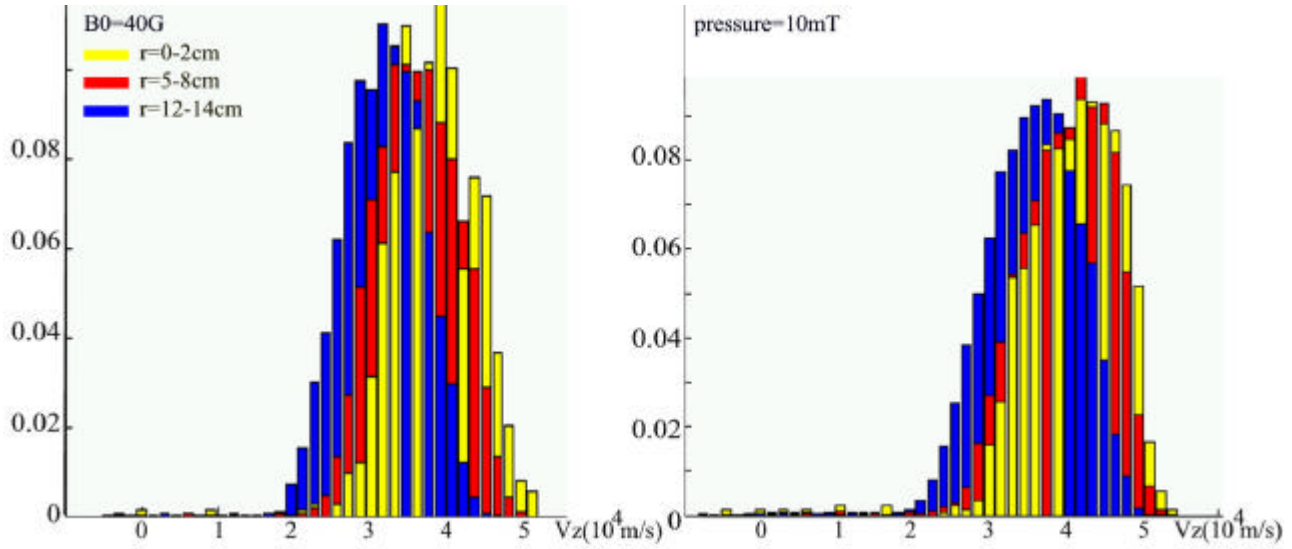

Fig 6.7b: Ions relative density as function of the axial velocity and radius, for z=40-45cm (10cm outside the helicon tube).

6.1.3 Axial velocity distribution

Fig 6.7 should represent the Ion Energy Distribution Function (IEDF) measurements made by Charles and Plihon (see Fig 1.9-1.12). It is shown that the greater percentage of the ions inside the expansion chamber and at the source axis has velocities between 4 and 5 10^4m/s (yellow bars), while for higher radius the peak velocity decreases to 3-3.5 10^4m/s. The ion sound speed for hydrogenous and Te=7eV is $v(k\ Te/m_i)$~2.5 10^4m/s, so the peak velocity for r~0 is around two times C_s as reported by Charles and Plihon. The two peaks shape of the measurements, typical of the DL case, is better reproduced adopting a cold ions family at the source (Ti=0.01eV). The density of the ion beam is increased with the 20V dc biased left wall, while the ions velocity remains almost unchanged, comparing it with the present reference case (non-confining source wall). It has to be noted that several ions at two times the sound speed are registered also with a low or zero magnetic field.

6.1.4 Neutral pressure effects

Increasing the neutral pressure of a factor 10 the potential jump remains almost unchanged. To obtain significant differences the pressure has to grow of two order of magnitudes. Fig 6.8 shows how the ions' axial velocity distribution inside the diffusion chamber can be modified by the same factor: high pressures allow the gas ionization by the electrons that escape from the source. For pressures above 100mT the number of low velocity ions reaches the high energy ions, that forms the second peak of the distribution function.

ESA CONTRACT no.	SUBJECT	CONTRACTOR
Ariadna 05/3201	Numerical Simulations of the Helicon Double Layer Thruster Concept – Final report	CISAS "G. Colombo"

During the experiments the potential jump disappeared for pressures above 3-5 mTorr. Our simulations show a similar effect but for pressure greater than 100mTorr, so two orders of magnitude higher. The discrepancy can be explained considering that the real ions' density inside the helicon source was between 10^{15} and 10^{16} m^{-3} while for our studies we obtained values significantly lower: around 5 10^{12} m^{-3}.

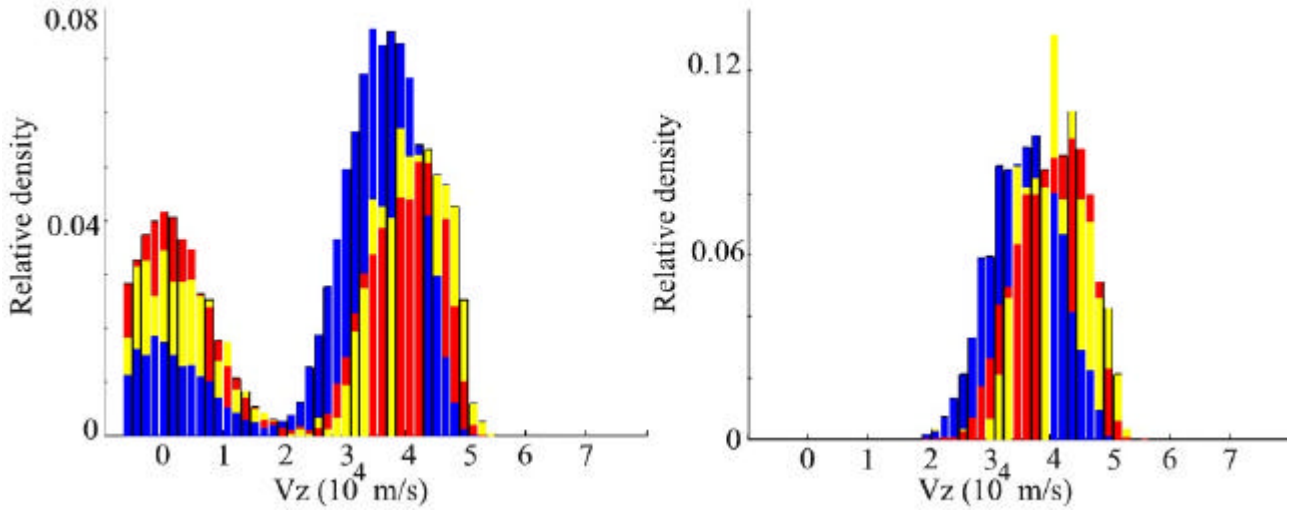

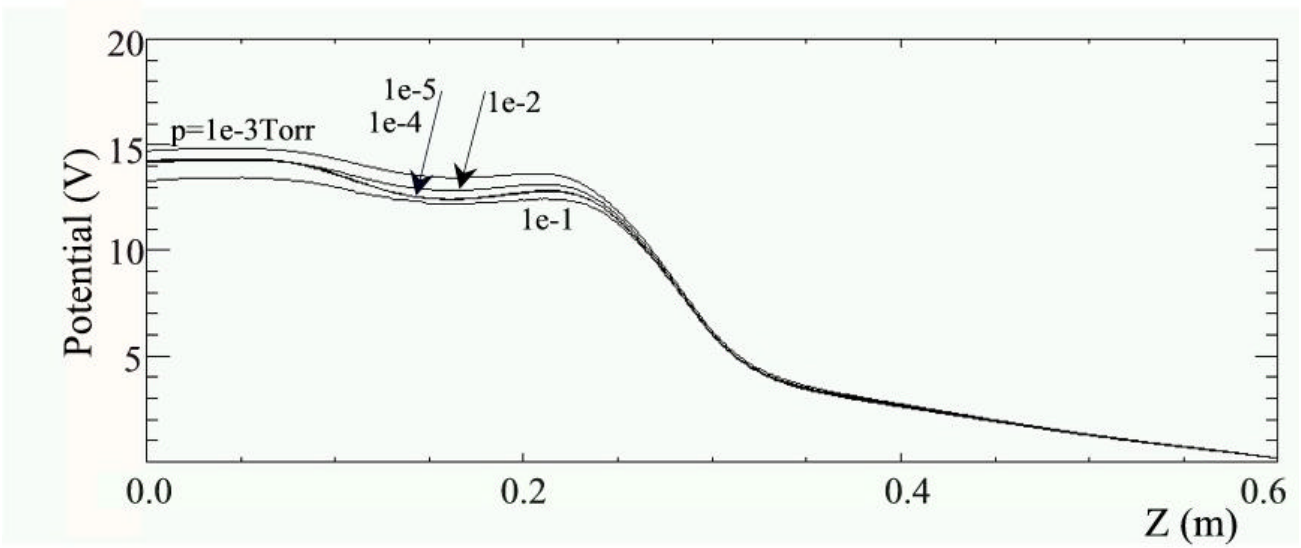

Fig 6.8: Up: Ions relative density as function of the axial velocity and radius, for z=40-45cm (10cm outside the helicon tube). Neutral pressures of 0.1Torr (left) and 0.1mTorr (right). Yellow bars represent the velocities for r=0-2cm, red r=5-8cm and blue r=12-14cm.
Down: Plasma potential after 11μs for five different neutral pressures: 0.01, 0.1, 1, 10 and 100 mTorr.

ESA CONTRACT no.	SUBJECT	CONTRACTOR
Ariadna 05/3201	Numerical Simulations of the Helicon Double Layer Thruster Concept – Final report	CISAS "G. Colombo"

The computed ionization process is therefore underestimated: the ions density is more than two orders of magnitude lower and the neutral pressure which shows a reduction of the potential jump is overestimated of almost the same factor. In fact the potential jump reduction happens for similar values of the Ni x Nn factor

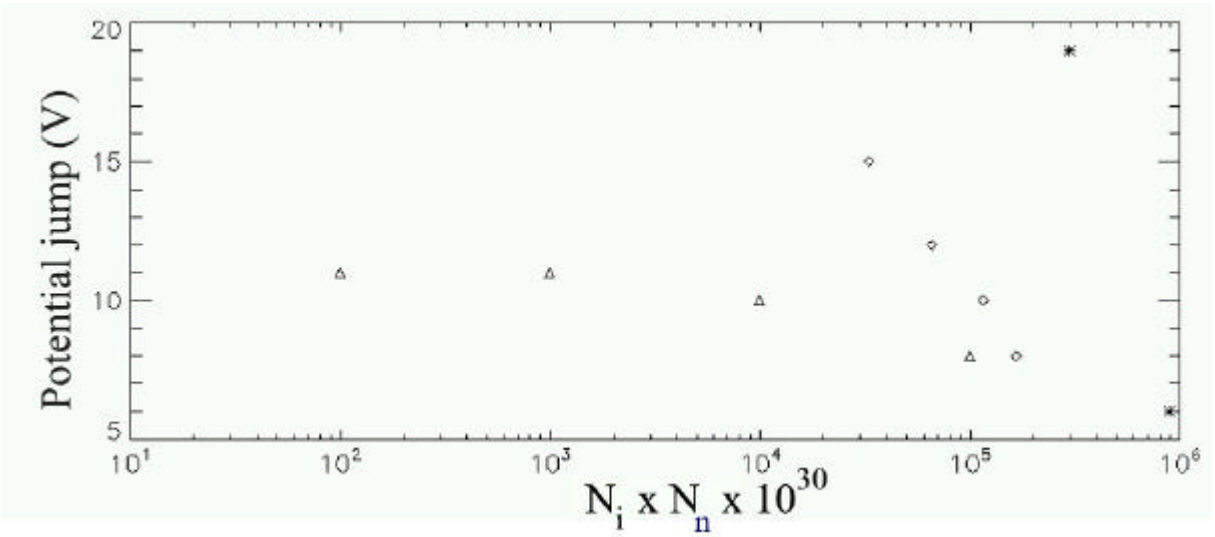

Fig 6.9: Potential jump amplitude as function of the ions times neutral density ratios. The results of the simulations (triangles) are shown together with the Plihon (squares) and Charles (stars) measurements.

6.2 HIGHER SOURCE RATE

Considering a spatial step of 1.2mm the maximum plasma density we can simulate is around $10^{14}m^{-3}$ in order to remain below $?_d$ with our grid dimension. Therefore into the simulations reported above we could increase the plasma production rate and analyze higher densities without changing the simulation scheme. Moreover OOPIC admits to restart a new simulation from the output file of another one that has to have the same dimensions and main border conditions. Inside the file are recorded the particles configuration (positions and velocities) of the old case, which the software will use as starting point for the new calculation. In this way, instead of begin new simulations, we propagated a starting condition increasing the source rate and changing some border conditions or plasma properties. This method saved some hours of computational time.

The diffusion chamber is now made only of grounded conducting walls (the *ExitPort* has been removed) while the dielectrics have ϵ_r=4. The propagations lasted for 6 μs and they started all from the same simulation at t=11μs. The starting condition, which was also propagated for the same 6 μs and then reported as reference case, was the one of the last paragraph except for the dielectric walls that had the

ESA CONTRACT no.	SUBJECT	CONTRACTOR
Ariadna 05/3201	Numerical Simulations of the Helicon Double Layer Thruster Concept – Final report	CISAS "G. Colombo"

accumulation charge property switched on. The propagations have a new source rate which has been set ten times bigger then the one of the last paragraph: 5 10^{18} m^{-3}/s^{-1}.

We have analyzed separately the main plasma parameters and their effects on the potential and ions density. The parameters we have varied are: electrons and ions temperatures, source walls characteristics and plasma production properties.

6.2.1 Ions temperature

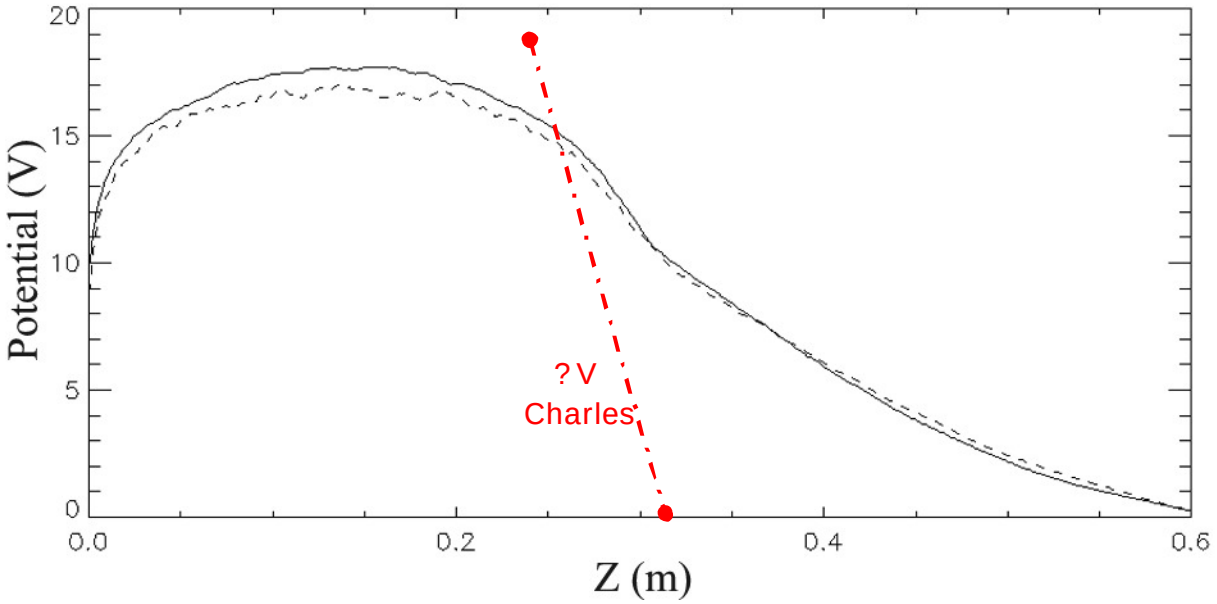

Fig 6.10: Comparison of axial plasma potential for Ti=0.01 and Ti=1 eV (dash). The red arrow represents the width of the potential jump measured by Charles. T_e=6eV final N_{ions}~10^{13} m^{-3}.

Increasing the ions' temperature and remaining below 1 eV, the plasma potential remains almost unchanged, see Figure 6.10. The main effect of this ions temperature enhancing is measured on the particles' axial velocity. Higher temperatures make the ions faster also at radii greater than the source tube. See Figure 6.11.

ESA CONTRACT no.	SUBJECT	CONTRACTOR
Ariadna 05/3201	Numerical Simulations of the Helicon Double Layer Thruster Concept – Final report	CISAS "G. Colombo"

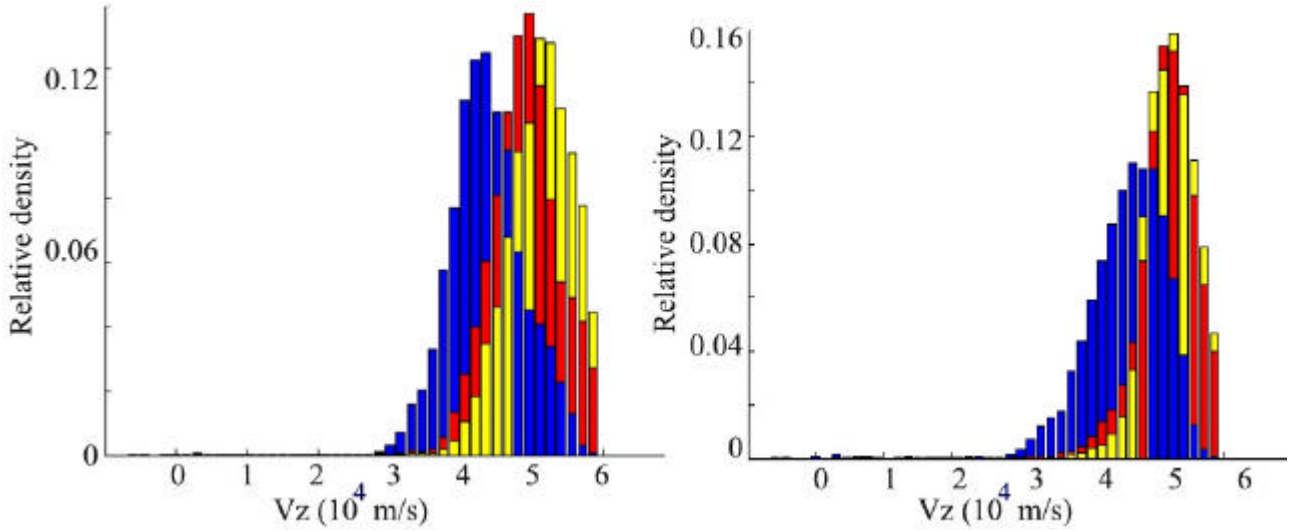

Fig 6.11: Ions relative density as function of the axial velocity, for z=40-45cm (10cm outside the helicon tube) and for Ti=1eV (right) and Ti=0.01eV. Yellow bars represent the velocities for r=0-2cm, red r=5-8cm and blue r=12-14cm.

6.2.2 Electrons temperature

As anticipated by Boswell the electrons temperature is responsible of the potential jump amplitude. Increasing the temperature from 5eV to 9eV the plasma potential inside the helicon tube increases of 5-6 V and the maximum ions axial velocity just downstream the source is enhanced from 5 to 6 10^4 m/s.

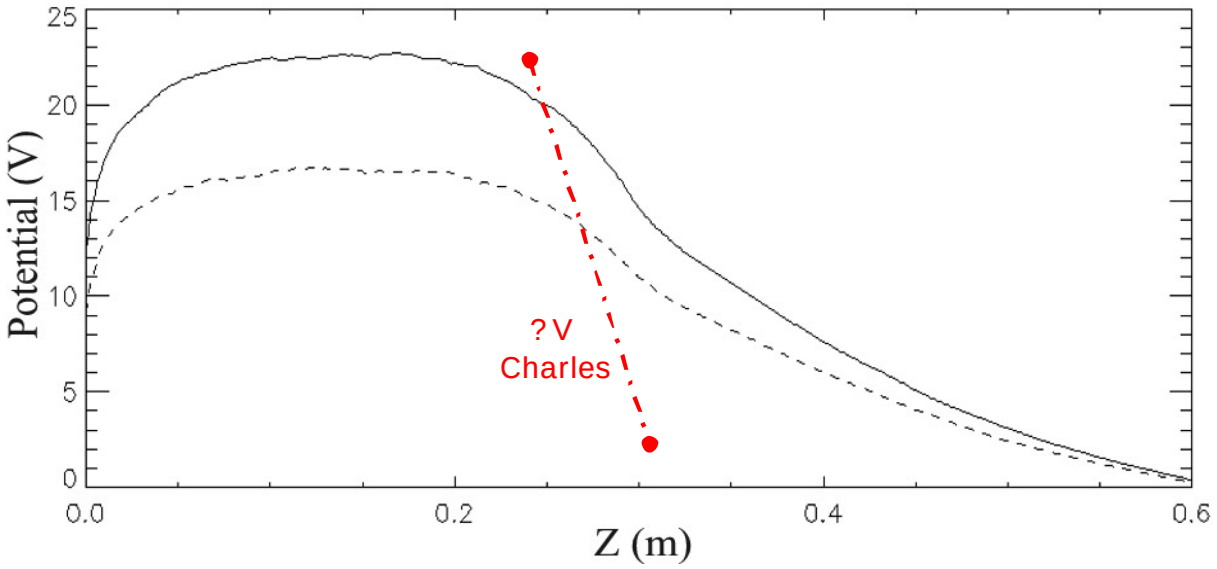

Fig 6.12: Comparison of axial plasma potentials for Te=9 and Te=5 eV (dash). The red arrow represents the width of the potential jump measured by Charles. Final N_{ions}~10^{13} m^{-3}.

ESA CONTRACT no.	SUBJECT	CONTRACTOR
Ariadna 05/3201	Numerical Simulations of the Helicon Double Layer Thruster Concept – Final report	CISAS "G. Colombo"

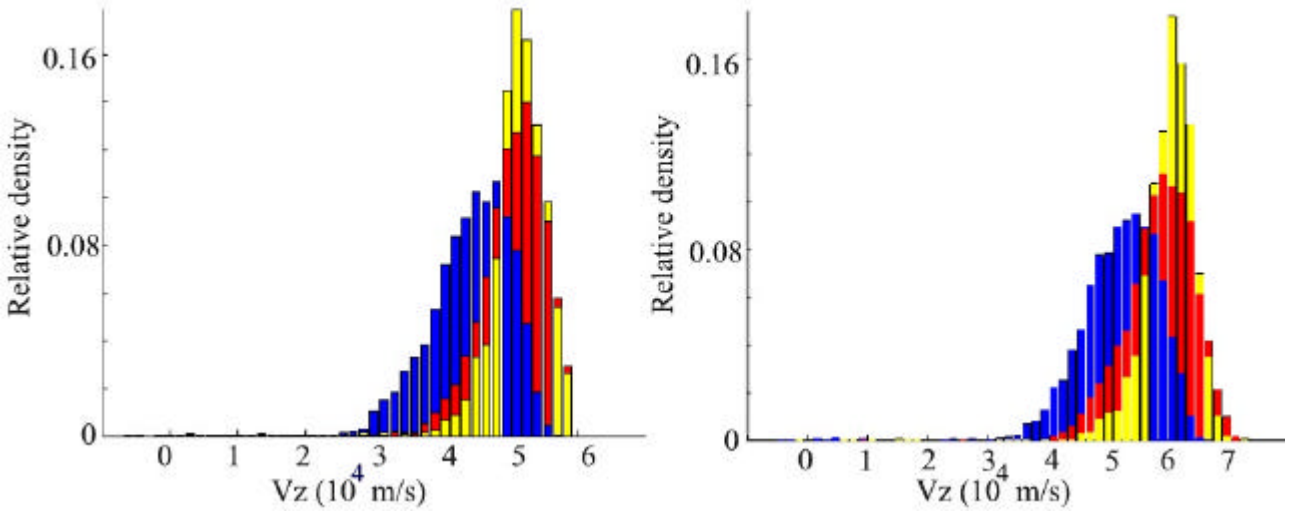

Fig 6.13: Ions relative density as function of the axial velocity, for z=40-45cm (10cm outside the helicon tube) and for Te=5eV (left) and Te=9eV (rigth). Yellow bars represent the velocities for r=0-2cm, red r=5-8cm and blue r=12-14cm.

6.2.3 Plasma production area

During the simulation, plasma is produced inside an area which is schematized in Fig 3.2 and 3.3. Here we have increased and reduced the length of the region where the plasma is produced of 6 cm. It has to be remembered that, as reported by bibliography, varying the magnetic field strength the position where most of the electromagnetic energy is absorbed, so where ionization happens, changes. Therefore this case should be one of the effects of the external magnetic field variation.

The results are shown in Fig 6.14 and 6.15. Enlarging the plasma's source area the potential becomes a little bit deeper, but the main differences concern the axial velocity. With a larger area the ions, just outside the helicon tube, are slower; this because a lot of particles are created downstream the potential jump and they can not be accelerated.

ESA CONTRACT no.	SUBJECT	CONTRACTOR
Ariadna 05/3201	Numerical Simulations of the Helicon Double Layer Thruster Concept – Final report	CISAS "G. Colombo"

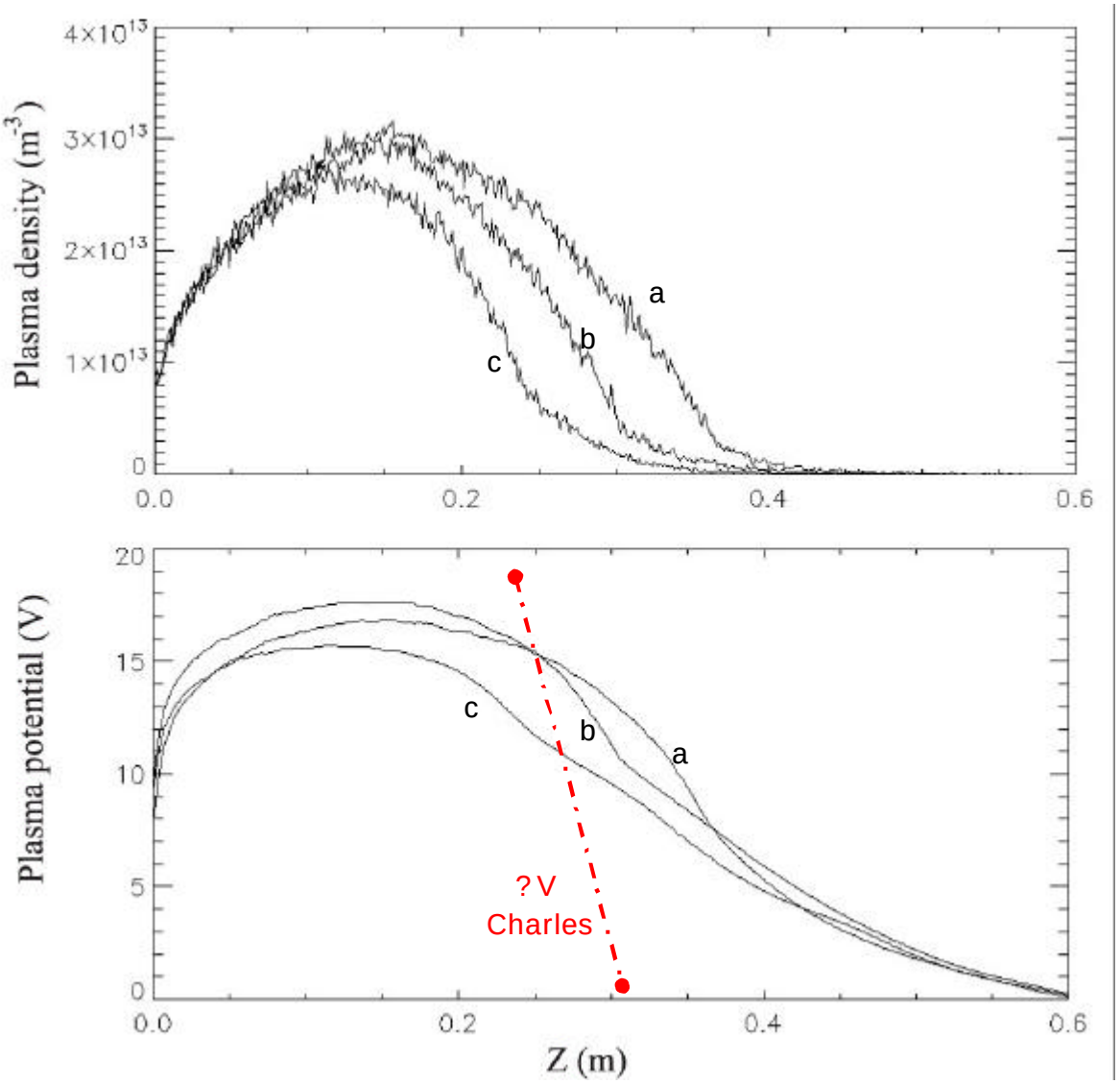

Fig 6.14: Ions plasma axial density and potential for large (a) and thin (c) plasma source regions, compared with the reference case (b). The red arrow represents the width of the potential jump measured by Charles. T_e=6eV final N_{ions}~10^{13} m^{-3}.

6.2.4 DC biased left wall and source tube length

As anticipated by the low density simulations the dc biased left wall can increase the plasma potential if its potential is fixed to a sufficiently high value. From Fig 6.17 we see that also the ions velocity is increased.

ESA CONTRACT no.	SUBJECT	CONTRACTOR
Ariadna 05/3201	Numerical Simulations of the Helicon Double Layer Thruster Concept – Final report	CISAS "G. Colombo"

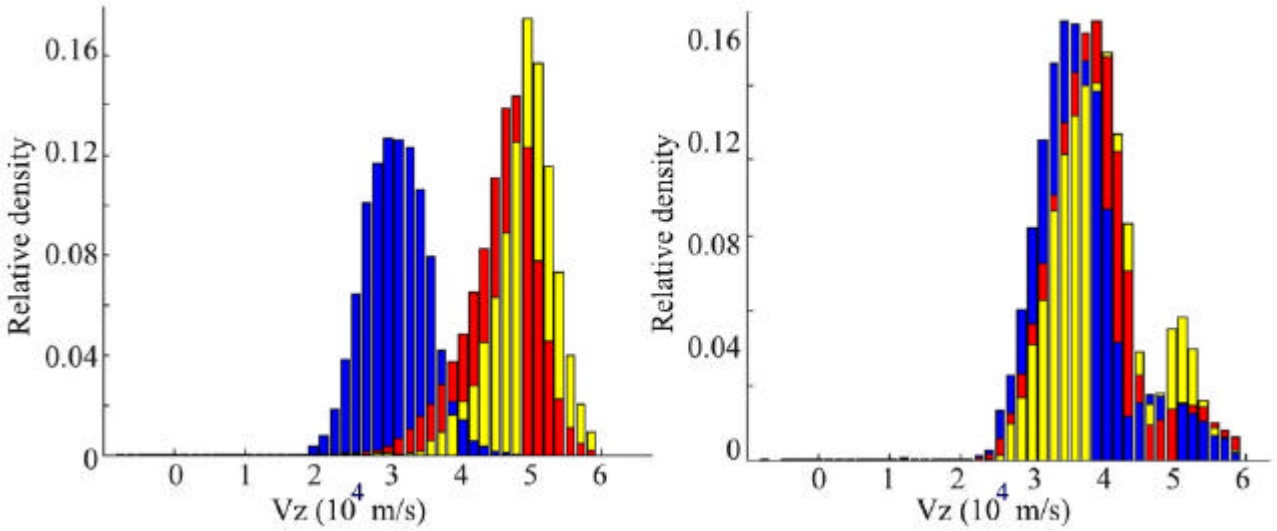

Fig 6.15: Ions relative density as function of the axial velocity, for z=40-45cm (10cm outside the helicon tube) and for large (right) and thin (left) plasma source areas. Yellow bars represent the velocities for r=0-2cm, red r=5-8cm and blue r=12-14cm.

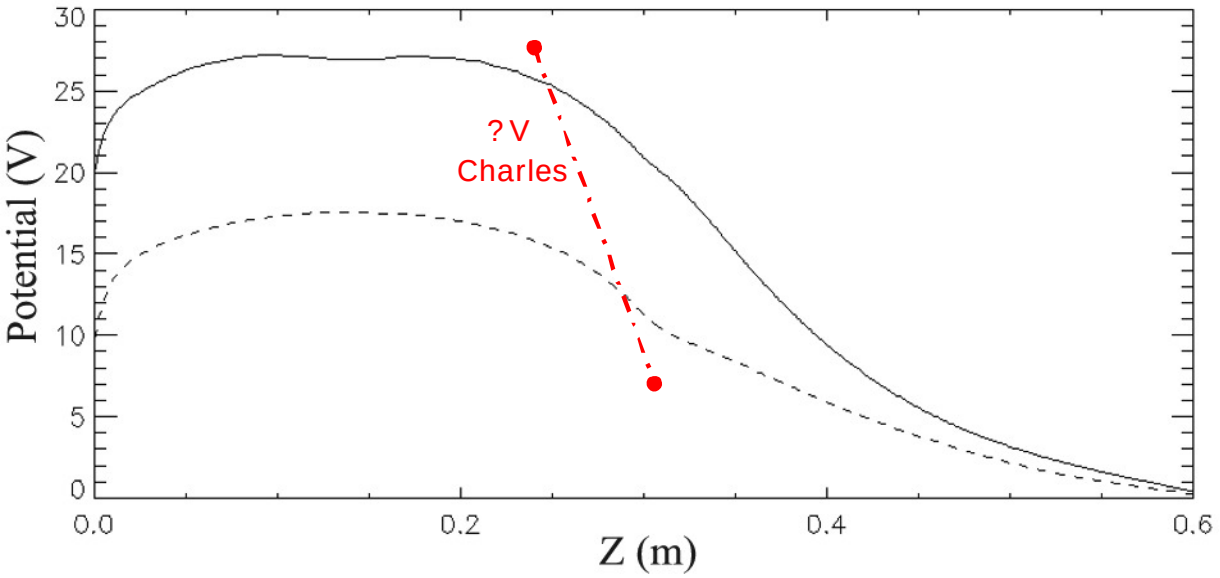

Fig 6.16: Axial plasma potential for 20V dc biased left wall (dash) and dielectric source wall. The red arrow represents the width of the potential jump measured by Charles. T_e=6eV final N_{ions}~10^{13} m^{-3}.

ESA CONTRACT no.	SUBJECT	CONTRACTOR
Ariadna 05/3201	Numerical Simulations of the Helicon Double Layer Thruster Concept – Final report	CISAS "G. Colombo"

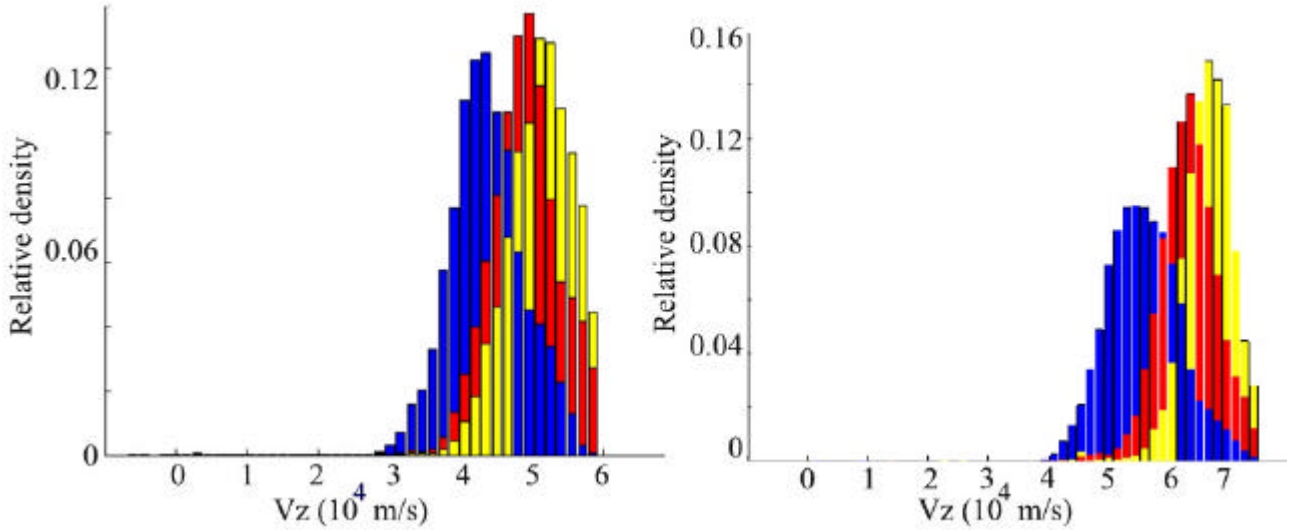

Fig 6.17: Ions relative density as function of the axial velocity, for z=40-45cm (10cm outside the helicon tube) and for 20V dc bias left wall (right) and reference case (left). Yellow bars represent the velocities for r=0-2cm, red r=5-8cm and blue r=12-14cm.

For the same case we have then increased the length of the dielectric tube (the dielectric up source wall) and the ions trajectories appear less divergent (Figure 6.18).

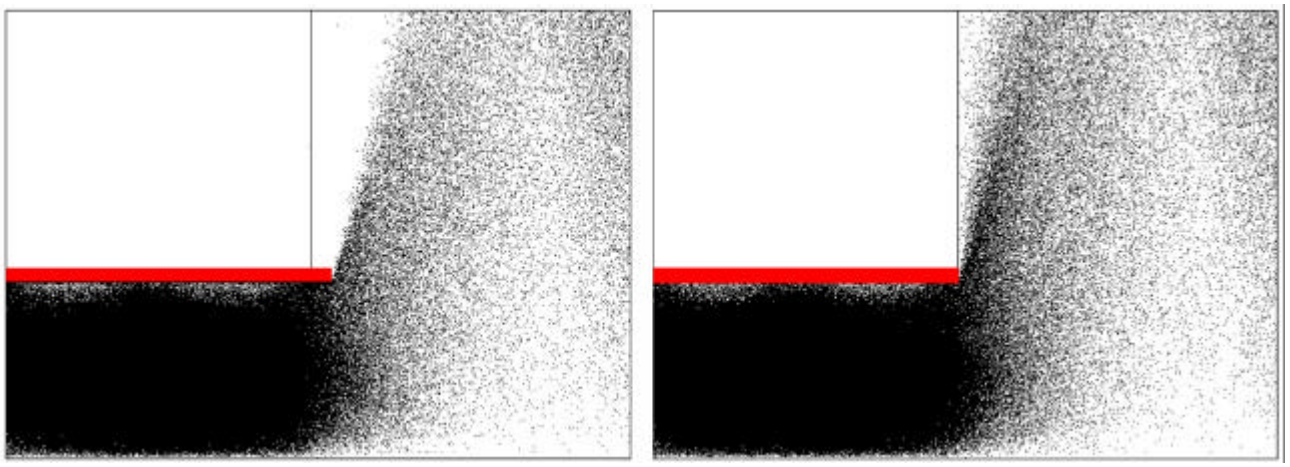

Fig 6.18: Ions trajectories for 20V dc bias left wall (left) and the same case but with a 2cm longer dielectric tube (right).

ESA CONTRACT no.	SUBJECT	CONTRACTOR
Ariadna 05/3201	Numerical Simulations of the Helicon Double Layer Thruster Concept – Final report	CISAS "G. Colombo"

7 OOPIC DENSER GRID SIMULATIONS

7.1 HIGH DENSITY

Trying to increase the plasma production rate we have halved the spatial step in order to allow a plasma density higher than $10^{14}m^{-3}$, which was the limit we had. In this way our grid dimension remains again below $?_d$ for higher densities. The nodes number goes from 128x512 to 256x1024 because using the *MultiGrid* solve they have to be $2^N X 2^M$.
As first step we have reproduced the reference simulation of Paragraph 6.1 in order to check the computational speed and compare the results with the case of sparser grid; as shown in Fig 7.1 non significant discrepancies have been met. The computation time grows with a factor around 4, it takes almost 3 days to have a simulation of 20 μs.

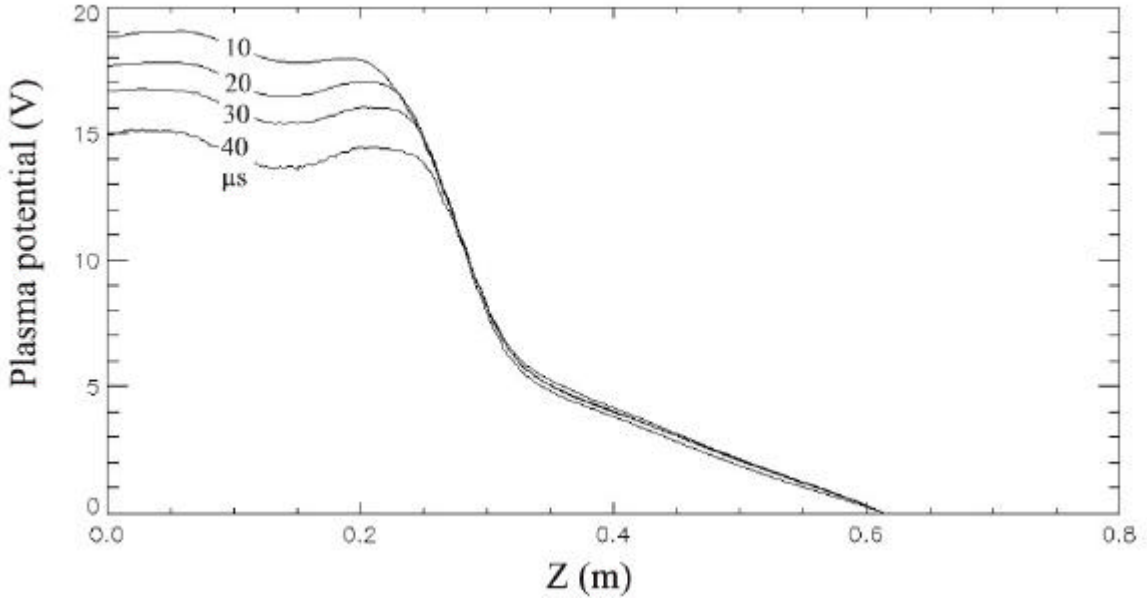

Fig 7.1: Reproduction of the low density simulation of the unconfined plasma with halved cells' length.

ESA CONTRACT no.	SUBJECT	CONTRACTOR
Ariadna 05/3201	Numerical Simulations of the Helicon Double Layer Thruster Concept – Final report	CISAS "G. Colombo"

The electrons temperature has been set at 6eV while ions at 0.01eV. We have simulated the most interesting cases: source tube completely made of dielectric and conducting DC biased left walls.
Using a dielectric source tube and source rate of $10^{20}m^{-1}s^{-1}$ the density does not reach a constant value. The potential becomes instable and almost disappears after 10μs, but this should be due to the plasma density which grows above the limit imposed by our grid dimension. In fact for densities around 8 10^{14} m^{-3} $?_d$ is higher than our cell length, so the simulation can not work properly. See Fig 7.2.

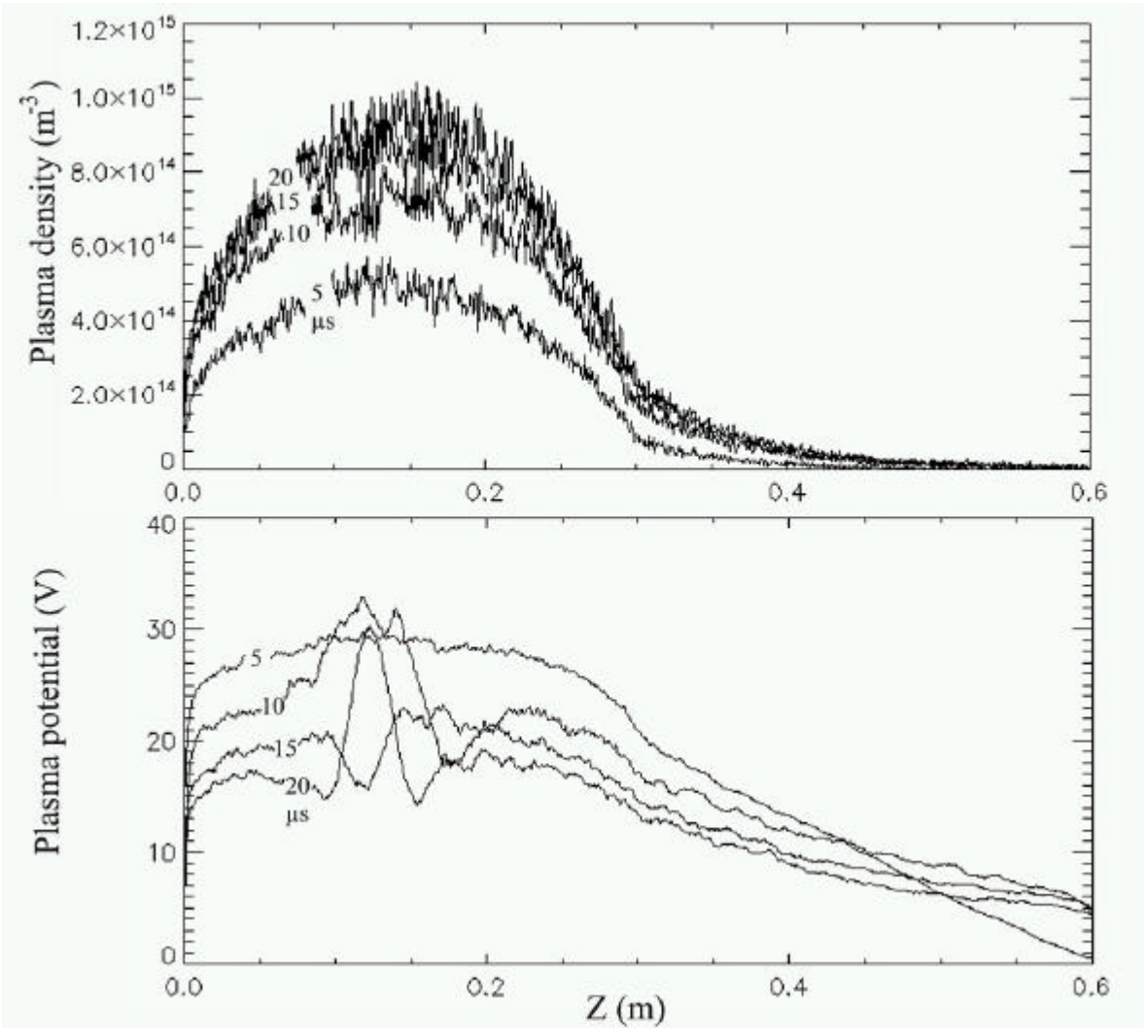

Fig 7.2: Ions plasma axial density and potential for source walls made of dielectrics with e_r=1, halved cell dimension and increased source rate at $10^{20}m^{-3}s^{-1}$. The potential becomes unstable due to the high plasma density which grows above the limit imposed by $?_d$ and our cell dimension.

ESA CONTRACT no.	SUBJECT	CONTRACTOR
Ariadna 05/3201	Numerical Simulations of the Helicon Double Layer Thruster Concept – Final report	CISAS "G. Colombo"

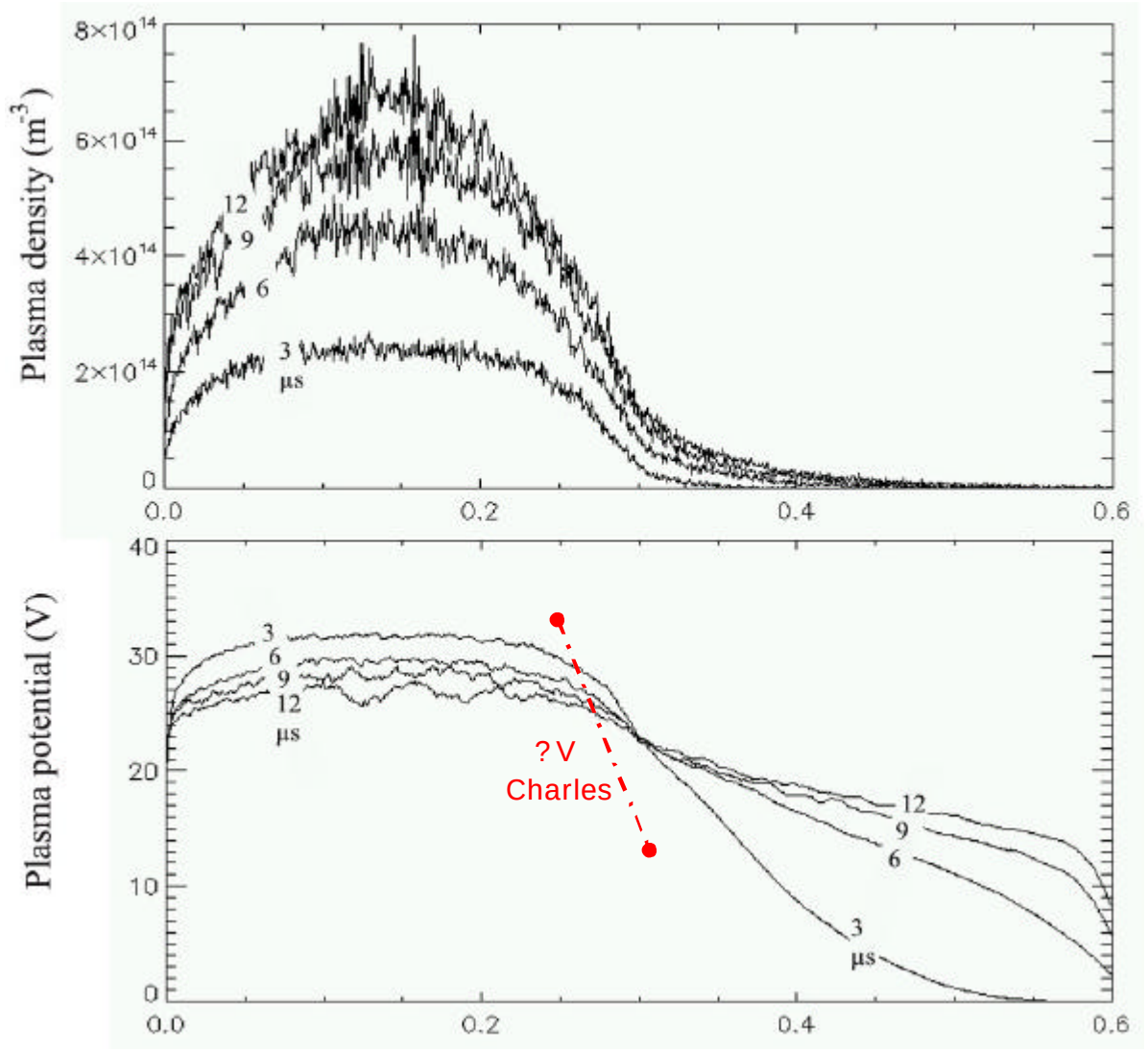

Fig 7.3a: Axial plasma ions density and potential for the 20V dc biased left wall and true dielectric as up source wall with e_r=4. Halved cell dimension. Source rate is $8\,10^{19} m^{-3}s^{-1}$. Below a zoom for t=12μs. The red arrow represents the width of the potential jump measured by Charles.

ESA CONTRACT no.	SUBJECT	CONTRACTOR
Ariadna 05/3201	Numerical Simulations of the Helicon Double Layer Thruster Concept – Final report	CISAS "G. Colombo"

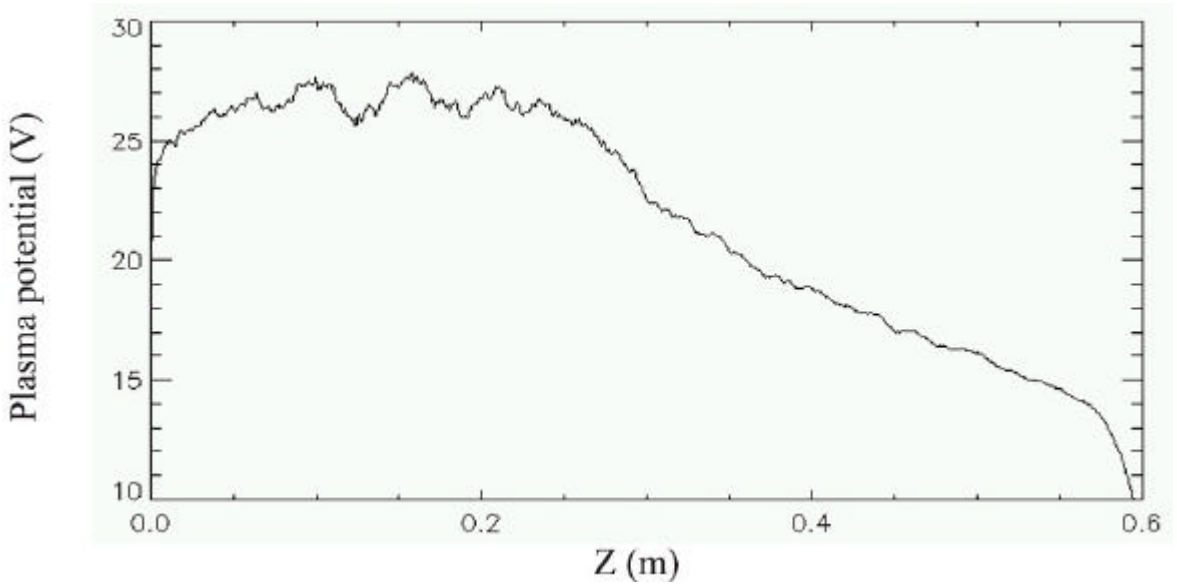

Fig 7.3b: Axial plasma potential, zoom for t=12μs of the picture above. 20V dc biased left wall and true dielectric as up source wall with e_r=4. Source rate is $8\,10^{19} m^{-3} s^{-1}$.

The simulations have been repeated changing the plasma generation rate and the source wall properties. In particular we gradually reduced the particles creation rate to find a stable configuration. The results are reported in Figure 7.3 – 7.6 and in Figure 7.8 the potential is compared with the experimental data. With a source rate of $8\,10^{19}$ m^{-3} s^{-1} the density does not stop to grow for a conducting left wall biased of 20V (see Figure 7.3) and the same happens for the 30V case (Figure 7.4). Reducing the source rate from $8\,10^{19}$ to 10^{19} m^{-3} s^{-1} the density starts to decrease (Figure 7.5) showing that the rate which comports a stable density has to bee between these two values.
Finally the simulation have been repeated with a source rate of $2\,10^{19}$ $m^{-1}s^{-1}$, this value gives a plasma density almost stable and around $5\,10^{14}$ m^{-3} , see Figure 7.7. In general it appears that the potential jump is smooth and not as deep as during the experiments.

ESA CONTRACT no.	SUBJECT	CONTRACTOR
Ariadna 05/3201	Numerical Simulations of the Helicon Double Layer Thruster Concept – Final report	CISAS "G. Colombo"

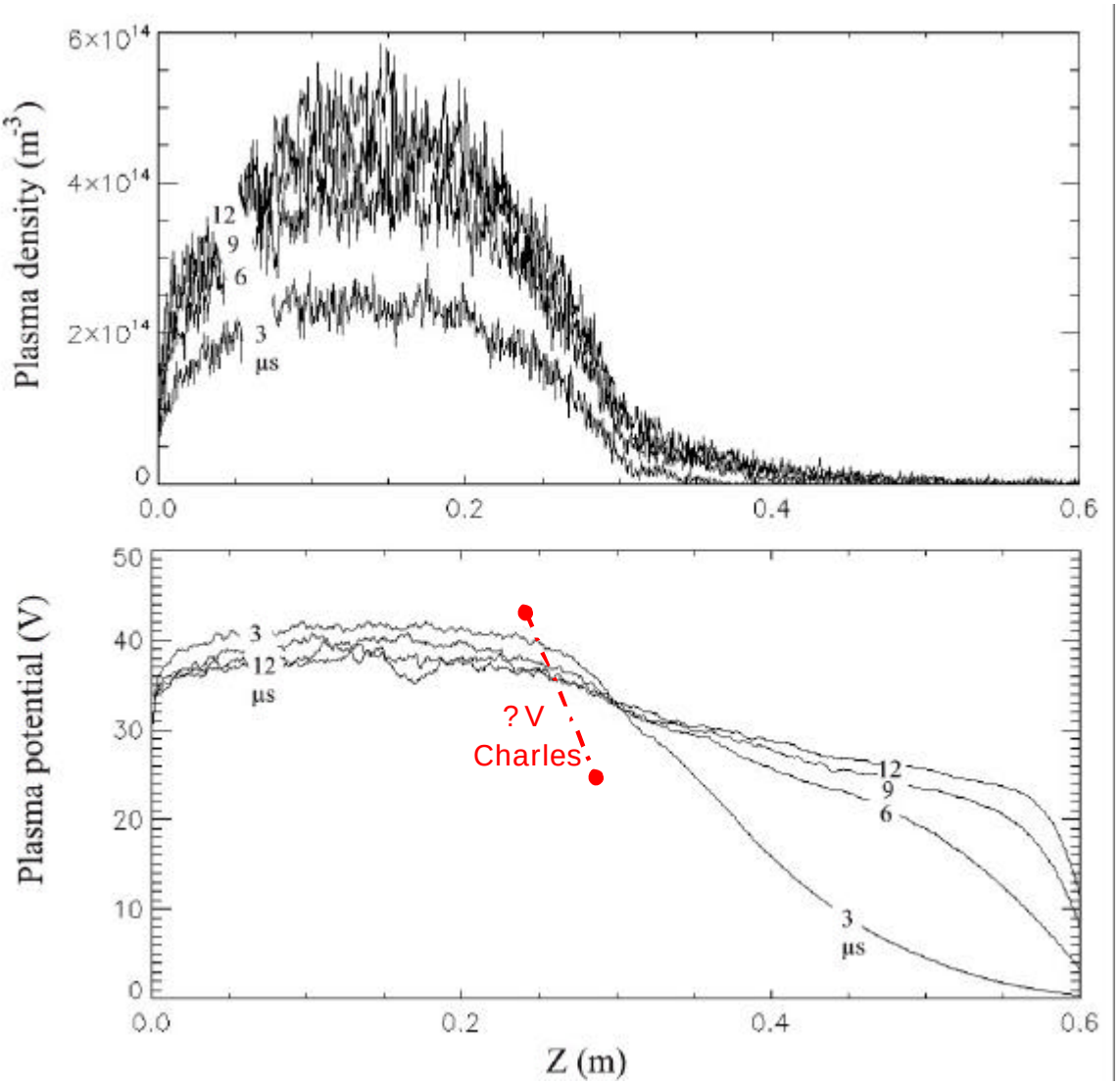

Fig 7.4: Axial plasma ions density and potential for the 30V dc biased left wall and true dielectric as up source wall with e_r=4. Halved cell dimension and source rate of 8 10^{19}m^{-3}s^{-1}. The red arrow represents the width of the potential jump measured by Charles.

ESA CONTRACT no.	SUBJECT	CONTRACTOR
Ariadna 05/3201	Numerical Simulations of the Helicon Double Layer Thruster Concept – Final report	CISAS "G. Colombo"

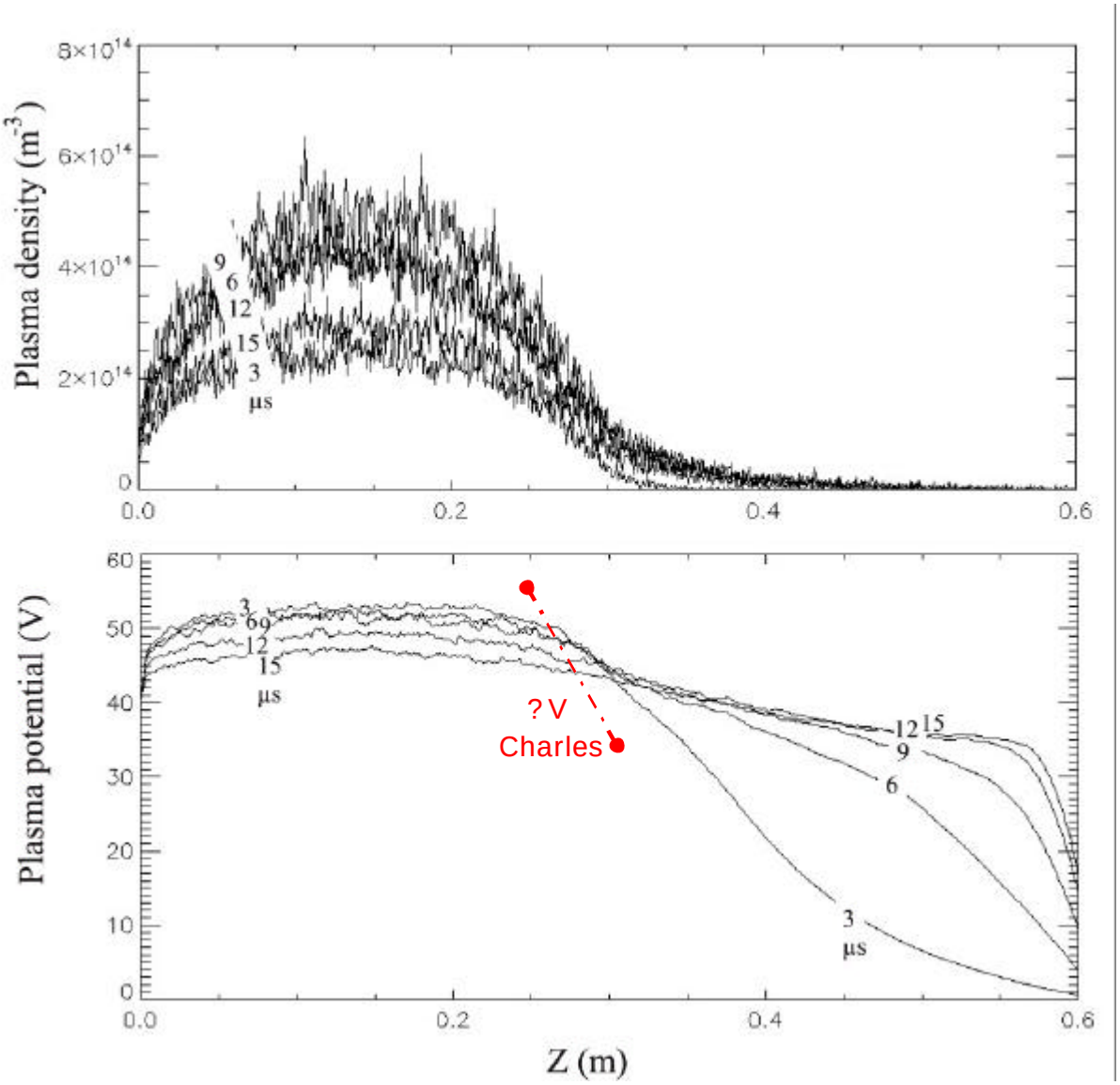

Fig 7.5: Axial plasma ions density and potential for the 40V dc biased left wall and true dielectric as up source wall with e_r=4. Halved cell dimension and source rate of $8\,10^{19} m^{-3} s^{-1}$ for the first 10µs and 10^{19} after. The red arrow represents the width of the potential jump measured by Charles.

ESA CONTRACT no.	SUBJECT	CONTRACTOR
Ariadna 05/3201	Numerical Simulations of the Helicon Double Layer Thruster Concept – Final report	CISAS "G. Colombo"

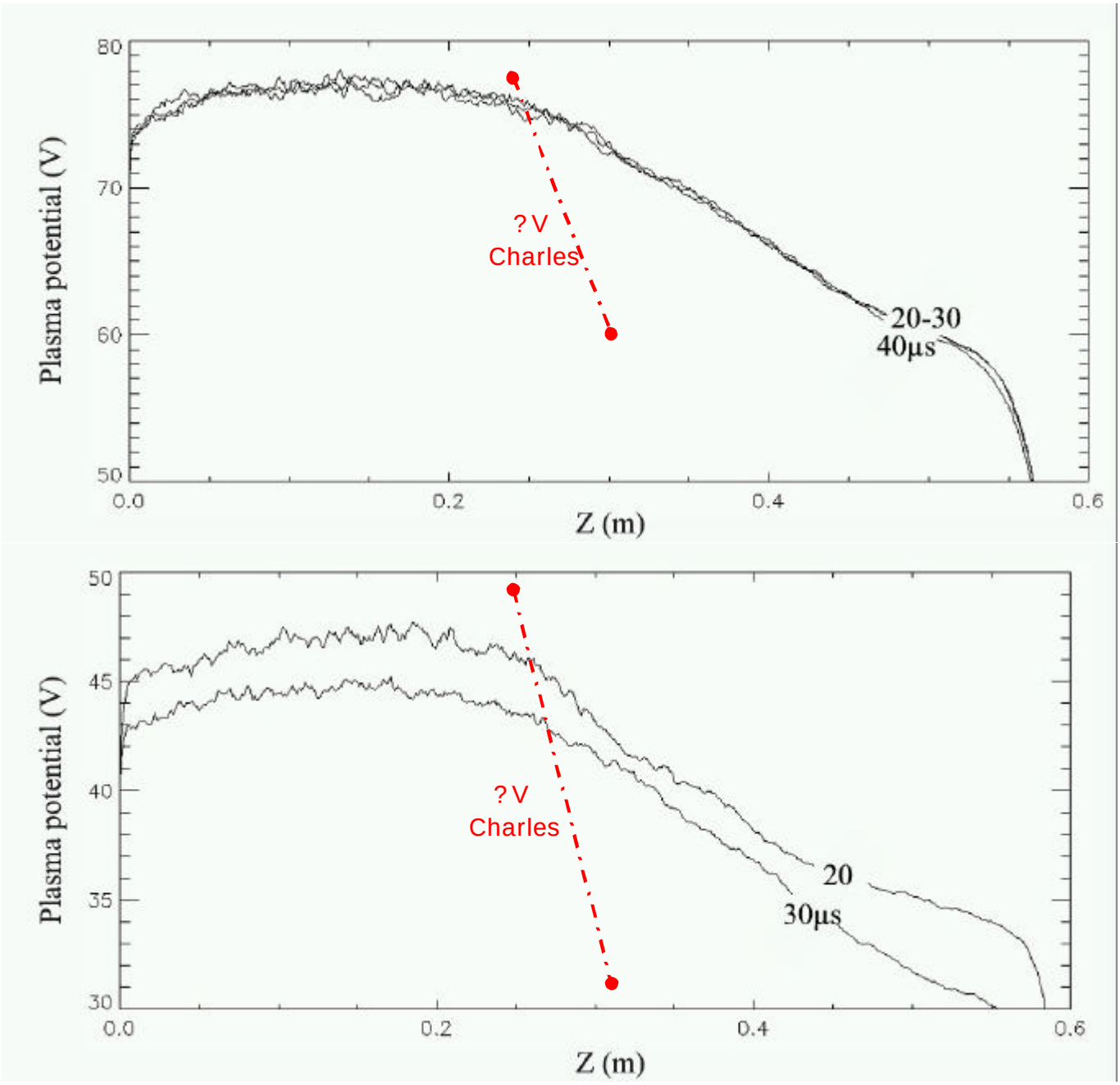

Fig 7.6: Plasma potential for 40 (up) and 70 (down) V DC biased conducting left walls and halved cell dimension. The simulations are made with a plasma production rate of 2 10^{19} $m^{-3}s^{-1}$ which gives a constant plasma density inside the source tube around 5 10^{14} m^{-3}. The red arrow represents the width of the potential jump measured by Charles.

ESA CONTRACT no.	SUBJECT	CONTRACTOR
Ariadna 05/3201	Numerical Simulations of the Helicon Double Layer Thruster Concept – Final report	CISAS "G. Colombo"

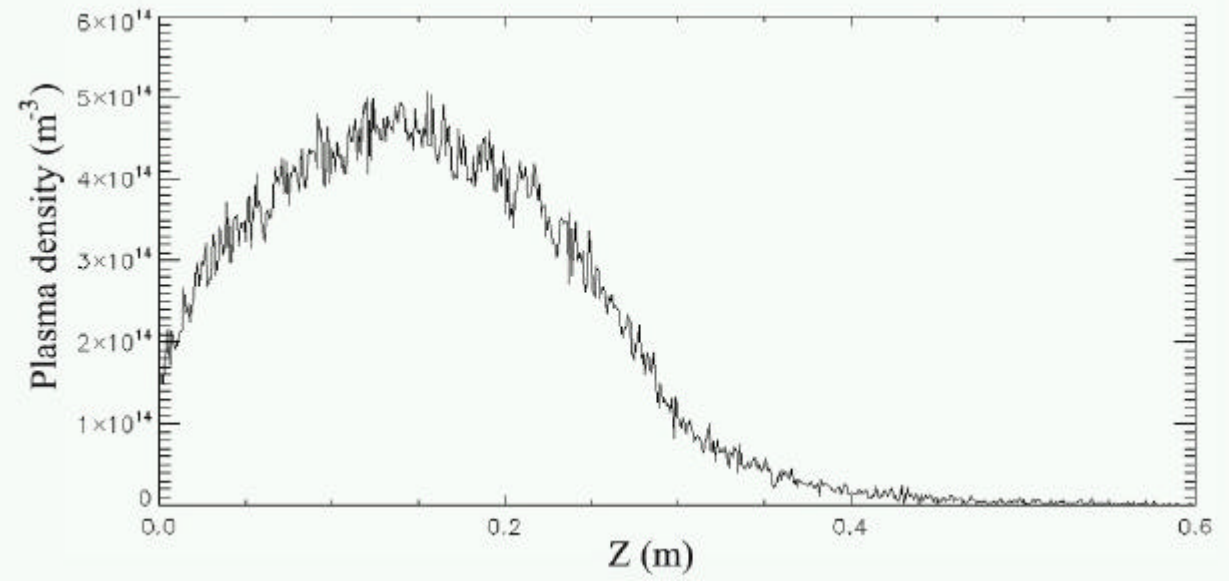

Fig 7.7: Axial plasma density for the case with source rate of 2 10^{19} $m^{-3}s^{-1}$ and 70V conducting dc biased left wall. After 15μs the density remains almost constant.

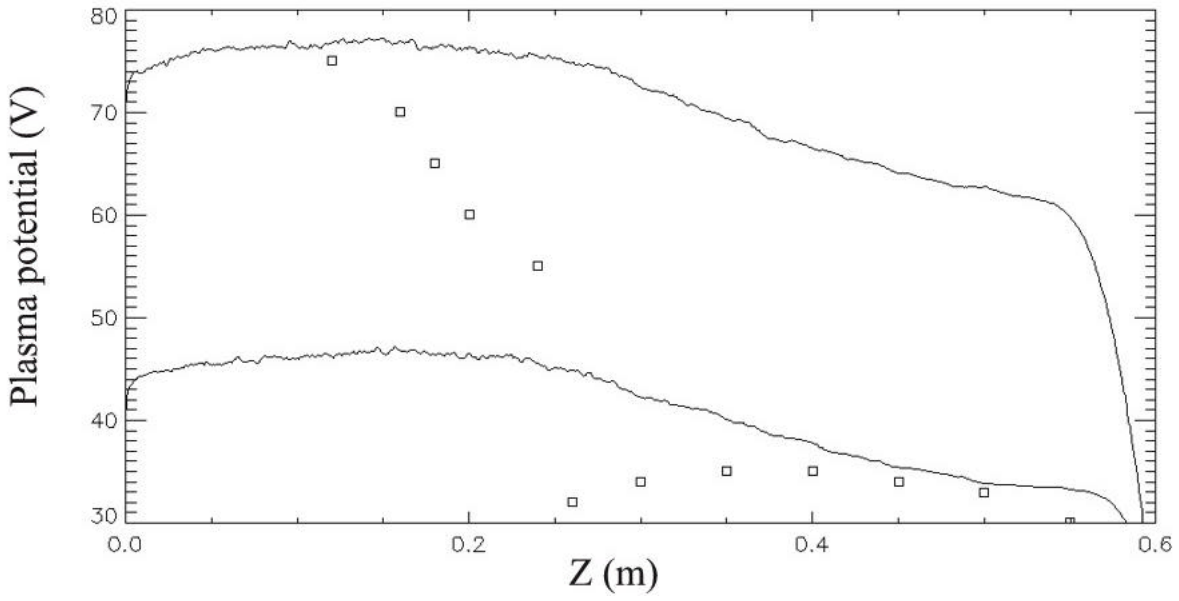

Fig 7.8: Potential of the 40 and 70 DC biased left wall simulations after 22μs compared with the measurements made by Charles (squares).

ESA CONTRACT no.	SUBJECT	CONTRACTOR
Ariadna 05/3201	Numerical Simulations of the Helicon Double Layer Thruster Concept – Final report	CISAS "G. Colombo"

7.2 LONGER DIFFUSION CHAMBER

To evaluate the performances in space and the ions detachment we have increased the chamber dimension by maintaining the node numbers of Sec 7.1 (the denser grid of 256x1024) and increasing the spatial step (returning to the value of 1.2mm of Sec 7.1). In this way we obtained a expanding chamber 1.2 m long. The best OOPIC configuration to simulate out space can be obtained by substituting the grounded walls with *ExitPorts*. The simulations started to diverge after 15-20 μs, therefore we repeated the calculations with a diffusion chamber having grounded conducting walls. It is also necessary to neglect the neutral pressure inside the expanding chamber. The plasma ions are again H because with Ar the sound speed decreases too much and the time necessary to fill the diffusion chamber is prohibitively high.
To evaluate the detachment from the magnetic field lines we have analyzed the ions' trajectories inside the diffusion chamber. The particle velocity is curvilinear until the magnetic field acts on it, after a certain distance from the source the trajectory starts to be almost rectilinear, there we can suppose the detachment takes place. From the next picture we can argue that the detachment is function of the radius and it happens not before z of 0.7 and 1.2 m respectively for r=0 and 15 cm, so at a distance between 0.4 and 0.8 m from the source tube.

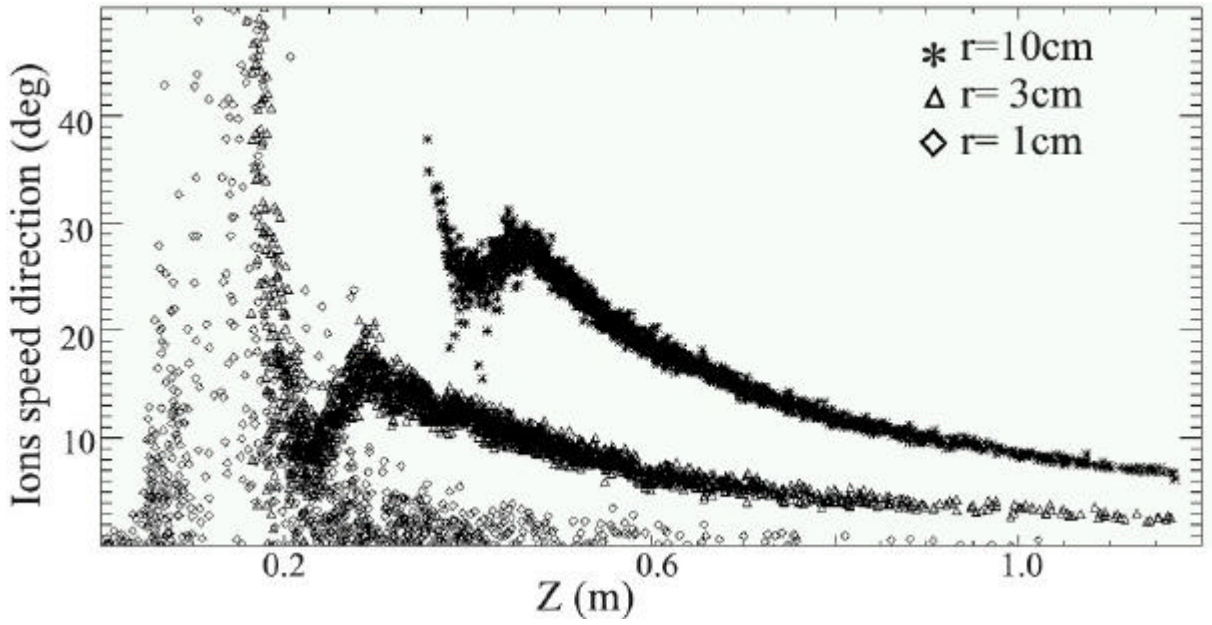

Fig 7.9: Ions speed direction inside the diffusion chamber for r between 1 and 10 cm. The trajectories are almost rectilinear after 0.7, 1 and 1.2 meters respectively for r=1, 3 and 10cm. The detachment should happen there.

ESA CONTRACT no.	SUBJECT	CONTRACTOR
Ariadna 05/3201	Numerical Simulations of the Helicon Double Layer Thruster Concept – Final report	CISAS "G. Colombo"

7.3 THRUST AND SPECIFIC IMPULSE EVALUATION

The thrust is evaluated by means of the formula $T=m\ N\ V_a^2 A$ iterated for every r_i along the supposed detachment line:

$$T = \sum_{i=1}^{Nm} m \cdot N_i^{\det} \cdot (Va_i^{\det})^2 \cdot A_i$$

and where:

m is the ion mass
N is the density of ions inside the detachment cell at radius r_i
Va is the average axial velocity inside the detachment cell
A is the cross surface of the cell revolution along $f = p\ [(r_i+dr)^2-r_i^2]$
N_m is the number of cells along the radius

Thrust and specific impulse have been calculated for 4 detachment lines, that are represented in Figure 7.10, defined as the positions where, at a particular r, the ions' speed direction changes of almost 2 (lines 1 and 2), 6 (line 3), and 8° (line 4) for higher z.
For all the cells that follow the selected line, we have evaluated the ions' density, which is a default output of OOPIC, and the average ions' axial velocity. The results are reported in Table 7.1, that is an average of three simulations made with Te=8eV, 70V dc bised left wall and diffusion chambers represented by *ExitPorts* or grounded *Equipotential*. The simulations we made reached a density, inside the source tube, around $5\ 10^{13}\ m^{-3}$, the source rate has been set between 10^{18} and $3\ 10^{18}\ m^{-3}\ s^{-1}$.

ESA CONTRACT no.	SUBJECT	CONTRACTOR
Ariadna 05/3201	Numerical Simulations of the Helicon Double Layer Thruster Concept – Final report	CISAS "G. Colombo"

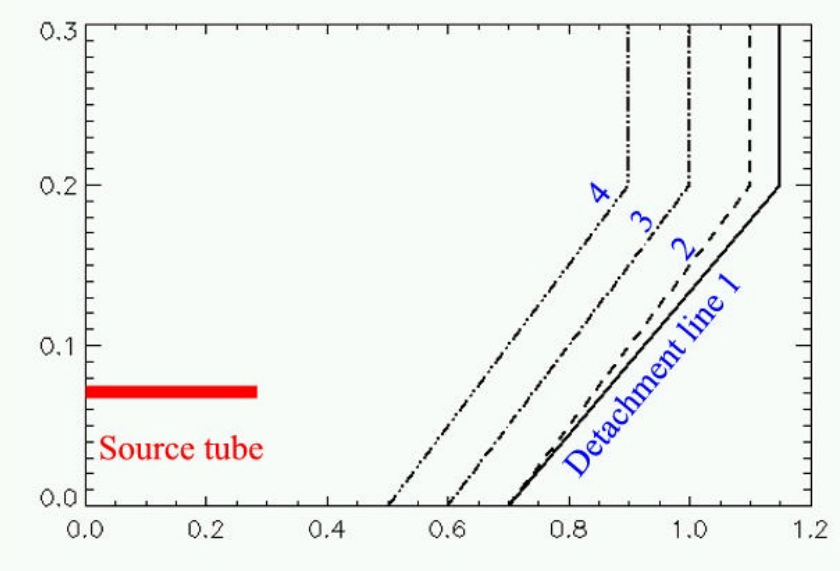

Fig 7.10: Detachment lines adopted for the thrust evaluation

The specific impulse (Is) can be calculated by means of the following formula, where *g* is gravitational acceleration:

$$I_S = \frac{\sum_{i=1}^{N_m} N_i^{\det} \cdot Va_i^{\det}}{\sum_{i=1}^{N_m} N_i^{\det}} \frac{1}{g}$$

Detachment line	Ions	Specific Impulse (s)	Thrust (N)
1	H	~2800	~2E-9
2	H	~2900	~3E-9
3	H	~3600	~7E-9
4	H	~4000	2E-8

Table 7.1: Thrust performance as function of the detachment line, computed as average of three simulations with same geometry and Te=8eV but different electrical properties of the diffusion chamber and dc biased of 70V. Final N_{ions}~5 10^{13} m^{-3}.

ESA CONTRACT no.	SUBJECT	CONTRACTOR
Ariadna 05/3201	Numerical Simulations of the Helicon Double Layer Thruster Concept – Final report	CISAS "G. Colombo"

8 PPDL RESULTS

results.xls is a summary of all the simulations done.

Description of reports.xls

In this file useful simulations data are reported.
The first two columns identify the simulation: first column DIR represents the directory where the simulation is stored, while in the second column FILE the simulation input filename is presented.
The other columns report some simulation characteristics.
In the following table, each column ID and its meaning are presented, and, if present, the correspondent variable name stored in the input file is reported.

COLUMN ID	DESCRIPTION	INPUTFILE VARIABLE
lg	System Length	length
sr	Source Rate	Srate
time	Simulation Time Length	Time
ned	Initial particle density	Ne
te	Electron Temperature in eV	Te
ti	Ion Temperature in eV	Ti
mi	Ion Mass	Mi
fix	FIXED-FIXED case Flag [1=fixfix, 0=fixflo]	fixfix
dcb0	Left boundary DCBIAS - for FIXED-FIXED case only	dcb0
dcbN	Right boundary DCBIAS - for FIXED-FIXED case only	dcbN
iw0	Coil 0 current per wire	iw0
iw1	Coil 1 current per wire	iw1
Bconf	Magnetic configuration [A or C][1]	--
dir	Direction of main plasma flow	--
Vmax	Maximum value of Potential (V)	--
? v	Potential damp (V)	--
? s	Potential damp width	--
M	Mach number	--

1 See text explanation

Det	Detachment occurrence	--
Note	Notes on simulation configuration / results	--
dv %	Potential damp percentage with respect to potential maximum	--
c_s	Ion Bohm Velocity	--
Ion beam Isp	Ion beam Specific Impulse	--

c_s is calculated as

$C_s = \sqrt{1.67\,10^{-19} T_e / m_i}$

where T_e is the electron temperature and m_i is the ion mass.

The Ion beam Isp is calculated as

$I_{sp} = M \cdot c_s / g$

where M is the Mach number, c_s is the Ion Bohm velocity and g is 9,806645 m/s^2.

n the follow explanation we put two letters before the name of every simulation to specify the directory where is contained.

every simulation has a report in .pdf format with all the significant data: (DESCRIZIONE)

8.1 IONS AND ELECTRON TEMPERATURES

As expected the maximum potential is increased by the temperature due to sheath effect: as shown in the figure 8.1.1 where:

MAlongtime3: Te=Ti=60 eV
MAlongtime4: Te=10 Ti=10 eV
MAlongtime6: Te=100 Ti=1 eV
MAlongtime7: Te=60 Ti=1 eV
MAlongtime8: Te=30 Ti=1 eV
MAlongtime9: Te=10 Ti=1 eV
MAlongtime5: Te=6 Ti=.1 eV

The ratio between Δv and V_max increase with V_max, so it seems that some advantage can derive increasing the temperature. A larger difference between electron and ion temperature increases the potential drop as in Fig 8.1.2, where we use MAlongtime3: Te=Ti=60 eV and MAlongtime7: Te=60eV Ti=1 eV.

ESA CONTRACT no.	SUBJECT	CONTRACTOR
Ariadna 05/3201	Numerical Simulations of the Helicon Double Layer Thruster Concept – Final report	CISAS "G. Colombo"

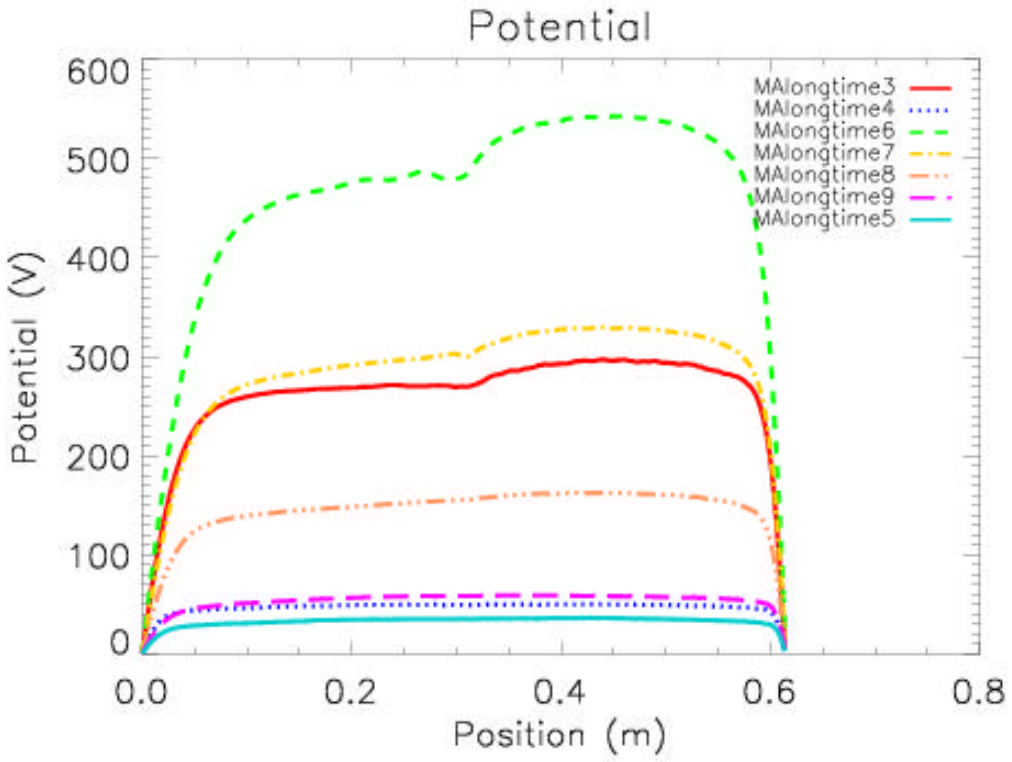

Fig. 8.1.1 - Comparison for several temperature of the same system: MAlongtime3: Te=Ti=60 eV MAlongtime4: Te=10 Ti=10 eV MAlongtime6: Te=100 Ti=1 eV MAlongtime7: Te=60 Ti=1 eV MAlongtime8: Te=30 Ti=1 eV MAlongtime9: Te=10 Ti=1 eV MAlongtime5: Te=6 Ti=.1 eV

ESA CONTRACT no.	SUBJECT	CONTRACTOR
Ariadna 05/3201	Numerical Simulations of the Helicon Double Layer Thruster Concept – Final report	CISAS "G. Colombo"

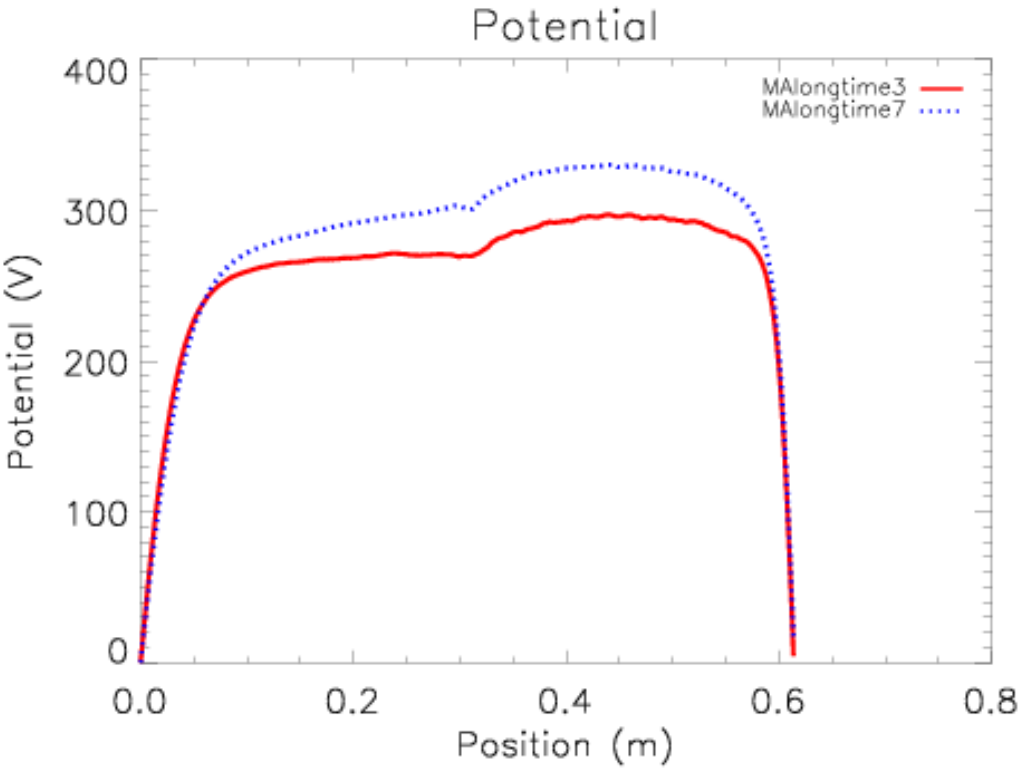

Fig. 8.1.2 - Comparison for different ion temperature of the same system: MAlongtime3: Te=Ti=60 eV and MAlongtime7: Te=60eV Ti=1 eV.

8.2 MAGNETIC FIELD COIL CONFIGURATION

We used two different configuration of magnetic field: the first one (C) uses line without inversion, with a long solenoid also in the expansion camera as shown in Fig 8.2.1.

ESA CONTRACT no.	SUBJECT	CONTRACTOR
Ariadna 05/3201	Numerical Simulations of the Helicon Double Layer Thruster Concept – Final report	CISAS "G. Colombo"

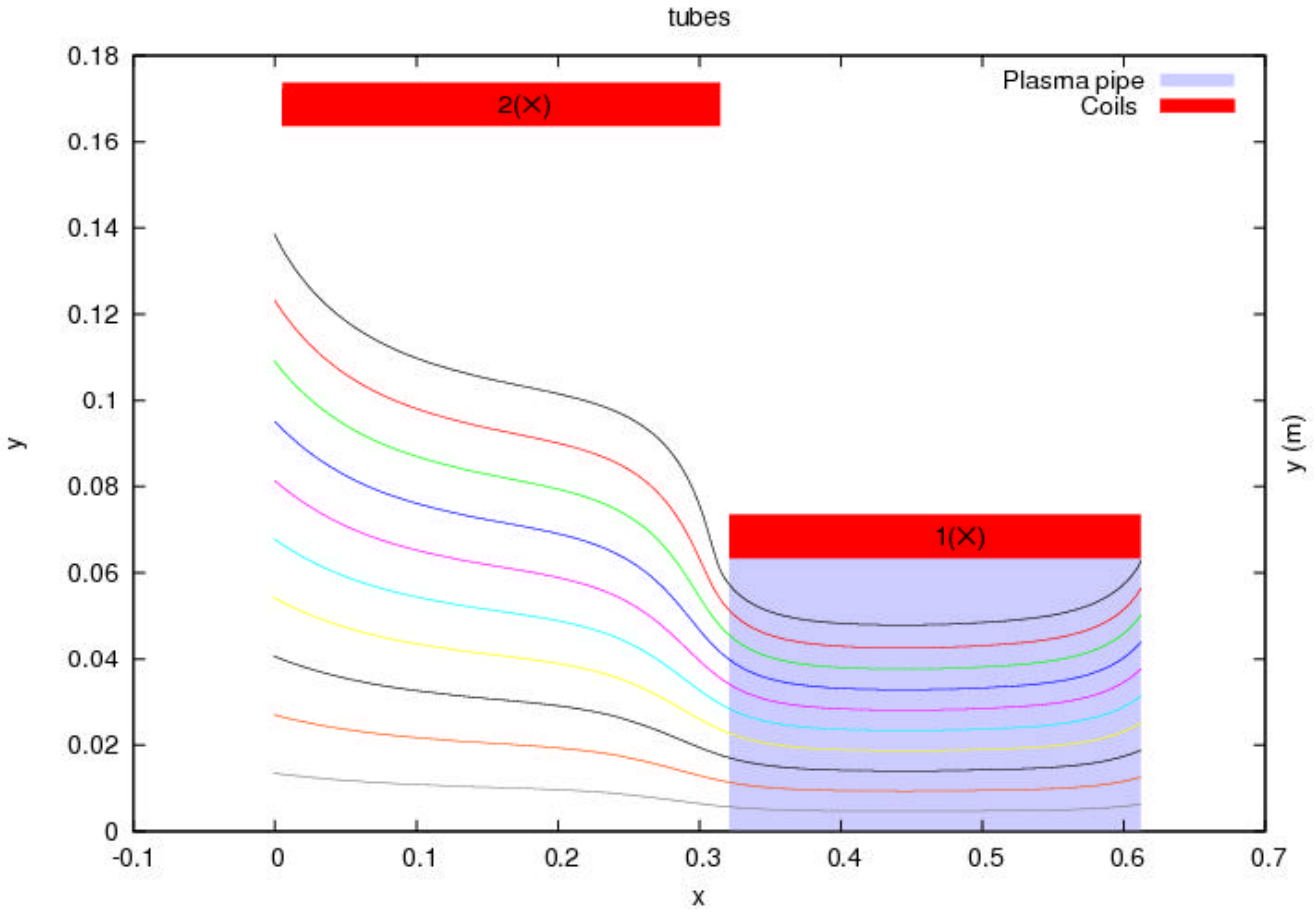

Fig 8.2.1 – magnetic field lines with solenoid in expansion chamber

The second one (A) use two solenoid only over the source as shown in Fig 8.2.2.

ESA CONTRACT no.	SUBJECT	CONTRACTOR
Ariadna 05/3201	Numerical Simulations of the Helicon Double Layer Thruster Concept – Final report	CISAS "G. Colombo"

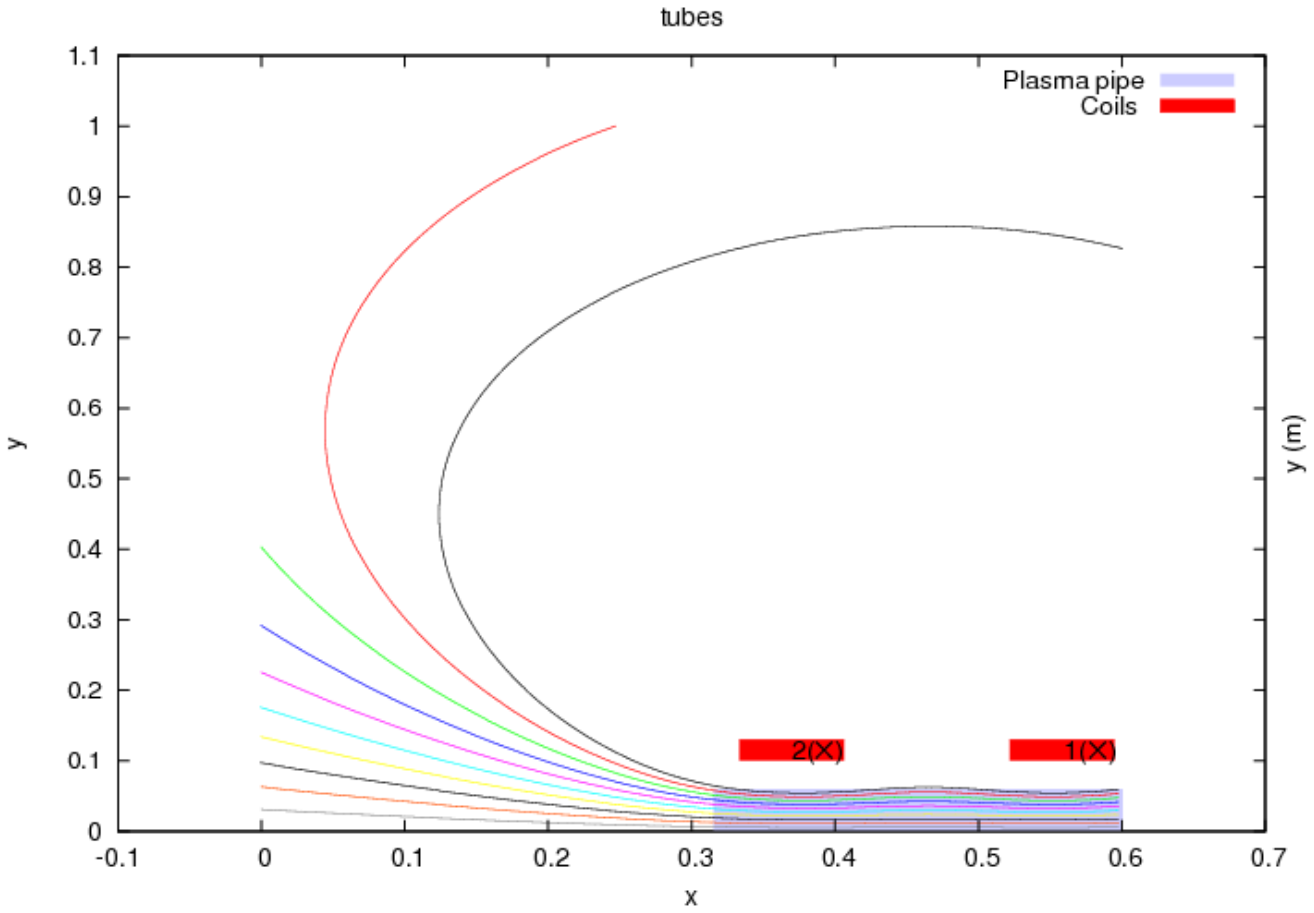

Fig 8.2.2 - Magnetic field lines with two solenoid only over the source

In this case we use a plasma frozen to the magnetic lines, so we use only the magnetic line that does not turn. PPDL uses the first of the magnetic tube that do not invert: in that case we keep the plasma frozen so we can calculate the density dilution because we have the magnetic tube radius for each z in

$$\frac{n(z)}{n_o} = \frac{B(z)}{B_o} = \left(\frac{r_0}{r(z)}\right)^2$$

8.3 MAGNETIC FIELD

There's no significant difference if we simply increase the wire current, from B_max 150G to B_max 300G

ESA CONTRACT no.	SUBJECT	CONTRACTOR
Ariadna 05/3201	Numerical Simulations of the Helicon Double Layer Thruster Concept – Final report	CISAS "G. Colombo"

8.4 MAGNETIC GRADIENT

The gradient of magnetic field does not seem that can change the potential profiles as shown in Fig 8.4.1

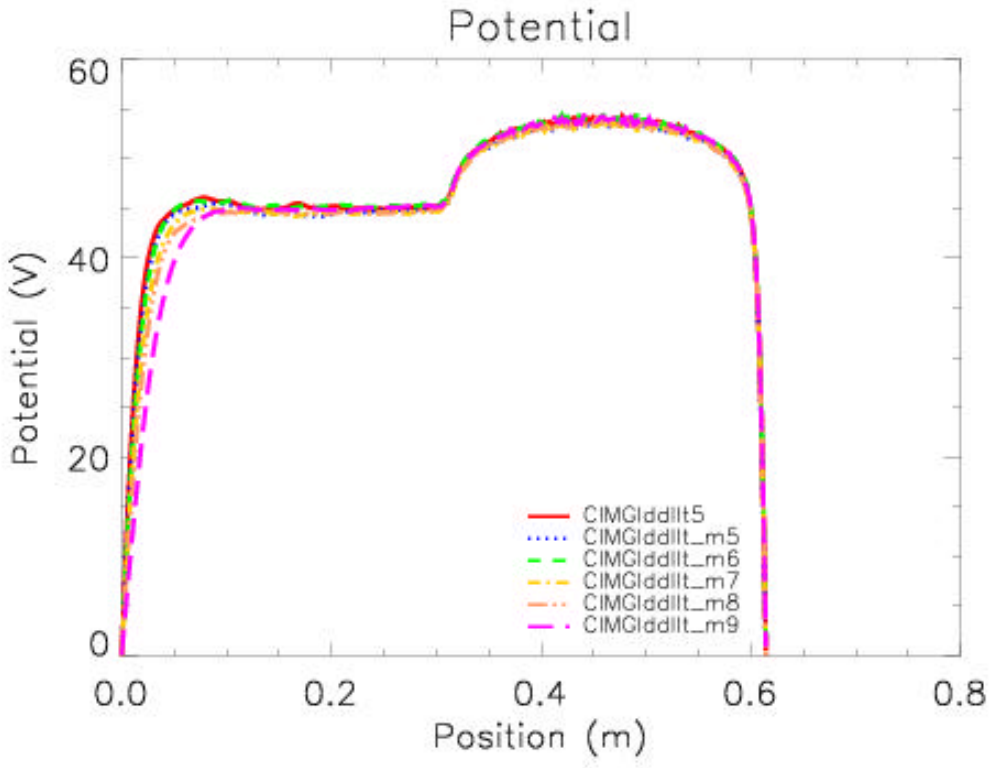

Fig 8.4.1 - Potential profile for simulations where the current is decreasing in the chamber coil, changing the magnetic field gradient

8.5 SOURCE POSITION

The position of source rate is very important for the localization of potential drop as shown in Fig 8.5.1 where the CIxcomp_invpd14 has the source in the normal position (0.35-0.55 m), Cixcomp_invpd15 has the source between 0.45 to 0.55 m and Cixcomp_invpd16 between 0.35 to 0.45 m

ESA CONTRACT no.	SUBJECT	CONTRACTOR
Ariadna 05/3201	Numerical Simulations of the Helicon Double Layer Thruster Concept – Final report	CISAS "G. Colombo"

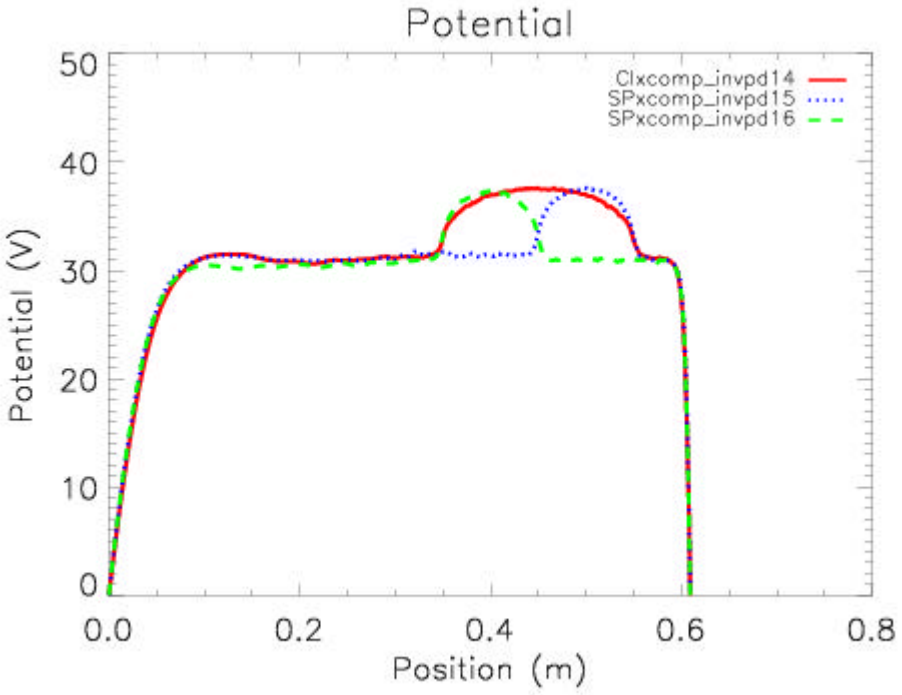

Fig 8.5.1 – Potential profile for different length and position of the plasma source

8.6 SOURCE RATE

It seems that it's very important for the position and for the width of potential drop. In the simulation input files, the source rate of value of 1e32 means that the source maintain the constant density inside the system. Every particle that go out of the system at wall is replaced inside the source. The influence of source rate is shown in Fig 8.6.1 and 8.6.2

ESA CONTRACT no.	SUBJECT	CONTRACTOR
Ariadna 05/3201	Numerical Simulations of the Helicon Double Layer Thruster Concept – Final report	CISAS "G. Colombo"

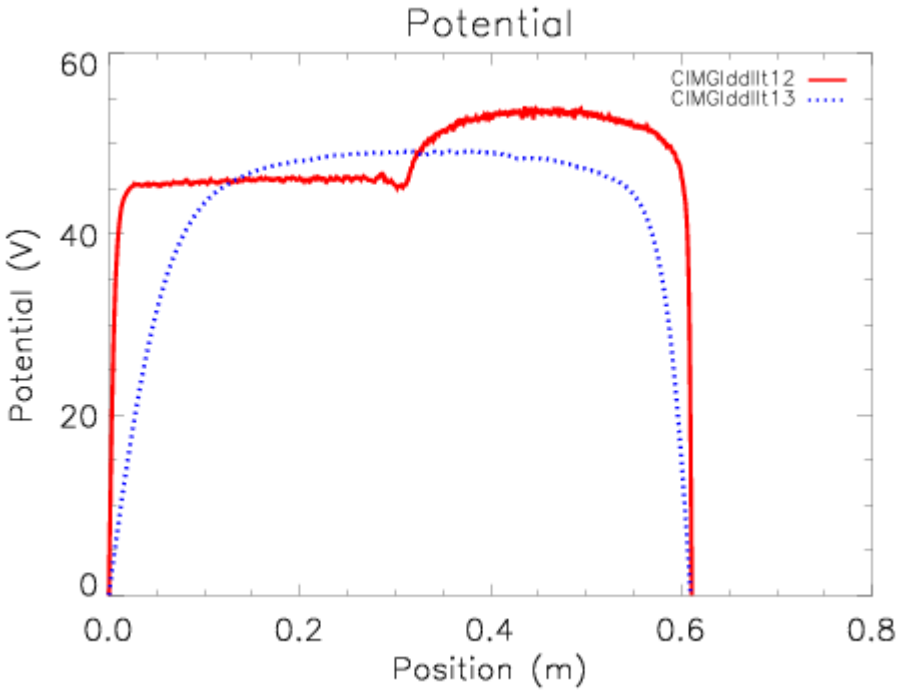

Fig 8.6.1 – Potential profile for different source rate (CIMGlddllt12 SR=Mant., CIMGlddllt13 SR=1 · 10^{17}

ESA CONTRACT no.	SUBJECT	CONTRACTOR
Ariadna 05/3201	Numerical Simulations of the Helicon Double Layer Thruster Concept – Final report	CISAS "G. Colombo"

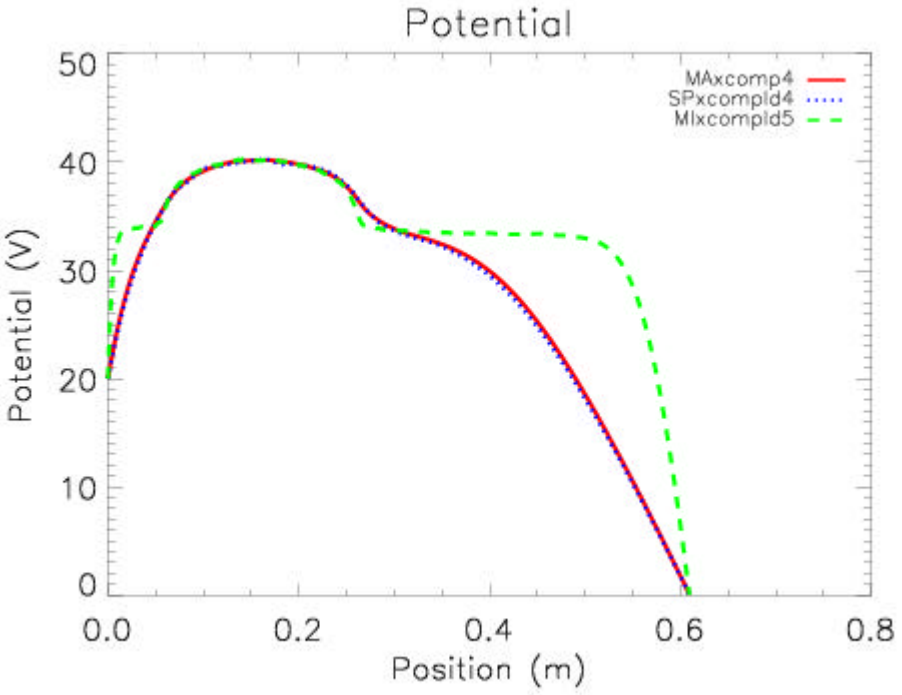

Fig 8.6.2- Hydrogen simulation with 20 V Dc bias (MAxcomp4 ne=4 · 1012 SR=5 · 10^{17}, SPxcompld4 ne=1014 SR=5 · 10^{17}, MIxcompld5 ne=10^{14} SR=Mant

If the source rate is very low density decrease very quickly.

8.7 NEUTRAL PRESSURE

The collision probability between plasma and neutrals, calculated with the method explained above, shows no collisions for pressure around 0.1-3 mTorr (so there is no influence of neutral by collisions). Probably the neutral pressure influences only the source rate of plasma production.

8.8 GAS

We simulate both Hydrogen and Argon. Argon shows a maximum potential higher than hydrogen, as shown in Fig 8.8.1, but Dv is similar. The specific impulse reach by argon is around 650s and 3800 s for H.

ESA CONTRACT no.	SUBJECT	CONTRACTOR
Ariadna 05/3201	Numerical Simulations of the Helicon Double Layer Thruster Concept – Final report	CISAS "G. Colombo"

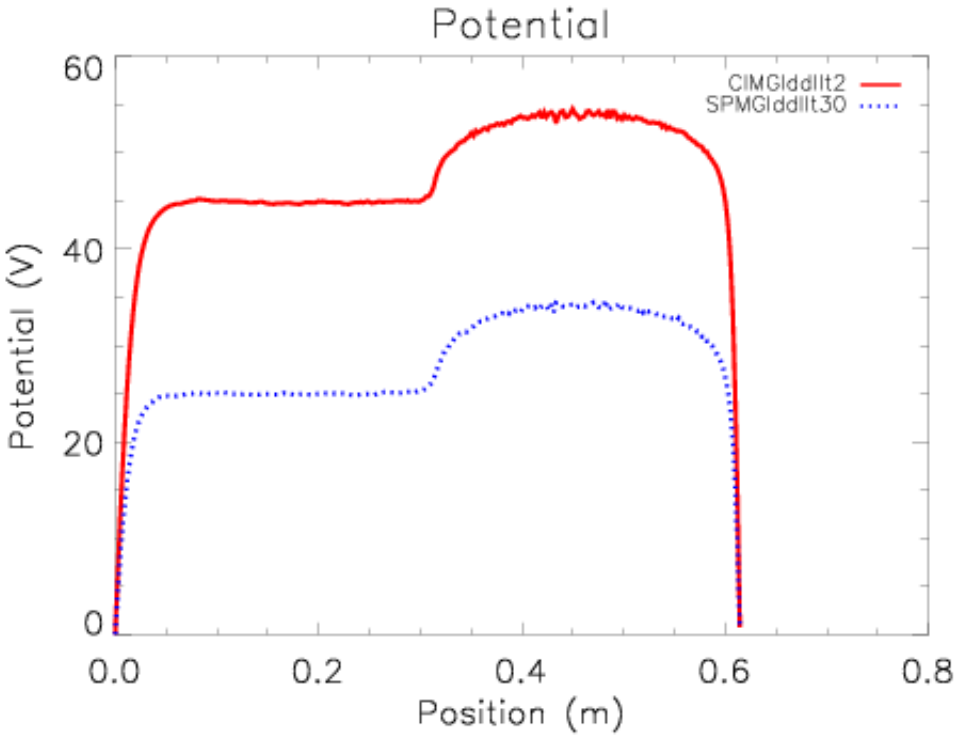

Fig 8.8.1 – comparison between Argon (CIMGlddllt2) and Hydrogen (SPMGlddllt30)

8.9 DENSITY

From the comparison of the same simulations with different plasma density we can see that the influence of density is not important for Dv. The density can change the kinetic energy for the detachment

ESA CONTRACT no.	SUBJECT	CONTRACTOR
Ariadna 05/3201	Numerical Simulations of the Helicon Double Layer Thruster Concept – Final report	CISAS "G. Colombo"

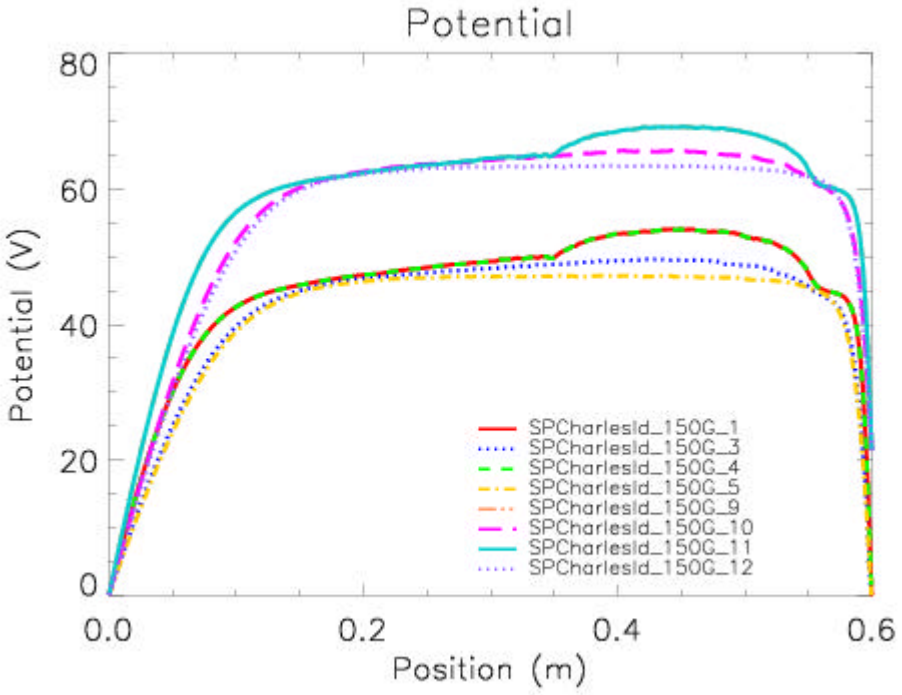

Fig 8.9.1 – Potential profile of several simulation: all simulations present density = 10^{14}

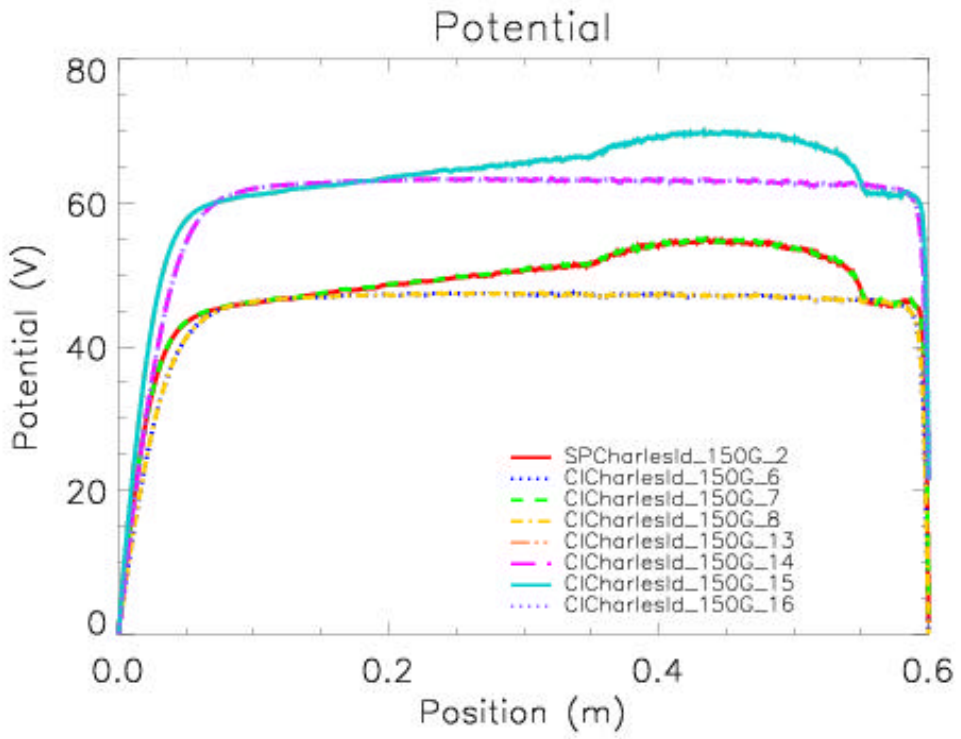

Fig 8.9.2 – Potential profile of several simulation: all simulations present density = 10^{15}

ESA CONTRACT no.	SUBJECT	CONTRACTOR
Ariadna 05/3201	Numerical Simulations of the Helicon Double Layer Thruster Concept – Final report	CISAS "G. Colombo"

8.10 DC BIAS

The influence of DC bias is only related to the value of maximum potential as shown in Fig 8.10.1. In Fig 8.10.2 the lower curves (SPESA_Bosdld4 SR=5e18 and CIESA_Bosdld13 SR =1e32) are at 0V-0V DCbias. The upper curves (SPESA_Bosdld5 SR=5e18 and CIESA_Bosdld14 SR =1e32) are at 10V-0V Dcbias

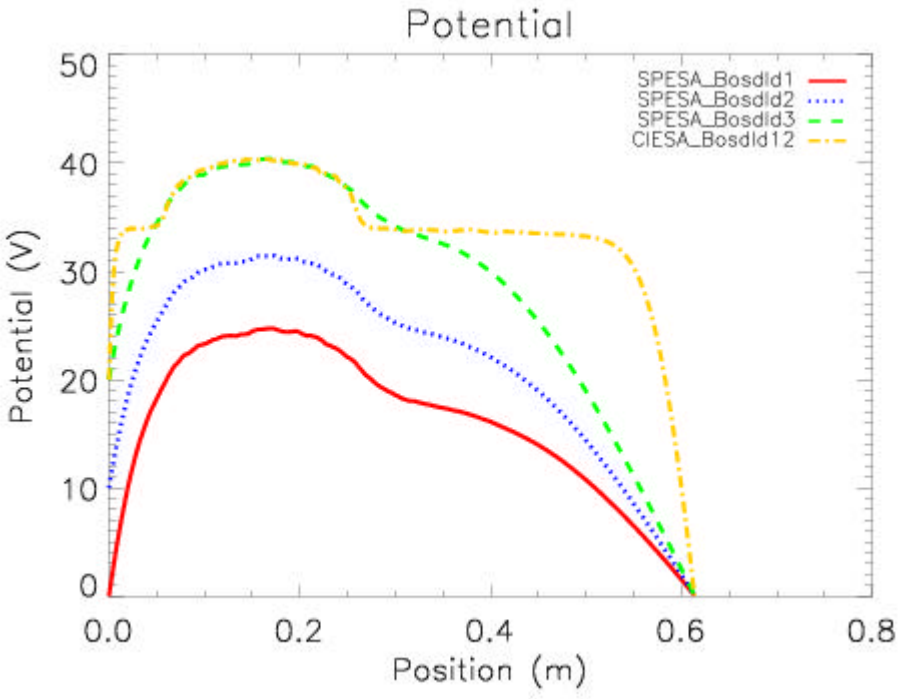

Fig 8.10.1 – Dc Bias influence: SPESA Bosdld1 (Dc bias 0V) SPESA Bosdld1 (Dcbias 10V) SPESA Bosdld1 (Dc bias 20V) CIESA Bosdld12 (Dc bias 20V and SR = Mant.)

ESA CONTRACT no.	SUBJECT	CONTRACTOR
Ariadna 05/3201	Numerical Simulations of the Helicon Double Layer Thruster Concept – Final report	CISAS "G. Colombo"

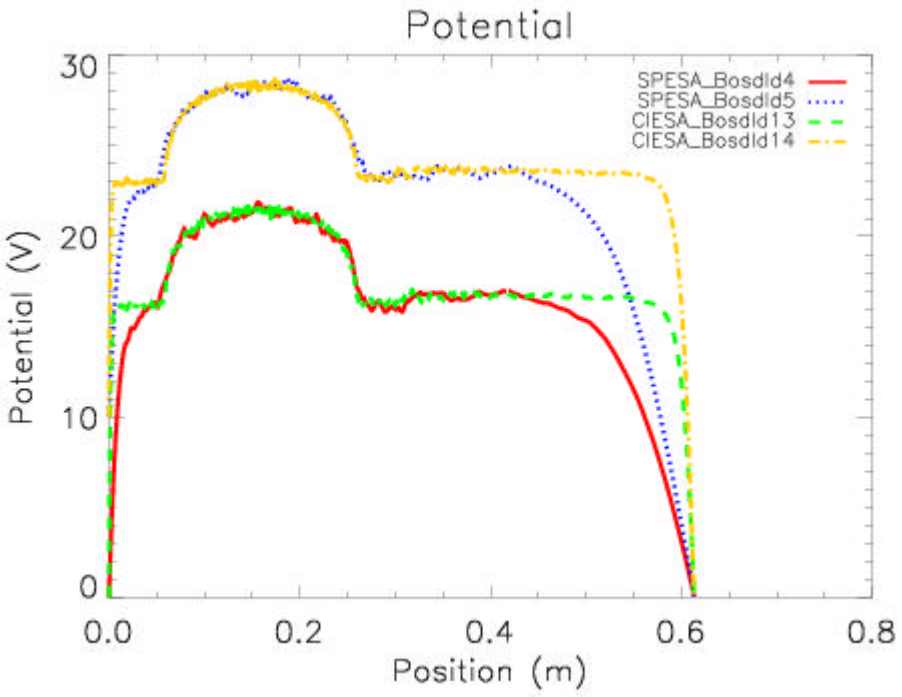

Fig 8.10.2 - DC bias influence: The lower curves (SPESA Bosdld4 SR=5e18 and CIESA Bosdld13 SR =Mant.) are at 0V-0V DC bias. The upper curves (SPESA Bosdld5 SR=5e18 and CIESA Bosdld14 SR = Mant.) are at 10V-0V Dcbias

8.11 TIME STABILITY

The time stability of potential drop is shown in Fig 8.11.1 for a time length of 1 ms. The graph shows the potential profile time history, and you can see that the profile does remains constant for all the time after a short transient period.

ESA CONTRACT no.	SUBJECT	CONTRACTOR
Ariadna 05/3201	Numerical Simulations of the Helicon Double Layer Thruster Concept – Final report	CISAS "G. Colombo"

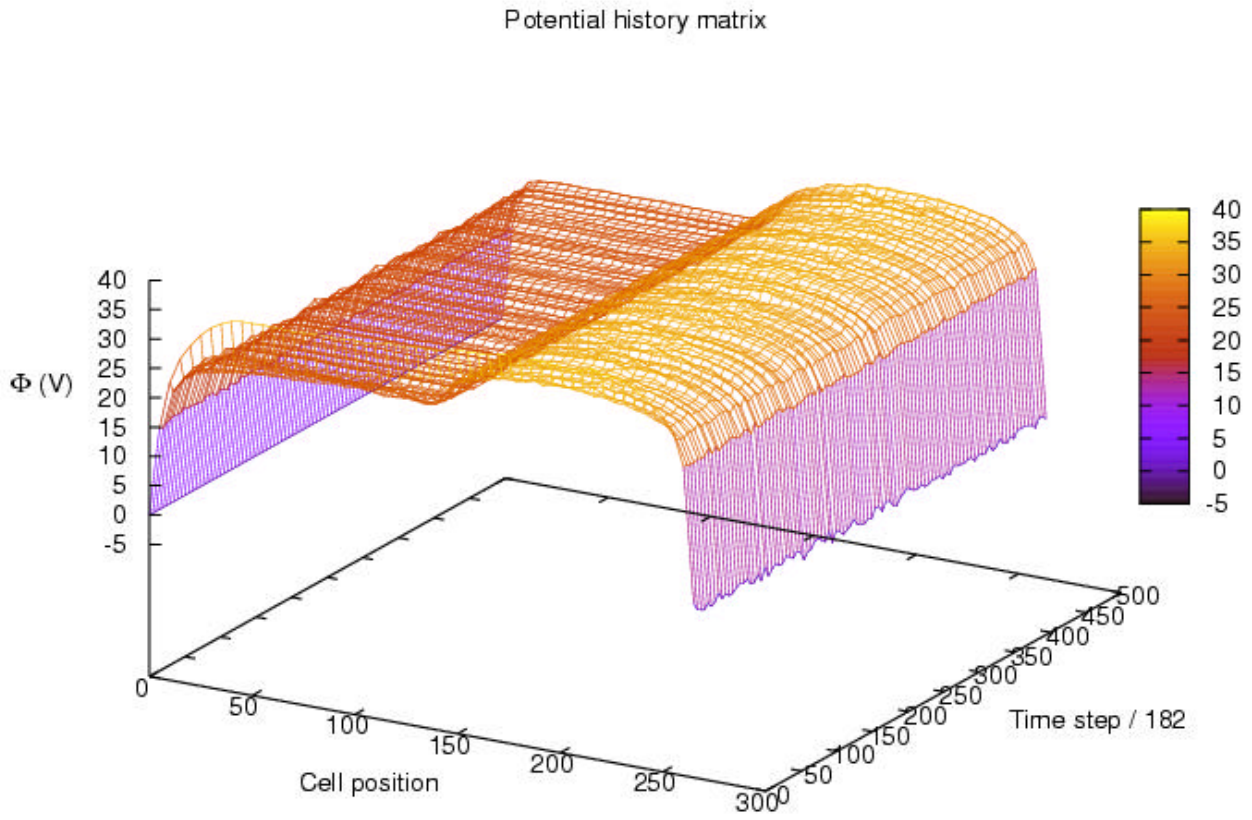

Figure 8.11.1 – Time history of potential profile

8.12 SYSTEM LENGTH

The system length does not seem to influence the results as shows in Fig 8.12.1

ESA CONTRACT no.	SUBJECT	CONTRACTOR
Ariadna 05/3201	Numerical Simulations of the Helicon Double Layer Thruster Concept – Final report	CISAS "G. Colombo"

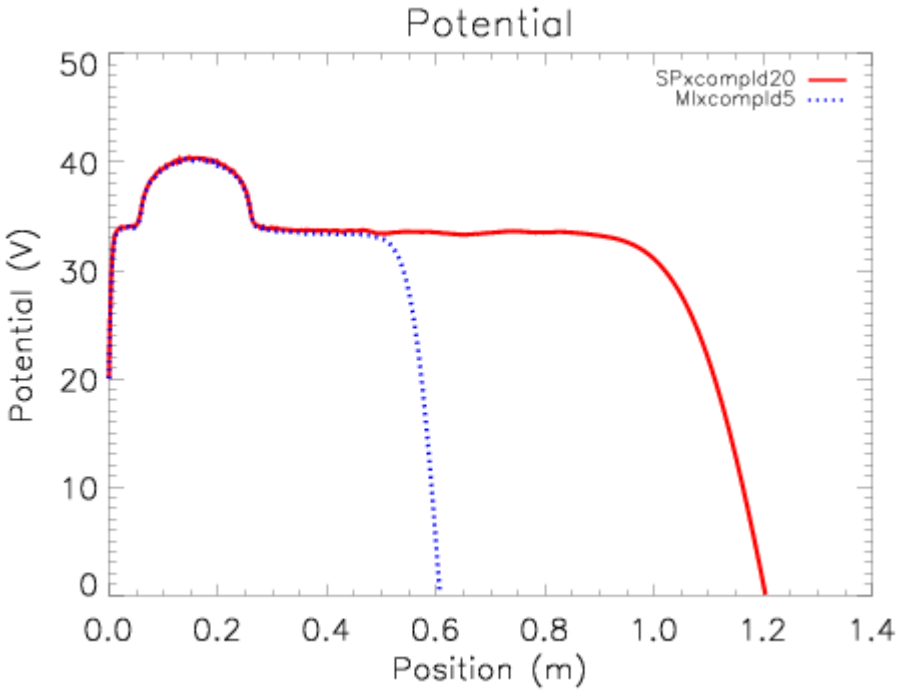

Fig 8.12.1 – Same simulation with different system length

8.13 MACH NUMBER

In some simulation we observed a ion beam velocity around 1.4 times the ion Bohm velocity. Every ion beam velocity is reported in xls file.

ESA CONTRACT no.	SUBJECT	CONTRACTOR
Ariadna 05/3201	Numerical Simulations of the Helicon Double Layer Thruster Concept – Final report	CISAS "G. Colombo"

9 OOPIC AND PPDL COMPARISON

The PPDL results will be here compared with the OOPIC simulations and the measurements made by Charles. Figures 9.1-9.4 compare the low density simulations of Chapter 6 while Figures 9.5 and 9.6 show the results of the two models for some of the conditions of Chapter 7. Finally the last pictures show some PPDL results for higher source rates and for the fixed/floating case.
The axial potential calculated by OOPIC is lower than the one computed by PPDL for the same border conditions. In particular for the case of low density (the conditions of Chapter 6) the OOPIC simulations have been done with the not confining dielectric walls, this reduces the plasma potential inside the source and therefore the differences between the two models. When the true dielectric walls are utilized and the border conditions are the same, the OOPIC/PPDL discrepancies seam to reduce around 10V (see pictures 9.5 and 9.6).
Both models show a potential jump between source and diffusion chamber almost 10V high and 10cm large, so lower and larger than the measured one.

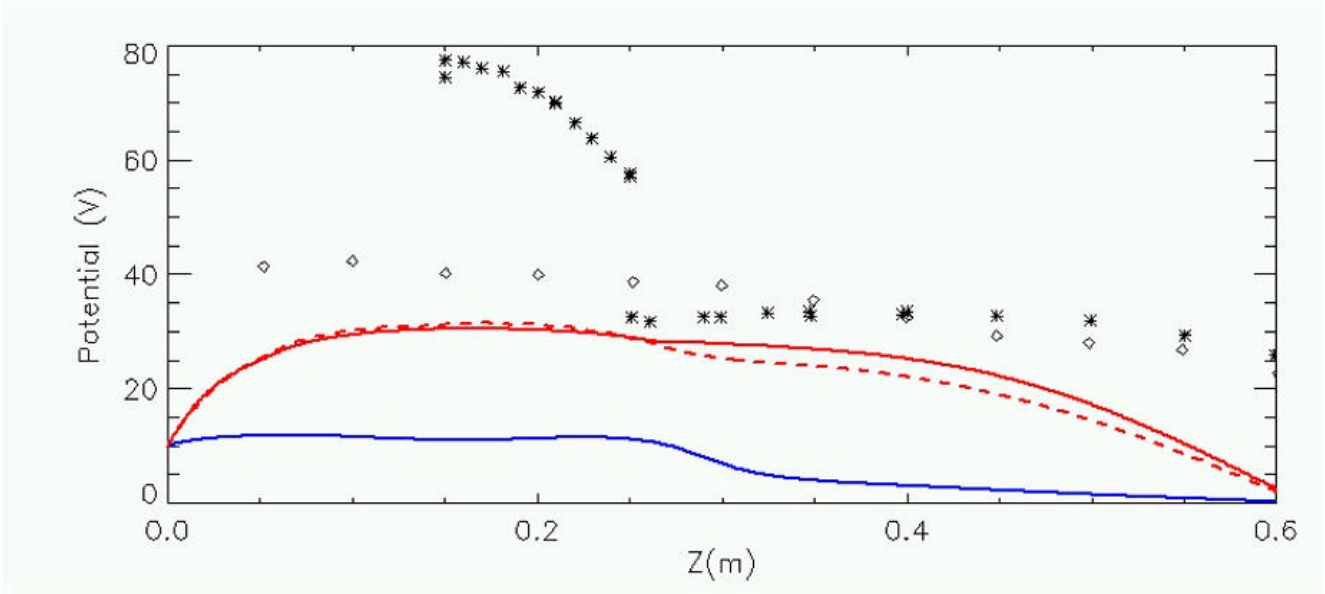

Fig 9.1: Simulations with source rate of 5e17 $m^{-3}s^{-1}$ and duration of 15µs. The blue line is the OOPIC simulation , PPDL simulations are red, red dashed is the simulation of 150µs. The left source wall is a 10V dc biased. Stars are the Charles measurements with DL (high magnetic field and low neutral pressure) and squares are the measurements without DL.

ESA CONTRACT no.	SUBJECT	CONTRACTOR
Ariadna 05/3201	Numerical Simulations of the Helicon Double Layer Thruster Concept – Final report	CISAS "G. Colombo"

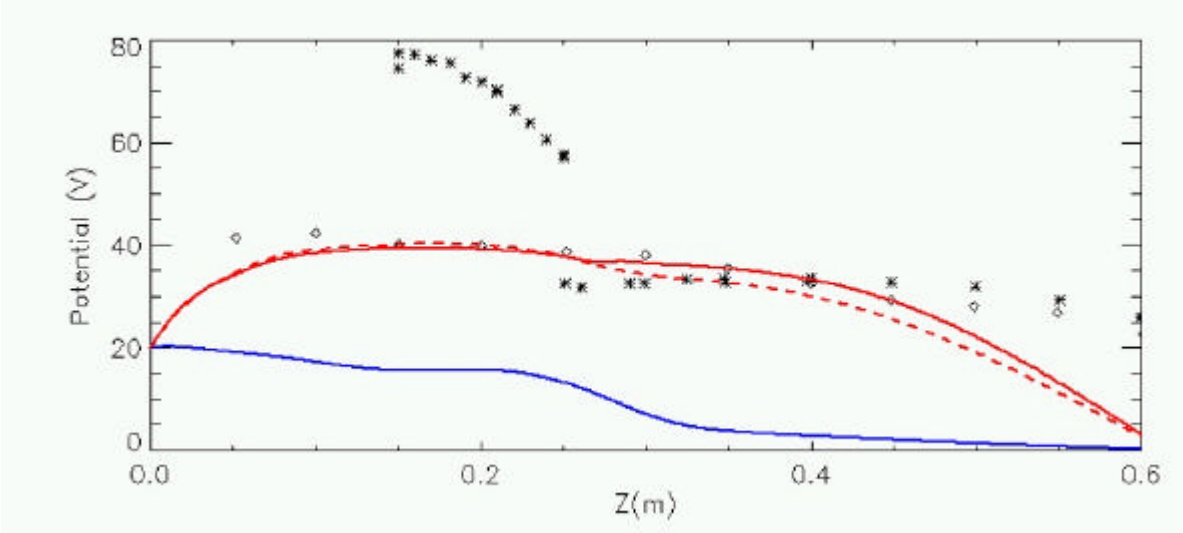

Fig 9.2: Simulations with source rate of 5e17 $m^{-3}s^{-1}$ and duration of 15µs. The blue line is the OOPIC simulation , PPDL simulations are red, red dashed is the simulation of 150µs. The left source wall is a 20V dc biased. Stars are the Charles measurements with DL (high magnetic field and low neutral pressure) and squares are the measurements without DL.

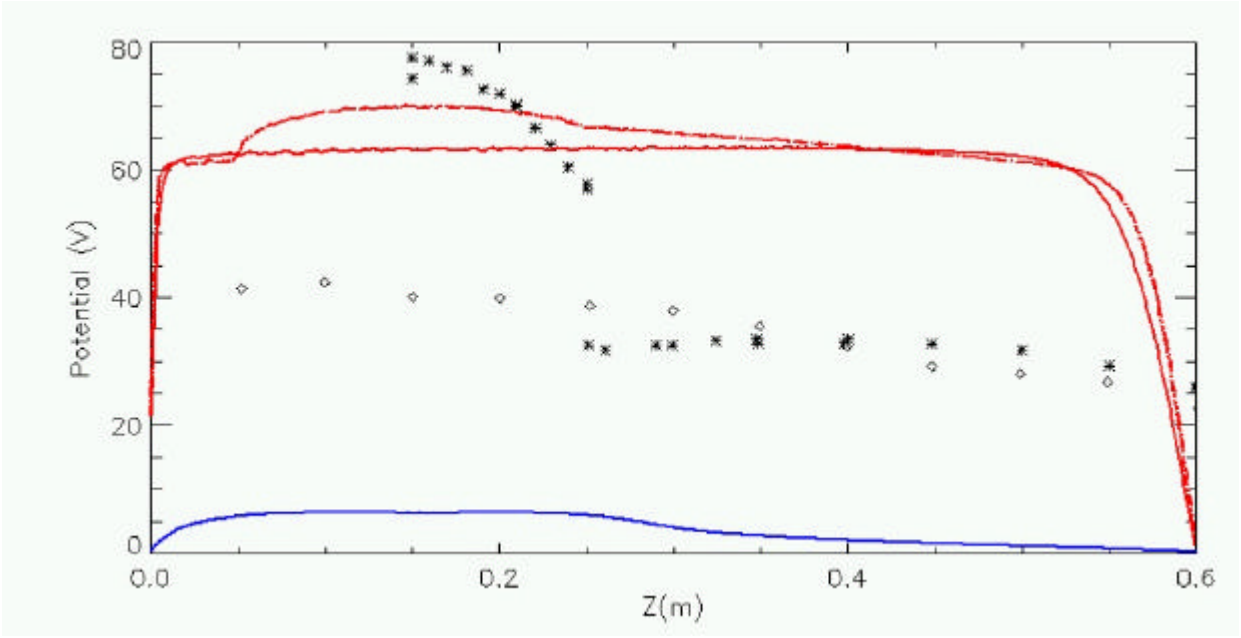

Fig 9.3: The blue line is the OOPIC simulation with source rate of 5e17 $m^{-3}s^{-1}$ and duration of 15µs. PPDL simulations are red, dashed is the simulation of 1e20 $m^{-3}s^{-1}$ both have a duration of 100µs.The left source wall is a 0V dc biased. Stars are the Charles measurements with DL (high magnetic field and low neutral pressure) and squares are the measurements without DL.

ESA CONTRACT no.	SUBJECT	CONTRACTOR
Ariadna 05/3201	Numerical Simulations of the Helicon Double Layer Thruster Concept – Final report	CISAS "G. Colombo"

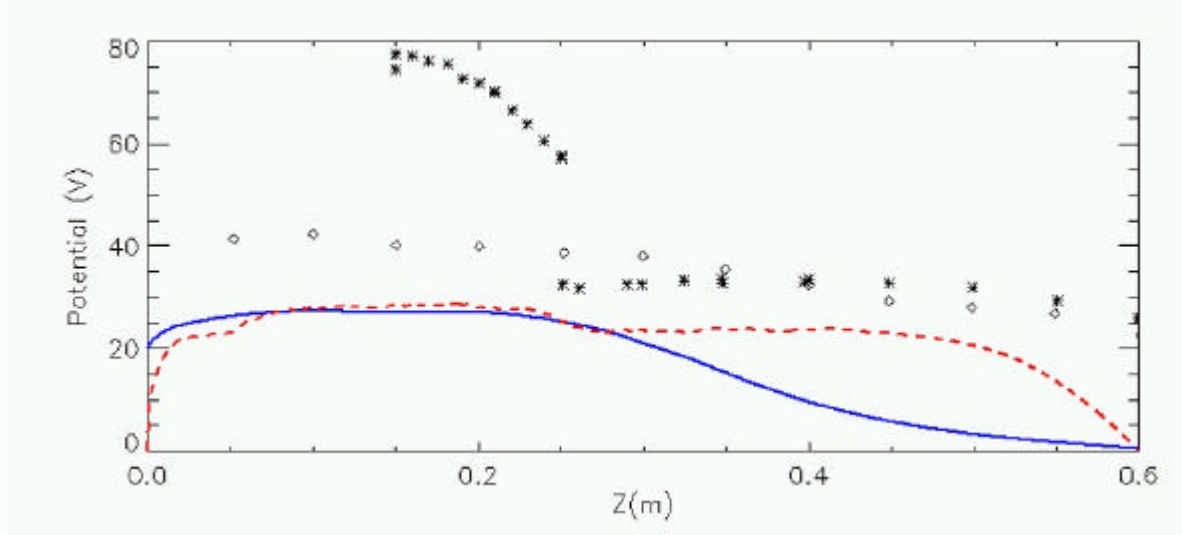

Fig 9.4: Simulations with source rate of 5e18 $m^{-3}s^{-1}$. The OOPIC simulation with dc bias of 20V and duration of 17μs is reported by the blue line. The PPDL simulation with dc bias of 10V lasts 170μs and it is drawn as red dashed line. Stars are the Charles measurements with DL (high magnetic field and low neutral pressure) and squares are the measurements without DL.

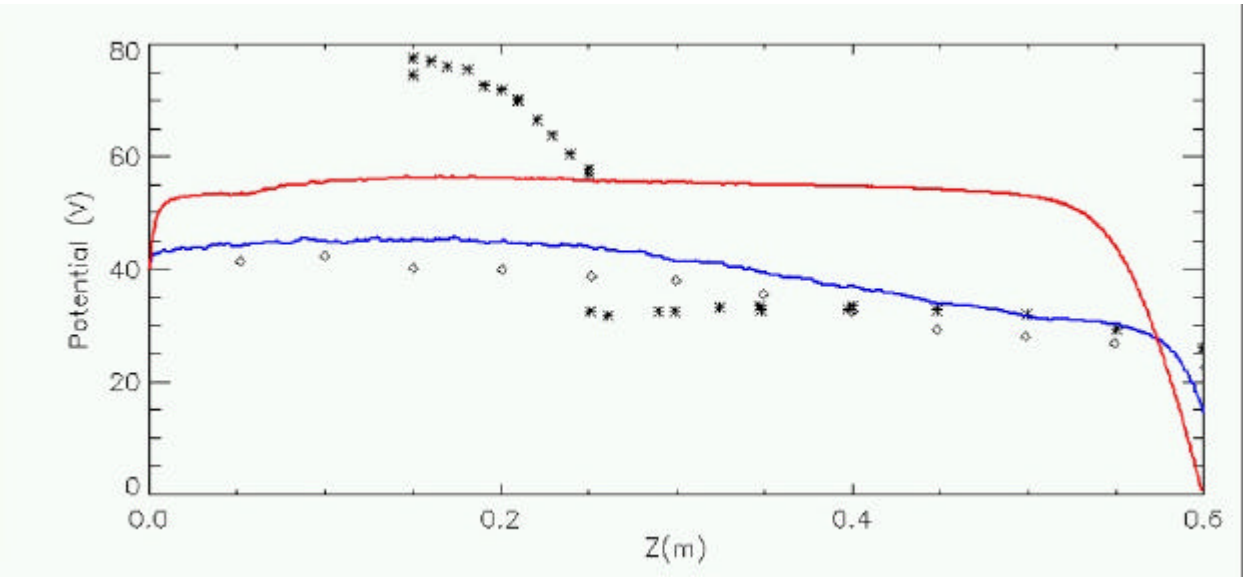

Fig 9.5: Simulations with source rate of 2e19 $m^{-3}s^{-1}$, duration of 30 μs and dc bias of 40V. The OOPIC results are reported by the blue line, the PPDL simulation is drawn as red line. Stars are the Charles measurements with DL (high magnetic field and low neutral pressure) and squares are the measurements without DL.

ESA CONTRACT no.	SUBJECT	CONTRACTOR
Ariadna 05/3201	Numerical Simulations of the Helicon Double Layer Thruster Concept – Final report	CISAS "G. Colombo"

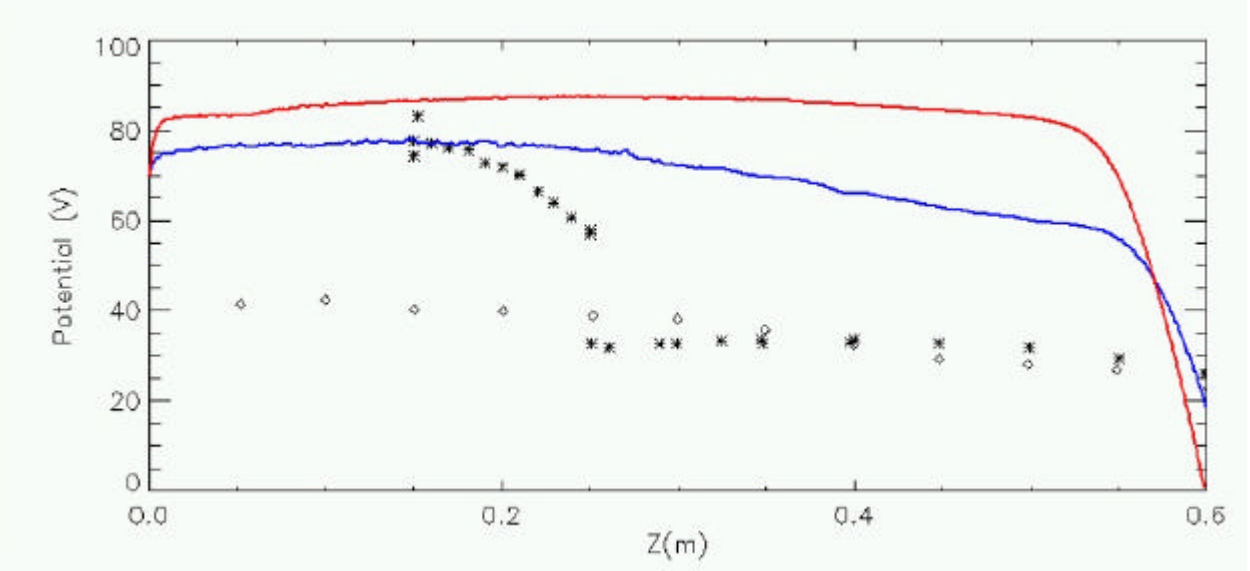

Fig 9.6: Simulations with source rate of 2e19 $m^{-3}s^{-1}$, duration of 30 μs and dc bias of 70V. The OOPIC results are reported by the blue line, the PPDL simulation is drawn as red line. Stars are the Charles measurements with DL (high magnetic field and low neutral pressure) and squares are the measurements without DL.

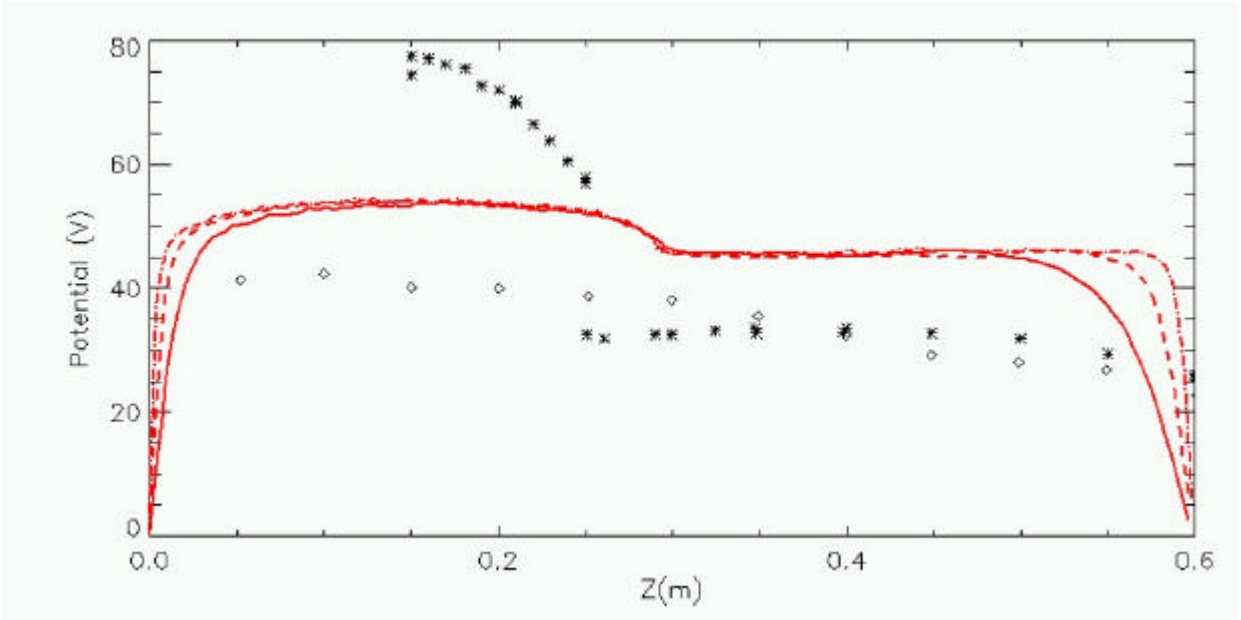

Fig 9.7: PPDL simulations of 600 μs with fixed/floating walls and growing source rates: 5e17, 1e14 (dashed) and 1e20 $m^{-3}s^{-1}$ (dashed-dotted). Stars are the Charles measurements with DL (high magnetic field and low neutral pressure) and squares are the measurements without DL.

ESA CONTRACT no.	SUBJECT	CONTRACTOR
Ariadna 05/3201	Numerical Simulations of the Helicon Double Layer Thruster Concept – Final report	CISAS "G. Colombo"

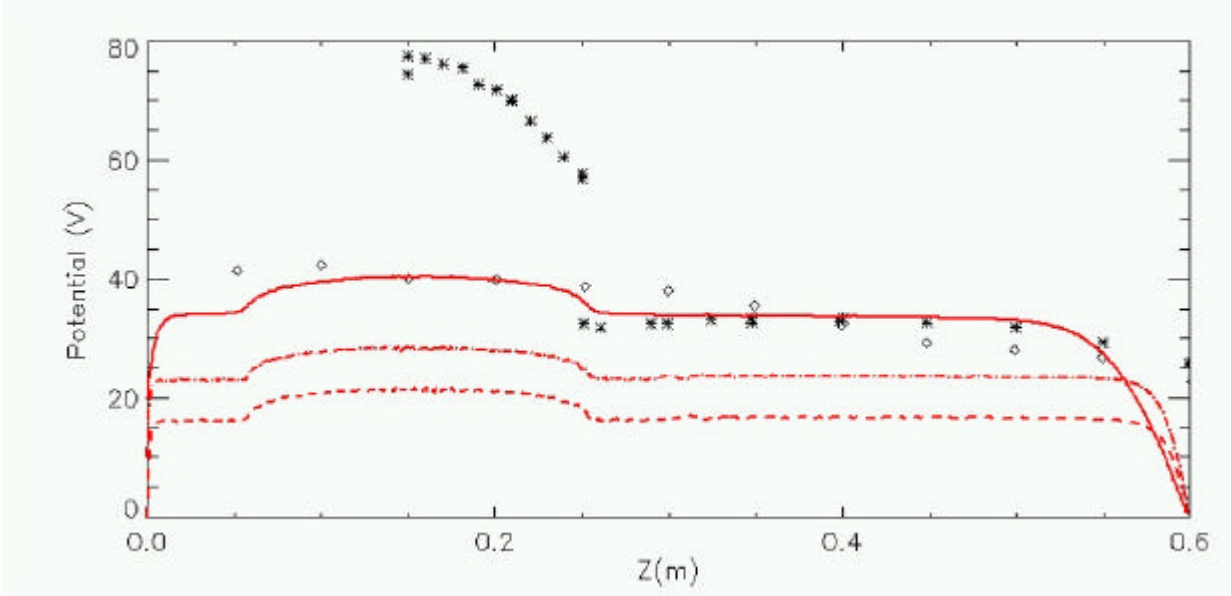

Fig 9.7: PPDL simulations of 170 μs, source rate of 1e32 $m^{-3}s^{-1}$ and dc biased walls of 0, 10 and 20V. Stars are the Charles measurements with DL (high magnetic field and low neutral pressure) and squares are the measurements without DL.

ESA CONTRACT no.	SUBJECT	CONTRACTOR
Ariadna 05/3201	Numerical Simulations of the Helicon Double Layer Thruster Concept – Final report	CISAS "G. Colombo"

10 CONCLUSIONS

The simulations have shown the formation and evolutions of plasma potential and ions axial velocity. The jump on the potential has not been seen as deep as reported by measurements but an ion flux at two times the ions sound speed has been obtained, in accordance with the bibliography.
The source walls, in particular the left one, have a great influence on the potential reached by the plasma. A conducting left wall biased at a sufficiently high potential can significantly increase the value registered inside the source tube and, sometimes, influence the stabilization of the plasma density there.
Increasing the neutral pressure we can switch off the high energy ion flux and reduce the potential jump. These effects happen at pressures greater than the measured but at almost the same value of $N_i \times N_n$ (neutral particles density times ions density) which is directly proportional to the ionization factor.
Along the helicon tube two solenoids make a static magnetic field which has as main effect the variation of the electrons trajectories. Neglecting the field intensity the ions flux at two times the sound speed remains, this fact does not correspond to the Charles' measurements.
The density of the ions high energy flux can be modulated by shaping the plasma formation area, in particular enlarging the area outside the diffusion chamber, we can obtain results that are similar to the experimental ones. The dimension and shape of this area in fact depends on several factors (i. e. magnetic field strength, antenna power, neutral pressure) so it is a sort of indirect effect of those factors.
Finally we evaluated the thrust and specific impulse, for H ions and source densities around 10^{13} m^{-3}, around $2\ 10^{-9}$ N and 3000 s.
Finally comparing our 1d and 2d simulations we met some differences but great agreement studying the general properties of the phenomenon. In particular, for the geometry of the Charles experiment, the potential jump remains below the measured one and we can have a 20-30% discrepancy between the two models; but the high energy ions flux and the main effects of the border conditions, like electrons and ions temperatures and walls characteristics, registered in the laboratory has been almost reproduced here.

ESA CONTRACT no.	SUBJECT	CONTRACTOR
Ariadna 05/3201	Numerical Simulations of the Helicon Double Layer Thruster Concept – Final report	CISAS "G. Colombo"

BIBLIOGRAPHY

1. M. A. Raadu, "Particle Acceleration Mechanisms in Space Plasmas", Phys. Chem. Earth (C), Vol. 26, No.1-3, pp. 55-59, 2001
2. M. Raadu, "The physics of double layers and their role in astrophysics", Physics Reports 178, No2, 1989, pp25-97
3. F.W. Perkins and Y.C. Sun "Double Layers without current" Phys. Rev. Lett. 46, 115 (1981)
4. C. Chan, M.H. Cho, N. Hershkowitz, T. Intrator, " Experimental observation of slow ion acoustic Double Layers" Phys. Rev. Lett. 57, 3050 (1986)
5. C. Chan, M.H. Cho, N. Hershkowitz, T. Intrator, "Laboratory Evidence for Ion-Acoustic-Type Double Layers" Phys. Rev. Lett. 52, 1782 (1984)
6. C. CHARLES, R.W. BOSWELL, "Time development of a current-free "helicon" double-layer". Accepted in Phys. Plasmas, (May 2004).
7. C. CHARLES, R.W. BOSWELL, "Laboratory evidence of a supersonic ion beam generated by a current-free helicon double-layer". Phys. Plasmas 11, 1706-1714 (2004).
8. C. CHARLES, "Hydrogen ion beam generated by a current-free double-layer in a helicon plasma". Applied Physics Letters 84, 332-334 (2004).
9. C. CHARLES and R.W. BOSWELL, "Current-free double-layer formation in a high-density helicon discharge". Applied Physics Letters 82, 1356-1358 (2003).
10. Temerin, "Observations of double layers and solitary waves in the auroral plasma", Phys. Rev Lett., 48, 17, 1982, pp1175
11. C. Birdsall, Langdon A. "Plasma Physics via computer simulation" Iop, Bristol, 1991
12. J.P. Verboncoeur, A.B. Langdon and N.T. Gladd, "An Object-Oriented Electromagnetic PIC Code", Comp. Phys. Comm., 87, May11, 1995, pp199-211
13. T. Sato, H. Okuda "Ion-Acustic Double Layers" Phys. Rev. Lett. 44, 740 (1980)
14. K. Y. Kim, "Weak monotonic Double Layers", Physics Letters, v 97A, n1, Aug 1983, pp45
15. F. Gesto, B. Blackwell, C. Charles, R. Boswell, "Ion Detachment in the Helicon Double-Layer Thruster Exhaust Beam", Journal Propulsion and Power Vol. 22, No. 1, January–Feb 2006, pp24
16. A. Meige, R. W. Boswell, C. Charles "One-dimensional Particle-in-Cell simulation of a current-free doublelayer in an expanding plasma" Physics of plasmas 12, 052317 (2005)
17. A. Meige, G. Hagelaar, R.W. Boswell, C. Charles, J.P. Boeuf, "Numerical modeling of electronegative electric double-layers", XXVIIth ICPIG, Eindhoven, the Netherlands, 18-22 July, 2005
18. Francis F. Chen, "Physical mechanism of current-free double layers", report *University of California, Los Angeles, California 90095-1594*
19. G. Hairapetian, R. Stenzel, "Particle dynamics and current-free double layer in an expanding,

ESA CONTRACT no.	SUBJECT	CONTRACTOR
Ariadna 05/3201	Numerical Simulations of the Helicon Double Layer Thruster Concept – Final report	CISAS "G. Colombo"

collisionless, two-electron-population plasma", Physics of Fluids B: Plasma Physics, 3, 4, p899, (1991)
20. S. Choen, N. Siefert, S. Stange, "Ion acceleration in plasmas emerging from a helicon-heated magnetic mirror device", Physics of Plasma, v10, N6, pp2593, (2003)
21. X. Sun, C. Biloiu, R. Hardin, "Parallel velocity and temperature of Ar ions in a expanding, helicon source driven plasma", v13, pp359, (2004)
22. X. Sun, A. Keesee, C. Biloiu, C. Charles, R. Boswell, "Observations of ion-beam formation in a currentfree double layer", Physical Rev Letters, v95, 025004, (2005)
23. N. Plihon, C. Corr, P. Chabert, "Double layer formation in the expanding region of an inductively coupled electronegative plasma", Applied Physics Lett, v86, 091501, (2005)
24. N. Plihon, C. Corr, P. Chabert, "Periodic formation and propagation of double layers in the expanding chamber of an inductive discharge operating in Ar/SF6 mixture", Journal of Applied Phys, v98, 023306, (2005)
25. A. Fruchtman, "Electric Field in a Double Layer and the Imparted Momentum", Physical Review Letters, 96, 065002 (2006)
26. J.P. Verboncoeur 1, A.B. Langdon 2, N.T. Gladd 3, "An object-oriented electromagnetic PIC code", Computer Physics Communications 87 (1995) pp199-211
27. G D Conway, A J Perry and R W Boswell, "Evolution of ion and electron energy distributions in pulsed helicon plasma discharges", Plasma Sources Sci. Technol. 7 (1998) pp337–347
28. N. Plihon, C. Chabert, "Helicon Double Layer Thruster Concept for High Power NEP Missions", ESA Ariadna ID: 04/310 final report
29. C. Charles, A. W. Degeling, T. E. Sheridan, J. H. Harris, M. A. Lieberman, "Absolute measurements and modeling of radio frequency electric fields using a retarding field energy analyzer", Physics of Plasmas 7, 12
30. M. Tuszewski, S. Gary, "Downstream instability of electronegative plasma discharges", Phys of Plasmas, v10, N2, pp539, (2003)
31. Christine Charles, "High source potential upstream of a current-free electric double layer", Phys. Of Plasmas, 12:044508, 2005.
32. K.L. Cartwright, J. P. Verboncoeur, C.K. Birdsall "Nonlinear hybrid Boltzmann-Particle-in cell acceleration algorithms" Physics of Plasmas 7 (3252-3264) 2000
33. Francis F. Chen, "Physical mechanism of current-free double layers" Physics of Plasmas 13 (034502-1-034502-3) 2006
34.. M. A. Lieberman C.Charles, R.W. Boswell "A theory of formation of a low pressure, current free double layer" Journal of Physics D: Applied Physics 39 (3294-3304) 2006
35. A. V. Phelps. "The application of scattering cross sections to ion flux models in discharge sheaths", Journal of Applied Physics 76 (747-753) 1994